CHARACTERISING THE ROLE OF MICROGLIA IN THE EARLY STAGES OF BRAIN METASTASIS



Kleopatra E. Andreou

St. Edmund Hall

Department of Oncology

Trinity Term, 2016

A thesis submitted to the Medical Sciences Division of the University of Oxford in partial fulfilment of the requirements for the degree of Doctor of Philosophy

Acknowledgments

I would like to thank my supervisor, Prof. Nicola Sibson, for giving the opportunity to undertake this DPhil and study such an exciting project. I would like to thank her for her support and patience throughout the years. I would also like to thank Dr. Manuel Sarmiento Soto and Dr. James Larkin for their help with experiments and scientific advice. Also, a huge thank you to all the members of the Sibson lab, past and present, for their friendship and for always sharing their chocolate with me.

I dedicate this thesis to my family, who always believed in my abilities.

Abstract

Brain metastasis is a common complication of breast cancer patients with poor survival. Histological analysis of autopsy samples from patients with brain metastases suggests that microglia, rather than lymphocytes, are the major immune population activated around the metastatic foci. Microglia and macrophages are versatile immune cells with the ability to polarise to different functional phenotypes depending on the microenvironment they reside in. Clinical and preclinical data report both tumourigenic and cytotoxic effects of microglia and macrophages in the tumour microenvironment. However the role and phenotype of microglia during the early stages of metastatic growth in the brain has not yet been fully determined. The aim of this thesis, therefore, was to determine the temporal and spatial profile of microglial activation in a mouse model of brain metastasis, and to assess the effect of M2 (anti-inflammatory) microglial depletion on tumour growth.

Iba1, a specific marker for microglia, was robustly expressed around 4T1 metastatic foci. Quantitatively, microglial activation positively correlated with tumour volume over a 28 day study. Moreover mixed populations of classically (M1) and alternatively (M2) activated microglia were identified by co-localisation of Iba1 with inducible nitric oxide synthase (iNOS) and cyclooxygenase 2 (COX2), or mannose receptor 1 (MRC1) and arginase 1 (Arg1), respectively. M1 and M2 microglia were found within the tumour microenvironment as well as adjacent to the 4T1 foci. Temporally, $MRC1^+$ M2 microglia maintained their levels across the time-course, as did $iNOS^+$ M1 cells. *In vivo* depletion of $MRC1^+$ microglia at an early stage significantly reduced intracranial tumour burden in the metastatic brain. Moreover, increased levels of apoptosis, indicated by cleaved caspase 3 expression, were associated with 4T1

tumour foci in the animals injected with clodronate liposomes compared to those injected with control liposomes.

A genetic model of deficient M2 polarisation of myeloid cells was also employed as an alternative approach. However, there was no significant decrease in intracranial metastasis burden, possibly due to lack of microglial targeting in the specific model. Further validation of this model is needed in order to draw conclusions on the effect on tumour burden.

Our findings suggest that microglia are effectors of the inflammatory response in the early stages of brain metastasis. We have shown that mixed M1 and M2 phenotypes co-exist within the tumour microenvironment and that targeting the anti-inflammatory M2 microglial population could be of therapeutic benefit. Further research will provide insights into the M2 molecular signatures that sustain metastatic outgrowth in the brain with the aim of therapeutic intervention.

Contents

Acknowledgments i

Abstract ii

Contents iv

List of tables vii

List of figures viii

List of abbreviations x

Chapter 1: Introduction 1

1.1 Cancer 2

1.2 Cancer metastasis 3

1.2.1 Introduction 3

1.2.2 Steps of the metastatic cascade 4

1.2.2.1 Invasive carcinoma 5

1.2.2.2 Intravasation and haematogenous spread 7

1.2.2.3 Extravasation and metastatic growth 8

1.3 Tumour associated macrophages (TAMs) 10

1.3.1 TAMs during tumour progression 10

1.3.2 TAM polarisation 13

1.3.3 TAMs as therapeutic targets 16

1.4 Brain metastasis 17

1.4.1 Treatment of brain metastases 17

1.4.2 Mechanistic insights 19

1.4.2.1 Molecular characterisation of brain seeking cancer cells 20

1.4.2.2 Role of brain endothelial cells 21

1.4.2.3 Role of astrocytes 23

1.4.2.4 Role of microglia and macrophages 24

1.5 Microglia 26
1.5.1 Microglial cell origin 26
1.5.2 Role of microglia in brain homeostasis 28
1.5.3 Microglial polarisation in disease 30
1.6 Research motivation 33
Chapter 2: Materials and methods 35
2.1 Chemicals and buffers 36
2.2 Cell lines and tissue culture 36
2.2.1 Cell lines 36
2.2.2 Tissue culture 38
2.3 Cell treatments 38
2.4 MTT cell viability assay 39
2.5 *In vivo* procedures 40
2.5.1 Experimental brain metastasis 41
2.5.1.1 Tumour cell injections 41
2.5.1.2 Mouse models of brain metastasis 42
2.5.2 Model of CNS inflammation 42
2.5.3 *In vivo* depletion of microglia 43
2.5.4 Injection of free clodronate 43
2.6 Brain harvest 44
2.7 Lung/Liver harvest 44
2.8 Immunohistochemistry 44
2.9 Immunohistochemical scoring 46
2.10 Double immunohistochemistry 47
2.10.1 Sequential HRP and alkaline phosphatase double staining 47
2.10.2 Sequential double HRP staining 49

2.11 Matlab co-registration of sequential immunostained brain sections 50
2.12 Immunofluorescence 54
2.12.1 Immunofluorescence on tissue sections 54
2.12.2 Immunofluorescence on cells 58
Chapter 3: Microglial infiltration in an experimental model of breast cancer brain metastasis 59
3.1 Introduction 60
3.2 Aims 62
3.3 Methods 63
3.4 Results 64
3.4.1 Microglial infiltration in the metastatic brain 64
3.4.2 Expression of M1 and M2 markers in the metastatic brain 68
3.4.3 M1 and M2 microglia in the metastatic brain 71
3.5 Discussion 79
Chapter 4: *In vivo* depletion of MRC1^{+} microglia in the mouse metastatic brain 86
4.1 Introduction 87
4.2 Aims 90
4.3 Methods 91
4.4 Results 92
4.4.1 Effect of mannosylated liposomes on cell viability *in vitro* 92
4.4.2 IL-4 model of CNS inflammation 99
4.4.3 The mannosylated liposomes approach in the metastatic brain 104
4.4.3.1 Validation of MRC1 depletion in the 4T1-GFP model 104
4.4.3.2 Metastasis burden 107
4.4.3.3 Tumour apoptosis 109
4.4.3.4 Tumour vascularity 112

4.4.4 Control experiments in naïve mouse brains....113
4.5 Discussion....119
Chapter 5: Effect of myeloid specific Krüppel-like factor 4 knock out on the growth of experimental brain metastases....127
5.1 Introduction....128
5.2 Aims....129
5.3 Methods....130
5.4 Results....130
5.4.1 Intracranial metastasis burden in LYSM and LYSK mice....130
5.4.1.1 Metastasis burden in LYSM/LYSK mice injected with EO771 cells....130
5.4.1.2 Metastasis burden in LYSM/LYSK mice injected with LLC cells....132
5.4.1.3 Metastasis burden in LYSM/LYSK mice injected with B16F10 cells....135
5.4.2 Validation of the KLF4 knock-out in the LYS model....136
5.5 Discussion....139
Chapter 6: Discussion and future directions....142
6.1 General discussion....143
6.2 Future directions....145
References....148

List of tables

Table 2.1: Mouse models of brain metastasis....42
Table 2.2: Antibodies used for immunohistochemistry....45
Table 2.3: Antibody, enzyme and substrate combinations for double immunohistochemistry....50
Table 2.4: List of antibodies used for fluorescent staining....57

List of figures

Figure 1.1: Steps of metastasis 5

Figure 1.2: Traits of malignancy promoted by TAMs 12

Figure 1.3: Macrophage polarisation in the tumour microenvironment 15

Figure 1.4: Cellular composition of the brain 20

Figure 2.1: Schematic of the enzymatic reaction of the MTT assay 40

Figure 2.2: Demarcation of areas of interest for quantitation of tumour and microglial volumes 47

Figure 2.3: Matlab co-registration of sequential immunostained brain sections 52

Figure 3.1: Schematic of the brain regions used for the Matlab analysis 63

Figure 3.2: Validation of the intracerebral 4T1-GFP model 65

Figure 3.3: Sustained microglial infiltration during the early stages of breast cancer brain metastasis 67

Figure 3.4: Expression of M1 and M2 markers in the metastatic brain 69

Figure 3.5: Detection of M1 and M2 microglia in the metastatic brain by immuno fluorescence 72

Figure 3.6: Double immunohistochemistry to identify M2 microglia and macrophages 73

Figure 3.7: Detection of M1 and M2 microglia in the metastatic brain using Matlab 75

Figure 3.8: Spatiotemporal expression of M1 and M2 microglia in the metastatic brain 77

Figure 4.1: The clodronate liposome approach for macrophage depletion 90

Figure 4.2: Mannosylated liposomes do not affect viability of 4T1-GFP tumour cells *in vitro* 92

Figure 4.3: Mannosylated clodronate liposomes decrease viability of BV2 microglia and RAW264.7 macrophages *in vitro* 94

Figure 4.4: *In vitro* polarisation of microglia/macrophages 95

Figure 4.5: *In vitro* M1 polarisation subsides the decrease of cell viability upon treatment with mannosylated clodronate liposomes 98

Figure 4.6: Microglial response after intracerebral injection of IL-4 100

Figure 4.7: MRC1 upregulation after intracerebral injection of IL-4 101

Figure 4.8: *In vivo* depletion of $MRC1^{+}$ cells by intracerebral injection of mannosylated clodronate liposomes 103

Figure 4.9: *In vivo* depletion of $MRC1^{+}$ microglia in the 4T1-GFP metastatic brain 105

Figure 4.10: Metastatic tumour burden after intracerebral injection of mannosylated clodronate liposomes 108

Figure 4.11: Levels of apoptosis in metastatic brains injected with mannosylated control or clodronate liposomes 110

Figure 4.12: Vascularity of 4T1-GFP tumours in metastatic brains injected with mannosylated control or clodronate liposomes 113

Figure 4.13: Effect of free clodronate on cell context *in vitro* and *in vivo* 114

Figure 4.14: Effect of mannosylated clodronate liposomes in the naïve brain 117

Figure 5.1: Tumour growth and microglia infiltration of EO771 tumours in LYSM and LYSK mice 131

Figure 5.2: Tumour growth and microglia infiltration of LLC tumours in LYSM and LYSK mice 133

Figure 5.3: Tumour growth and microglia infiltration of B16F10 tumours in LYSM and LYSK mice 135

Figure 5.4: Validation of the myeloid KLF4 knock out in LYSK mice 137

Figure 5.5: M2 microglia in the metastatic brains of LYSM and LYSK mice 138

List of abbreviations

ALCAM: activated leukocyte cell adhesion molecule

ANOVA: analysis of variance

ANGPTL4: angiopoietin like 4

Arg1: arginase 1

ATP: adenosine triphosphate

BBB: blood brain barrier

BMDMs: bone marrow derived macrophages

CC3: cleaved caspase 3

CD: cluster of differentiation

CNS: central nervous system

COX2: cyclooxygenase 2

CSF-1: colony stimulating factor 1

DAB: diaminobenzidine

EAE: experimental autoimmune encephalomyelitis

EGF: epidermal growth factor

EGFR: epidermal growth factor receptor

EMT: epithelial mesenchymal transition

FAK: focal adhesion kinase

FBS: fetal bovine serum

FGF: fibroblast growth factor

GFP: green fluorescent protein

HER: human epidermal growth factor receptor

HIF: hypoxia inducible factor

HRP: horseradish peroxidise

Iba1: ionised calcium-binding adapter molecule 1

ICAM: intercellular adhesion molecule

IFN: interferon

IgG: immunoglobulin G

IHC: immunohistochemistry

IL: interleukin

iNOS: inducible nitric oxide synthase

KLF4: krüppel like factor 4

LFA1: lymphocyte function associated antigen

LLC: Lewis lung carcinoma

LOX: lysyl oxidase

LPA: lysophosphatidic acid

LPS: lipopolysaccharide

MCP1: monocyte chemoattractant protein 1

MHCII: major histocompatibility complex II

MMP: matrix metalloproteinase

MRC1: mannose receptor 1

NSCLC: non-small cell lung cancer

NO: nitric oxide

PAMPs: pathogen-associated molecular patterns

PFA: paraformaldehyde

PTEN: phosphatase and tensin homolog

SDF-1α: stromal derived factor 1 alpha

STAT3: signal transducer and activator of transcription 3

TAMs: tumours associated macrophages

TEM: transendothelial migration

TGF-β: transforming growth factor beta

TLR: Toll like receptor

TNF: tumour necrosis factor

TREM2: triggering receptor expressed on myeloid cells 2

VCAM: vascular cell adhesion molecule

VEGF: vascular endothelial growth factor

VLA4: very late antigen 4

WBRT: whole brain radiation therapy

Chapter 1

Introduction

1.1 Cancer

Cancer is a disease characterised by neoplastic transformation of cells leading to uncontrolled cell division, tumour formation and ultimately death, if not treated. Initial conventional chemotherapies aimed to confer non-specific cytotoxicity to rapidly dividing malignant cells. Over the past few decades, however, research has unveiled complex molecular mechanisms that drive carcinogenesis and maintain malignant progression. This great effort has granted clinical oncology with numerous targeted treatment options, such as small-molecule agents against oncogenic kinases (Zhang et al, 2009), and has significantly improved the therapeutic outcome of molecularly defined subsets of patients.

Alongside the significant advances achieved towards better understanding cancer cells' traits came progress in understanding cancer as a multifactorial disease. A seminal study by Hanahan and Weinberg summarises the hallmarks of cancer and introduces the concept of tumour microenvironment in the maintenance and dissemination of cancer (Hanahan and Weinberg, 2000). The consolidated version of this proposition acknowledges tumour associated inflammation as an enabling characteristic of cancer and evasion of immune response as an additional hallmark (Hanahan and Weinberg, 2011). Indeed, data from biopsies have revealed that tumour masses are heterogeneous and comprise of a variety of neoplastic, host stromal and immune cells (Gajewski et al, 2013). The functional dependency of tumour progression on the host microecology is underlined by the promising outcomes of therapies against inflammatory cells, immune cells and components of the extracellular matrix.

1.2 Cancer metastasis

1.2.1 Introduction

Cancer metastasis, the dissemination of malignant cells from the primary site to distant organs, rather than primary tumours *per se* is the leading cause of morbidity and mortality amongst cancer patients. In the case of human breast cancer, metastasis-free interval is a strong favourable prognostic factor (Lobbezoo et al, 2015). Moreover, for a wide range of primary solid cancers such as lung, colorectal, cervical and melanoma, the survival rate for patients with metastatic disease remains very dismal compared to the respective rate for localised and regional disease (reviewed by Steeg, 2016).

Metastatic spread has been described as a naturally inefficient procedure (Luzzi et al, 1998). Experimentally, only an extremely small percentage of tumour cells injected into the circulation will successfully colonise secondary sites and give rise to metastases (Fidler, 1970). This inefficiency is attributed to the multiple challenges cancer cells need to overcome once detached from the primary tumour. Hemodynamic mechanical forces, recognition and destruction by the immune system, as well as the encounter with new cellular and molecular entities in the microenvironment of the secondary site, are all rate limiting factors for a successful metastatic colonisation (Luzzi et al, 1998). Clinical data from breast cancer patients also support the notion that metastasis is an inefficient process throughout its progression, since only a small percentage of breast cancer patients with bone marrow micrometastases at the time of diagnosis eventually developed clinically detectable distant macrometastases. Moreover, cancer patients who underwent surgical resection of their primary tumours presented with recurrent metastatic disease many years after the initial diagnosis (Tjensvoll et al, 2012).

Nevertheless, complex and enduring biological events, comprising of both genetic and epigenetic changes, can promote cancer metastasis. This process involves acquisition of traits that increase the metastatic potential of cancer cells, as well as adaptation of the stromal environment at the metastatic site to those traits. In this sense, metastasis resembles a Darwinian evolutionary process (Valastyan and Weinberg, 2011). Eventually, when overt metastases manifest in cancer patients, they usually represent the terminal stage of the disease. It is, thus, a great necessity to better characterise the metastatic process to distant organs with the aim of identifying targets for prevention and treatment.

1.2.2 Steps of the metastatic cascade

In an oversimplified view, metastasis comprises of three basic steps: tumour progression to invasive carcinoma, spread via haematogenous or lymphatic routes and infiltration and outgrowth at the distant site (Figure 1.1) (Nguyen et al, 2009). However, metastasis is a series of numerous sequential steps that also involve a plethora of host cells. Combination of histological techniques, elaborate mouse models and advanced preclinical imaging has provided important information about the complex steps characterising the metastatic cascade (Weiss et al, 1984; Khanna and Hunter, 2005; Beerling et al, 2011).

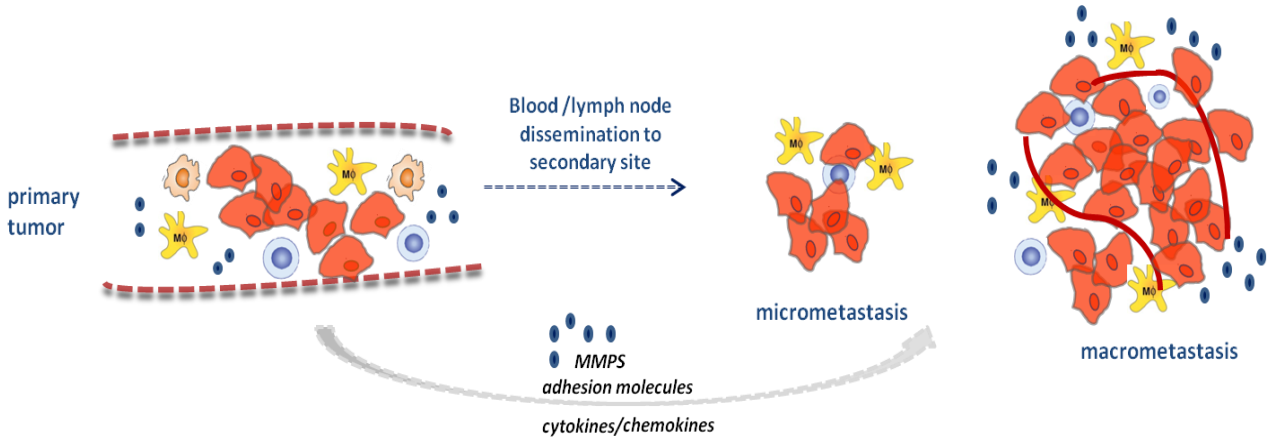


Figure 1.1: Steps of metastasis. Simplified schematic of the metastatic cascade. The primary tumours (light orange cells) progress to invasive carcinomas [orange cells in close association with breached stroma (red dotted lines)] and spread via blood or lymph node dissemination to the secondary site. There, cancer cells form metastatic foci which progress to well vascularised (red lines) macrometastases. Inflammatory cells [macrophages (yellow cells), leukocytes (blue cells)] and molecules (MMPS, cytokines) are present during the steps of the metastatic cascade.

1.2.2.1 Invasive carcinoma

The initiation of the metastatic cascade occurs at the site of the primary tumour and involves acquisition of an aggressive phenotype and local invasion. Accumulating genetic mutations and selective pressure can drive gene expression alterations in cancer cells. Commonly activated pathways at this stage bear the hypoxic signature known to promote cell proliferation, angiogenesis and invasion (Harris, 2002). Hypoxia inducible factor (HIF) is overexpressed in a variety of human solid tumours, including breast and lung, and their metastases (Zhong et al, 1999). Similarly, HER2, a member of the epidermal growth factor receptor (EGFR) family of receptors regulating cell survival and motility, is often overexpressed in breast cancer, and was recently implicated in the transition from *in situ* to invasive carcinoma (Roses et al, 2009). Other signalling pathways aberrantly activated in

cancer and implicated in the invasive phenotype of primary tumours are Wnt and KRAS driven, well characterised in the case of colorectal cancer (reviewed by Nguyen et al, 2009).

Once primary tumours become sufficiently mutagenic, cancer cells find their way out of the primary site and towards the bloodstream via the basement membrane and tumour associated stroma. An essential characteristic of this process is altered cellular adhesion properties that promote cell motility and epithelial-mesenchymal transition (EMT) (reviewed by Gupta and Massagué, 2006). Focal adhesion kinase (FAK) and downstream Rho-GTPase dependent signalling regulate cancer cells' motility and are implicated in cancer metastasis potentiation (Provenzano and Keely, 2009). Epithelial cadherin (E-cadherin), a key molecule of adhesion at the epithelial state, mediates the formation of cellular tight junctions, which are evidently lost at the invasive front of solid primary tumours. This is a small part of the complex EMT program resulting in increased cancer cell stemness and invasion (Thiery et al, 2009). Another class of adhesion related molecules, integrins, play paramount roles in induction of oncogenic signalling and extracellular matrix remodelling. For instance, integrins $\alpha_v\beta_6$ and $\alpha_v\beta_8$ induce the activation of transforming growth factor β (TGF-β), which subsequently promotes EMT and cancer cell invasion. $\alpha_v\beta_6$ also induces cell migration through the interstitial matrix due to its affinity to the glycoprotein fibronectin. Another mechanism implicated in enhanced migration through matrix degradation is the recruitment and activation of matrix metalloproteinase 2 (MMP2) by $\alpha_v\beta_3$. Notably, integrins are upregulated in human cancer (reviewed by Guo and Giancotti, 2004). Together, these processes allow local tumour invasion and initiation of the metastatic spread.

1.2.2.2 Intravasation and haematogenous spread

The next step for the colonisation of distant organs involves intravasation of invading cancer cells through the vasculature. In order to achieve that, cancer cells have to transmigrate through the vascular endothelial layer, a process often referred to as transendothelial migration (TEM). TEM can occur at the neovasculature, the angiogenic vessels locally induced by the primary tumour, or at pre-existing vessels where cancer cells pass through breached endothelial cell junctions. Cancer cell derived matrix metalloproteinase 1 (MMP1) and TGF-β can induce remodelling and retraction of endothelial cells thus facilitating their transmigration. Cleavage of vascular endothelial cadherin (VE cadherin) junctions on endothelial cells also promotes disruption of endothelial tight junctions and cancer cell passage through the endothelial layer. Alternatively, cancer cells may transmigrate the endothelium transcellularly (through the endothelial cell body) during a process that involves calcium triggered cytoskeletal and membrane remodelling of endothelial cells (reviewed by Reymond et al, 2013).

After successful intravasation into the bloodstream, cancer cells have to overcome several obstacles to reach secondary organs. Shear mechanical forces imposed by blood flow and surveillance by immune cells comprise a hostile environment. Nevertheless, invading cancer cells co-opt with circulating blood platelets, an interaction shown to actively promote cancer cell protection, survival and dissemination to distant organs (Jain et al, 2010). Activated platelets release numerous growth factors, chemokines and proteases that facilitate the metastatic process. Expression of p38 MAPK by platelets is important for tumour cell metastasis via upregulation of the adhesion molecules P- and E-selectin (Matsuo et al, 2006). Experimental models of lung metastasis have shed light on the role of P-selectin in

promoting the formation of platelet and cancer cell aggregates. Platelet derived lysophosphatidic acid (LPA) may also contribute to metastatic cell growth by inducing cytokine signalling, at least in the case of breast cancer bone metastasis. Fibrinogen, also implicated in increased metastatic potential, facilitates escape from immune surveillance and arrest of tumour cell emboli surrounded by platelets on the vasculature while tumour cells are in the circulation. Finally, integrin aIIbβ3, highly expressed on platelets and known to promote platelet aggregation, facilitates tumour cell emboli to firmly adhere to the vasculature and, thus, migrate into distant organs (Gupta and Massagué, 2004; Gay et al, 2011).

1.2.2.3 Extravasation and metastatic growth

Towards the end of their journey, metastatic cells enter the new microenvironment at the secondary site via the endothelial layer. Extravasation involves cancer cell adherence to the microvasculature of the distant organ and permeabilisation of its vascular barriers. Essentially, the process resembles TEM during intravasation. A report by Gupta and colleagues highlights the synergistic effect of MMP1, MMP2, cyclooxygenase 2 (COX2) and the EGFR ligand EREG on vascular remodelling as essential for breast cancer lung metastasis (Gupta et al, 2007). Those genes, which are clinically significant for metastasis to the lung, were involved in both the intravasation and extravasation of cancers cells to the bloodstream and to the pulmonary microvasculature, respectively. Vascular permeability of lung endothelial walls is also Src kinase dependent and induced by circulating malignant cells expressing VEGF (Criscuoli et al, 2005). Similarly, tumour cell derived angiopoietin like 4 (ANGPTL4) disrupts endothelial cell junctions and fosters pulmonary transendothelial

migration of breast cancer cells specifically (Padua et al, 2008). The notion that environmental signals originating from the primary tumour sites facilitate circulating cancer cells' extravasation to a secondary organ exists, and might partially justify the ability of metastatic cancer cells to passage through structurally solid, impermeable vessels.

Having survived this long and winding road, metastatic cancer cells face the final hurdle of successful outgrowth and formation of macrometastases at the secondary site. Although the microenvironment at the metastatic site usually differs significantly in terms of cellular and molecular composition from the primary tumour, cancer cells ease their homing there via the pre-metastatic niche. Fibronectin and stromal cell derived factor 1a (SDF-1a or CXCL12) have been described as important molecules of the pulmonary pre-metastatic niche. Another study identified increased expression of the cytokines S100A8 and S100A9 in the pre-metastatic lung, findings that provide additional mechanistic insight on the chemoattraction of migrating cancer cells towards the secondary site. Interestingly, the same molecules along with the chemokine CCL2 are highly expressed in the pre-metastatic brain of a murine model of mammary carcinoma (Liu et al, 2013). Upregulation of MMPs and lysyl oxidase (LOX), an enzyme involved in basement membrane cross-linking and remodelling, has been reported in the pre-metastatic lung, liver and brain, and their inhibition diminishes breast cancer cell invasion to the metastatic locus (Erler et al, 2009; reviewed by Psaila and Lyden, 2009).

Successful tumour cell seeding follows the establishment of a metastatic niche, which initially gives rise to micrometastases and eventually clinically detectable macrometastases. Molecular signatures that specifically support metastatic outgrowth in the lung, brain or bone have been described and consist of functionally different genes within and amongst

target organs (Minn et al, 2005; Kang et al, 2003; Bos et al, 2009). Although those signatures partially overlap, the differences mirror the heterogeneity of metastatic growth in different organs and underscore the necessity of studying organ specific metastasis into detail.

1.3 Tumour associated macrophages (TAMs)

As tumours constantly change and evolve over the course of the disease, so does the tumour associated microenvironment. Stromal and infiltrating immune cells are active participants of the metastatic process during every step. A plethora of evidence suggests that the tumour microenvironment plays a supportive role for the establishment of the primary niche and of macrometastases at the secondary site. Main components of the microenvironment are cells of the innate and adaptive immune system such as tumour associated macrophages (TAMs), neutrophils, immune suppressor cells, T cells and natural killers, as well as stromal fibroblasts and endothelial cells. Those populations are intensively studied for their contribution to the progression of different types of metastatic cancer and comprise an attractive target for therapeutic intervention. Of particular interest in the context of this thesis is the role of macrophages, both resident and circulating, in metastasis progression.

1.3.1 TAMs during tumour progression

The presence of macrophages and an exacerbated inflammatory milieu in cancer biopsies was considered to be proof of an immune response against the disease and, thus, consequently overlooked. However, it is now well established that tumour cells at the primary site hijack the microenvironment to circumvent their immune destruction and

establish their growth. TAMs comprise a large proportion of the tumour mass and data from clinical studies suggest that TAM density and TAM trophic factors (growth factors, chemokines) are associated with poor prognosis (Pollard, 2004). Experimental mouse models of cancer have confirmed the direct involvement of macrophages in tumour progression and metastasis (Figure 1.2). In the cases of breast cancer and glioma, TAMs promote tumour metastasis via a paracrine loop with tumour cells, which involves colony stimulating factor 1 (CSF-1) and EGFR signalling (reviewed by Quail and Joyce, 2013). Strikingly, a null mutation of CSF-1 led to decreased TAM infiltration of murine mammary carcinomas and almost completely abrogated their metastatic potential without significantly affecting their growth (Lin et al, 2001). Macrophages can also mitigate cancer progression in a CSF-1 dependent way mediated by the host cells as implicated by CSF-1 blockade studies of mice xenografted with human cancer cells negative for CSF-1 (Aharinejad et al, 2002).

Tumour derived chemokines, most prominently CCL2/MCP-1 (monocyte chemoattractant protein 1) are expressed in primary breast, lung, melanoma and brain tumours, and promote macrophage infiltration (Sica et al, 2006). TAMs can establish invasive cancer by modulating proliferation, angiogenesis, invasion and dissemination. As a major source of the growth factors TGF-β, fibroblast growth factor (FGF), epidermal growth factor (EGF) and VEGF, and TNF-α, TAMs induce tumour cell proliferation and chemotactic motility. TAMs also release proteases, such as MMP9 and cathepsins, in the tumour microenvironment, which promote stromal matrix remodelling and thus facilitate cancer cell invasion (Pollard et al, 2004). Wyckoff and colleagues used multiphoton microscopy to show that perivascular macrophages attract breast cancer cells towards vessels they are associated with and then promote their intravasation into the circulation (Wyckoff et al, 2007). In the case of breast cancer, tumour macrophages and bone marrow derived myeloid cells are implicated in

mesenchymal transition and invasion of the primary tumour and epithelial establishment at the secondary site via TGF-β signalling (as reviewed by Quail and Joyce, 2013). Interestingly, clusters of bone marrow derived cells form the pre-metastatic niche in the lung and the brain (Kaplan et al, 2005; Liu et al, 2013). Bone marrow myeloid progenitor cells positive for the receptor VEGFR1 create a permissive environment for lung colonisation by migrating tumour cells via a very late antigen 4 (VLA4)-fibronectin mechanism involving resident fibroblasts (Kaplan et al, 2005). TAMs expressing VLA4, also known as integrin α4β1, are essential for vascular cell adhesion molecule 1 (VCAM-1) positive breast cancer cell proliferation and invasion at the metastatic locus (Chen et al, 2011).

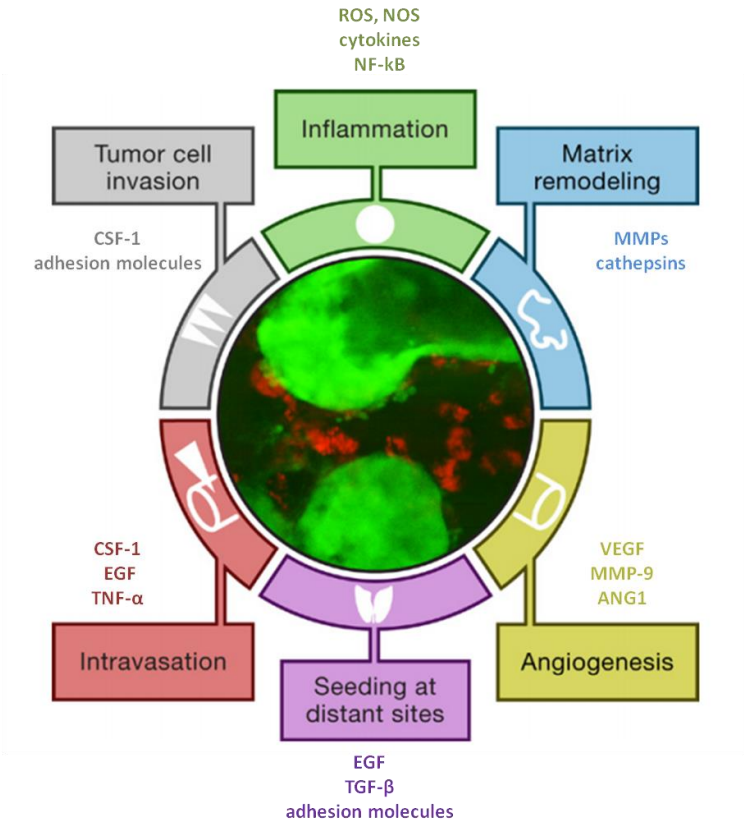


Figure 1.2: Traits of malignancy promoted by TAMs. Diagram showing 6 characteristic aspects of cancer progression promoted by TAMs, as described by Condeelis and Pollard. Molecules associated with each process are colour-coded and indicated next to each box. In the middle, a fluorescent multiphoton image of murine mammary cancer cells (green) associated with macrophages (red) in a living mouse. (Adapted by Condeelis and Pollard, 2006)

1.3.2 TAM polarisation

Macrophages are versatile cells of innate immunity that have the ability to express distinct functional programs depending on stimuli from the microenvironment they reside in. Activated macrophage classification resembles the well-established Th1/Th2 dichotomy applied for T helper cell immune response. Experimentally, macrophages polarise to the classical M1 phenotype upon stimulation with Toll-like receptor (TLR) agonists such as bacterial lipopolysaccharide (LPS) or the pro-inflammatory cytokine interferon gamma (IFNγ). M1 cells secrete pro-inflammatory cytokines such as tumour necrosis factor-α (TNFα) and interleukins IL-1β and IL6, inducible nitric oxide synthase (iNOS) and reactive species thus potentiating host defence against infectious intruders and eliciting a T cell immune response against neoplastic cells. The alternatively polarised M2 phenotype is induced by the interleukins IL-4 and IL-13, and is associated with high levels of anti-inflammatory molecules such as interleukin IL-10 and growth factor TGF-β as well as Th1 immune suppression. M2 polarisation promotes angiogenesis and tissue repair and ultimately accounts for the resolution of inflammation. M2 cell heterogeneity has emerged and M2 macrophages can be further subcategorised to M2a, M2b, M2c, with all of them still being involved in Th2 responses, immune regulation and tissue remodelling (as reviewed by Sica et al, 2006; Saijo et al, 2011; Martinez and Gordon, 2014).

In inflammation related pathology, there is a well accepted mode of action of macrophages: an initial pro-inflammatory M1 phase succeeded by an anti-inflammatory, resolving M2 phase. This temporal pattern almost perfectly reflects the macrophage associated response to infections. However, extensive research on TAM biology indicates that macrophage function is altered during tumorigenesis and solid cancer progression. Environmental signals

promote a functional switch towards the M2 phenotype, which in the context of neoplasia promotes evasion of immune destruction and tumour progression. Indeed, data from clinical studies and preclinical models support the notion that TAMs are skewed to a pro-angiogenic tumour supportive phenotype which resembles the M2 macrophage phenotype (Sica et al, 2006). TAMs preferentially upregulate the expression of non-opsonic receptors such as the mannose receptor (MRC or CD206) and scavenger receptors (CD163) unlike M1 cells, which are characterised by high expression of major histocompatibility complex (MHC) II and CD86 molecules. Macrophages infiltrating human tumours present with low levels of iNOS and COX2, while express high levels of IL-10 and arginase 1 (Arg1) (Figure 1.3) (Sica et al, 2006; Williams et al, 2016).

Arginine metabolism is an important determinant of macrophage polarisation. The functional diversity of M1 and M2 macrophages is often reflected by iNOS and Arg1 expression, respectively. Macrophages can convert L-arginine to nitric oxide (NO) and citrulline via iNOS, or alternatively to ornithine and urea via Arg1. The former pathway of arginine metabolism is connected to reduced cell viability and cytotoxicity, whilst the latter to cellular proliferation and tissue repair due to proline and polyamine production (Rath et al, 2014). Depletion of extracellular arginine by M2 polarised TAMs accounts for inhibition of T cell function and subsequent immunosuppression. Of note, the same mechanism has been also reported for M1 macrophages, although their roles in cancer are opposing (Rath et al, 2014; Williams et al, 2016). However, conversion of arginine to NO by M1 cells is linked to a “rescue” pathway of arginine replenishment (Rath et al, 2014). Thus, tight regulation of arginine bioavailability and metabolism by iNOS or Arg1 is fundamental for a balanced inflammatory response.

Although M1 and M2 cells are nice concepts to study macrophage plasticity *in vitro*, TAMs in human and rodent tumours are never fully M1 or M2 polarised. Instead, a spectrum of heterogeneous cells bearing characteristics of both M1 and M2 macrophages populate the tumour microenvironment (Figure 1.3) (Laoui et al, 2011; Noy and Pollard, 2014). Deeper knowledge of the spatiotemporal profile of TAMs infiltrating different types and stages of cancer warrants further investigation with the perspective to better understand and therapeutically exploit TAM biology.

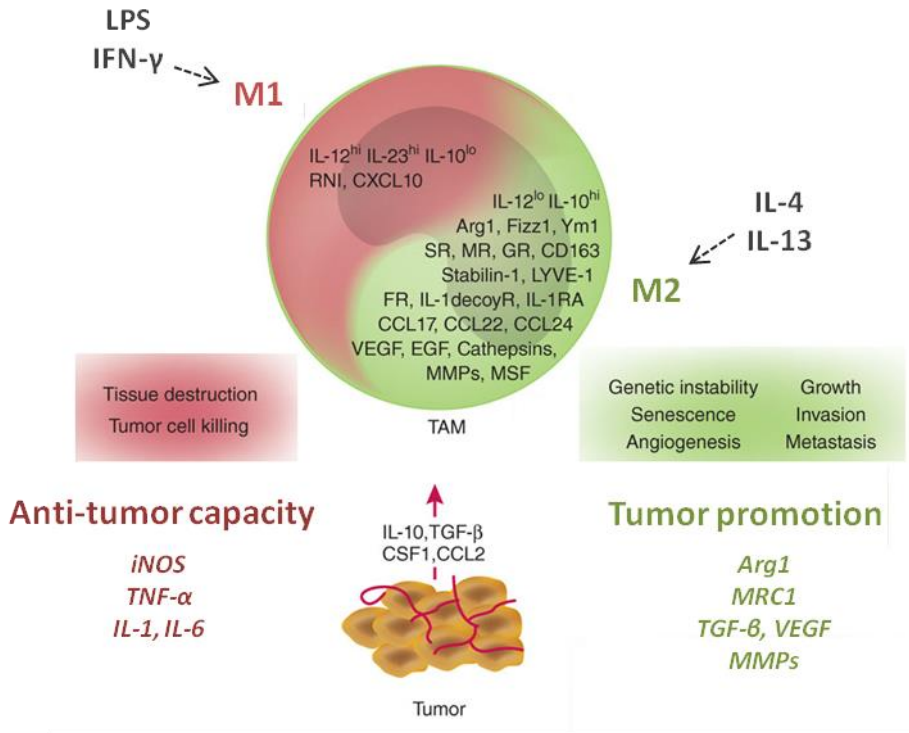


Figure 1.3: Macrophage polarisation in the tumour microenvironment. TAMs can polarise towards a classical (M1) or alternative (M2) phenotype under the influence of tumours. M1 cells, induced by stimuli like LPS and IFN-γ, are pro-inflammatory and cytotoxic to tumours by production of iNOS and TNF-α while M2 cells, induced by IL-4 and IL-13, promote tumour progression via their anti-inflammatory, pro-angiogenic properties. Molecules associated with each phenotype are indicated (adapted from Biswas and Mantovani, 2010).

1.3.3 TAMs as therapeutic targets

Following the unravelling of the tumour promoting properties of TAMs, efforts to target their recruitment and proliferation or to re-educate them towards tumour rejection have been the focus of numerous experimental approaches. Inhibition of the CSF-1/CSF-1R signalling axis has yielded promising results in pre-clinical models of invasive breast cancer, neuroblastoma and glioblastoma. Similarly, blocking of the CCL2 pathway reduces tumour growth and metastasis in rodent models of breast, lung and pancreatic cancer (Lin et al, 2001; Abraham et al, 2010; Qian et al, 2011; Pyonteck et al, 2012; Sanford et al, 2013; Williams et al, 2016). Small-molecule Inhibitors of those two important signalling axes (CSF-1/CSF-1R and CCL2/CCR2) are undergoing clinical trials for breast and other types of solid cancers (Panni et al, 2013; Noy and Pollard, 2014; Williams et al, 2016). Imiquimod, a TLR7 agonist shown to re-educate TAMs to adopt a tumoricidal phenotype in metastatic breast cancer models, is also under clinical trials. An antibody against IL-6R and an antisense oligonucleotide inhibitor of STAT3 as strategies for targeting macrophages are also under clinical trials in patients with solid tumours (Panni et al, 2013). Given the emerging functional and phenotypic heterogeneity of TAMs, novel approaches to target trophic subsets of TAMs in a cancer specific context should be considered in order to improve existing regimes of chemotherapy and radiotherapy (Noy and Pollard, 2014).

1.4 Brain metastasis

Haematogenous dissemination of cancer cells from the primary tumour to the brain is one feared complication in cancer patients, often manifested by severe seizures and cognitive dysfunction. Secondary brain tumours are the most common intracranial neoplasms, far

outnumbering primary brain tumours. It is estimated that 20-40% of cancer patients will develop brain metastases (Gavrilovic and Posner, 2005). The brain has been long considered as a "sanctuary" for cancer development due to the blood-brain barrier (BBB), which limits access to chemotherapeutic drugs (Pardridge, 2005). The increased incidence of brain metastasis partly reflects better control of systemic disease, but also improved diagnosis due to the development of more sensitive imaging techniques for early detection of metastatic tumours in the brain (Eichler and Loeffler, 2007). Nevertheless, the stage of diagnosis is still relatively late and prognosis remains poor for newly diagnosed patients even after whole brain radiotherapy (Pease et al, 2005). The high percentages of morbidity due to brain metastasis, in combination with the lack of pre-clinical models of CNS metastases compared to pulmonary and bone metastases, urge the need for delineation of the molecular and cellular mechanisms promoting metastasis to the brain with the aim of improved therapeutic intervention.

1.4.1 Treatment of brain metastases

Prognosis of patients diagnosed with CNS metastases is dismal because their treatment is a major challenge in clinical oncology. Current options include chemotherapy, whole brain radiation therapy (WBRT), surgical removal of tumours or combination of those (Eichler and Loeffler, 2007). Retrospective studies indicate that gefitinib, an inhibitor specific for EGFR, showed activity against brain metastases from NSCLC in almost one third of patients while other studies suggest that the CNS is the first site for disease recurrence after treatment of the primary non small cell lung cancer (NSCLC) with gefitinib (Ceresoli et al, 2004; Omuro et al, 2005). In the case of breast cancer brain metastases treated with trastuzumab, patients

positive for human epidermal growth factor receptor 2 (HER2) showed prolonged survival relatively to patients negative for the receptor. Trastuzumab is the gold standard for treating aggressive HER2 overexpressing breast cancer and the survival advantage observed in the case of $HER2^+$ breast cancer patients who developed brain metastases might be related to improved control of the systemic disease, especially since the degree of BBB penetration by trastuzumab is not yet very well established (Eicher et al, 2008; Pieńkowski and Zielinski, 2010). In the same context, combination of trastuzumab and lapatinib, an inhibitor targeting both EGFR and HER2, conferred survival benefit for breast cancer patients with brain metastases compared to each individual treatment alone (Hayashi et al, 2015). Moreover, clinical trials of systemic cytokine therapy for melanoma patients with resected brain metastases indicated a survival advantage for the therapy responders compared to non-responders (Lonser et al, 2011).

The interpretation of the afore-mentioned trials might suggest that the clinical benefit of the chemotherapy regimens used stems from control of the systemic disease rather than activity against brain metastases. This is a plausible scenario considering the chemoresistance of metastatic cancers (Acharya et al, 2012; Villanueva, 2012) and the drug delivery limitations imposed by the blood-brain and tumour-brain barrier (Pardridge, 2005). Thus, chemotherapy is often applied as an adjuvant therapeutic modality for patients with secondary brain cancer. Newly diagnosed patients typically undergo WBRT, which improves survival rate to 6 months (Pease et al, 2005). In the case of solitary brain metastases, combination of surgical removal of the lesion and WBRT has been reported to improve survival compared to WBRT alone (reviewed by Patchell, 2003; Eichler and Loeffler, 2007). However, adjuvant WBRT does not improve survival of patients with multiple brain metastases removed by surgery or radiosurgery, although it reduces the incidence of

intracranial relapse during the course of treatment (reviewed by Khan, 2013; Eichler and Loeffler, 2007). The standard treatment option for patients with brain metastases is currently WBRT, and multidisciplinary approaches to better manage the disease remain an unmet need.

1.4.2 Mechanistic insights

The brain represents a specialised environment due to its unique anatomical and cellular entities (Figure 1.4). Thus, cancer biology in the brain should be studied in the context of those intrinsic features. The BBB, structured by endothelial cells lining brain microvessels and astrocytic endfeet, and specialised glial cells, namely astrocytes and microglia, comprise the new microenvironment invading cancer cells should co-exist with. The seed and soil dogma predicts that only specific primary cancers have the propensity to colonise the brain (primarily carcinomas of breast, lung and melanomas) (Fidler et al, 2002) being actively supported by components of its vascular and stromal network (Carbonell et al, 2009; Hamilton and Sibson, 2013). Moreover, the brain microenvironment can contribute to tumour modulation via the effector functions of resident macrophage-like cells (microglia), astrocytes and inflammatory molecules (Lorger and Felding-Habermann, 2010).

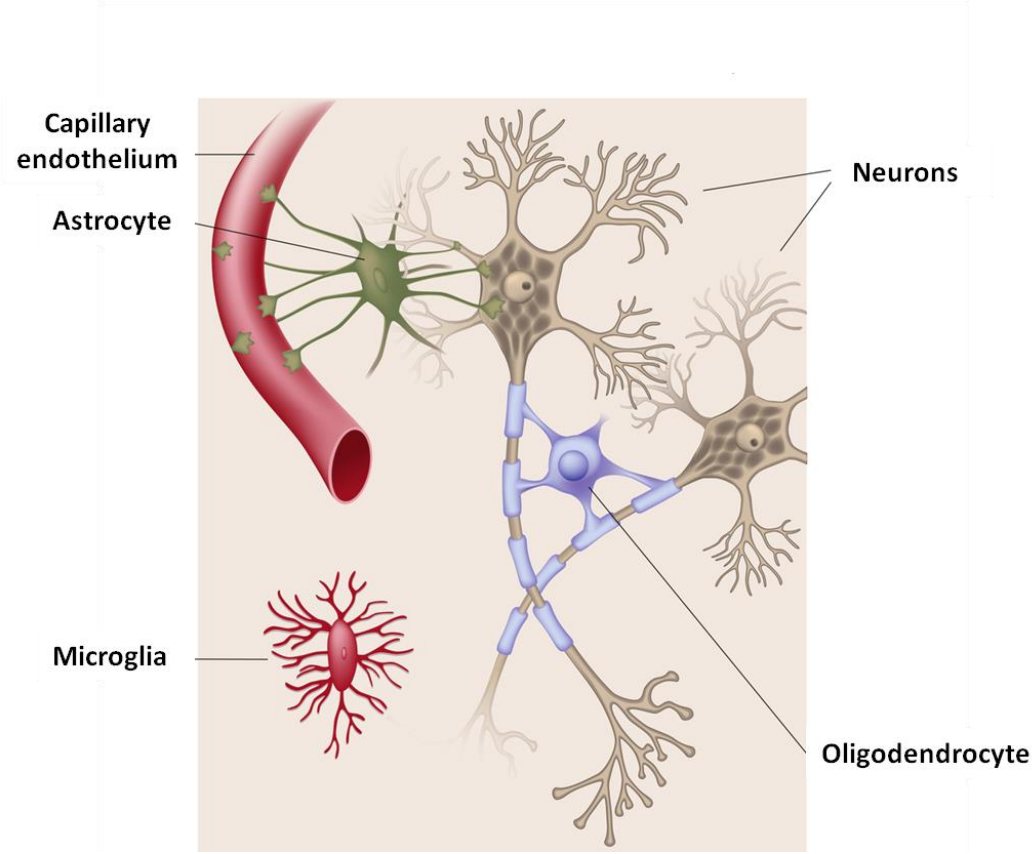


Figure 1.4: Cellular composition of the brain. Image depicting the main cellular components of the brain, neurons and neuroglia. Neuroglia comprise of microglia, the brain resident macrophages, and astrocytes and oligodendrocytes, which provide structural and functional support to neuronal functions. Astrocytes also interact with brain endothelial cells to form the protective BBB (Adapted from www.medicalsciencenavigator.com).

1.4.2.1 Molecular characterisation of brain seeking cancer cells

The molecular basis of the propensity of specific types of cancer to invade specific organs, such as the brain, is not yet fully understood. Elegant studies conducted by the Massagué team provide novel insights into the mechanisms governing breast cancer brain metastasis (Minn et al, 2005; Bos et al, 2009). The approach of using breast cancer cells that preferentially colonise the brain or lung to experimentally induce cerebral or pulmonary metastases, respectively, yielded information about the genetic signatures that promote metastasis to either organ. Both models shared COX2 and EGFR ligands as functional

mediators of breast cancer dissemination. Moreover ST6GALNAC5, a sialyltransferase highly expressed in the CNS, was identified as specific promoter of metastasis to the brain, but not to the lung, bone or lymph nodes. Importantly, the authors confirmed the clinical relevance of their findings thus further validating that a brain specific molecule is required for BBB extravasation of cancer cells. A similar approach provided evidence of significantly higher amounts of secreted VEGF and IL-8, both known for their pro-angiogenic properties, from brain colonising sub-clones of human breast cancer cells (Kim et al, 2004). The stem cell phenotype of cancer cells may also be associated with metastatic growth in brain. Studies have shown that reduced stemness of breast cancer cells, measured by expression of the mesenchymal marker CD44, accounted for less experimental brain metastases (McGowan et al, 2011). A proposed mechanism involves the expression of specific microRNAs by cancer stem like cells which modulate their invasive potential to the brain, but not to other organs (Okuda et al, 2013). Finally, patient derived breast cancer cells that preferentially colonise the brain after *in vivo* selection present with altered metabolic profiles as revealed by large scale proteomic analysis. Those cells appear to thrive in the brain due to adaptation to aerobic glycolysis and enhanced resistance to oxidative stress (Chen et al, 2007).

1.4.2.2 Role of brain endothelial cells

The BBB creates a form of natural separation between the periphery and the brain microenvironment, although not yet fully defined (reviewed by Hamilton and Sibson, 2013). Experimental models of brain metastasis induced by injection of tumour cells into the internal carotid artery revealed that the BBB is intact in the presence of micrometastases (tumours smaller than 0.25mm in diameter), but become leaky when they outgrow (Fidler et

al, 2002). The exact mechanisms of tumour cell extravasation to the brain are yet poorly defined. Although they might resemble leukocyte rolling and adhesion to the brain endothelium, different molecular signatures might account for tumour and immune cell entry into the brain (Strell and Entschladen, 2008).

The role of the brain endothelium as an active participant in the homing of metastatic cells has gained much interest. Brain metastatic cancer cells might breach the BBB by releasing extracellular vesicles containing microRNAs that disrupt actin dynamics in brain endothelial cells (Tominaga et al, 2015). It has been reported that human cancer cell subclones with high affinity for the brain overexpress the integrin $\alpha_3\beta_1$, a finding that might imply their extravasation via binding to endothelial laminin (Yoshimasu et al, 2004). Ongoing research in our laboratory has shed light on the functional interplay between the brain endothelium and invading cancer cells. Cellular adhesion molecules such as VCAM, intercellular adhesion molecule (ICAM) and activated leukocyte cell adhesion molecule (ALCAM) were highly expressed on the cerebral endothelium at early stages of metastatic seeding in the murine brain (Serres et al, 2012; Soto et al, 2014). Silencing the expression of or functionally blocking VLA-4, lymphocyte function associated antigen 1 (LFA-1), ALCAM (the ligands of VCAM, ICAM, ALCAM respectively) on breast tumour cells significantly reduced intracranial tumour burden (Soto et al, 2014; Soto et al, 2016). Similarly another adhesion molecule, namely L1CAM, has been identified as essential mediator of vascular co-option and metastatic outgrowth in the brain (Valiente et al, 2014). It is interesting to note that this particular CAM is commonly expressed in the brain, the implication being that features of the host organ foster cancer progression. Brain endothelium may also be involved in metastatic outgrowth by cell signalling via the chemotactic couple CXCR4/CXCL12. A functional interaction between CXCL12 expressing brain endothelial cells and $CXCR4^+$

glioblastoma cells has been reported as potential mechanism of intracranial tumour progression (Rao et al, 2012). Moreover, brain endothelial derived CXCL12 mediates immune cell mobility, adhesion and BBB transmigration (Liu et al, 2009). This finding corroborates the CXCR4/CXCL12 pathway in the entry of circulating cells entry into the brain. Importantly, this axis is a promising therapeutic target in breast and lung cancer brain metastasis (reviewed by Hinton et al, 2010; Cavallaro, 2013). Although blood vessel density in experimental and human brain metastases is lower than that of the normal brain parenchyma, cancer cells in close vicinity to endothelial cells are highly proliferative, the notion being that endothelial cells also support metastatic growth (Fidler et al, 2002).

1.4.2.3 Role of astrocytes

Another cellular entity of the BBB, which disseminating cancer cells encounter during extravasation into the brain parenchyma, is astrocytes. Astrocyte infiltration of brain metastases has been observed in human biopsies (He et al, 2006) and positively correlates with tumour burden in the murine metastatic brain (O'Brien et al, 2014). Research on their role in brain metastasis suggests that astrocytes are educated by environmental signals to sustain cancer cell survival and growth in the brain. It has been shown that IL-1β secreted by invading malignant cells activates astrocytes, which in turn stimulate Notch-1 dependent self-renewal of cancer cells and establish metastases in the brain (Xing et al, 2013). Additional features of the functional cross-talk between cancer cells and astrocytes were recently demonstrated by Zhang and colleagues. The team reported that astrocyte-derived exosomes induce PTEN loss in metastatic tumour cells. PTEN is a very well established tumour suppressor gene (Song et al, 2012) and its loss in the brain metastatic cells sustains

tumour outgrowth. Additionally, researchers identified increased microglial and myeloid infiltration, which further supports the establishment of metastatic lesions in the brain (Zhang et al, 2015). Invading breast and lung cancer cells create gap junctions with astrocytes which in turn activate IFN-α and TNF mediated immune signalling to promote cancer cell survival in the brain (Chen et al, 2016). Astrocyte-derived MMP9 may provide an additional mechanism of cancer cell survival and outgrowth in the early stages of experimental brain metastasis (Lorger and Felding-Habermann, 2010). *In vitro* co-cultures of primary astrocytes with cancer cells led to astrocyte activation and secretion of pro-inflammatoy cytokines IL-1β, IL-6 and TNF, which might be implicated in cancer cell survival and proliferation (Seike et al, 2011).

1.4.2.4 Role of microglia and macrophages

The macrophage populations of the CNS include microglia, perivascular macrophages and meningeal macrophages. Microglia are the most abundant resident cells populating the brain parenchyma, spinal cord and retina. Clustering of microglial cells around metastatic tumours has been described for both experimental and human brain metastases (Berghoff et al, 2013; Lorger and Felding-Habermann, 2010; O'Brien et al, 2014). In contrast, low numbers of scattered B- and T- lymphocytes were associated with human brain metastases (Berghoff et al, 2013). Moreover, minimal neutrophil infiltration of brain metastases in the mouse 4T1 mammary carcinoma model was reported by Granot and colleagues (Granot et al, 2011). Thus, the CNS resident macrophages appear to be important components of the immune response to metastatic growth in the brain.

Microglia are activated in response to brain tumours. Immunohistochemically, it is challenging to distinguish between brain resident microglia and circulating macrophages invading the brain due to their phenotypic similarities. Both populations express markers indicative of their myeloid origin, such as CD11b, F4/80 and CD45. However, the use of flow cytometry and classification of microglia and macrophages as $CD11b^{+}CD45^{low}$ and $CD11b^{+}CD45^{high}$ cells, respectively, or transgenic mouse models has allowed for the identification of blood derived myeloid cells in the brain. Rippaus and colleagues report both macrophage and microglial infiltration of experimental 4T1 parenchymal and dural metastases using flow cytometry (Rippaus et al, 2016). Another independent group has used bone marrow chimerism with GFP transgenic mice as donors to investigate circulating myeloid cell migration to the pre-metastatic brain (Liu et al, 2013). Those experiments showed bone marrow derived cell infiltration of 4T1 brain metastases, implicated this cell population in the formation of the brain pre-metastatic niche and, thus, assigned a pro-tumorigenic role for blood borne macrophages in the context of brain metastasis.

Despite great advances in understanding the contribution of brain resident cells in the pathology of brain metastases, the involvement of microglia in the progression of the disease remains poorly understood. The extent of microglial infiltration in human and rodent brain metastases is heterogeneous, ranging from no microglial activation to robust and spatially well-defined activation around metastatic foci. Moreover, different types of primary tumours present with different microglial responses in the metastatic brain (Berghoff et al, 2013; Lorger and Felding-Habermann, 2010; Fitzgerald et al, 2008). Both ramified and amoeboid microglial cells are reported in association with experimental metastatic tumours in the brain, an observation that might be indicative of different activation states and phagocytic properties of those cells (Lorger and Felding-Habermann, 2010; Fitzgerald et al,

2008). *In vitro*, murine microglia primed by LPS/IFN-γ treatment were tumouricidal against murine melanoma cells in a NO dependent manner, but did not affect the viability of other brain cells (endothelial cells, astrocytes). This experiment provided proof that appropriately educated microglia, in this case M1 skewed cells, may be of therapeutic benefit (Brantley et al, 2010). However, minimal expression of iNOS and other molecules involved in oxidative stress by microglial cells was reported for a small cohort of human brain metastasis samples, which is indicative of the lack of cytotoxic properties of those cells (Berghoff et al, 2013). Moreover, Pukrop and colleagues used living mouse brain slices to show that microglial cells promote invasion and metastasis of human breast cancer cells possibly via Wnt paracrine signalling (Pukrop et al, 2010). Further investigation of the role of brain resident microglia in response to metastasis is warranted to provide a more detailed and defined characterisation of the microglia elicited immune response associated with metastatic progression in the brain.

1.5 Microglia

1.5.1 Microglial cell origin

Microglia are haematopoietic cells that originate from the yolk sac and migrate into the CNS early during development. Although the myeloid nature of microglia is nowadays very well established, their origin has been an issue of extensive research and debate for many decades. Initial views supported the notion of neuroectodermal origin of microglia, as for all glial cells. However, del Rio Hortega was the first to propose a functional distinction between microglia and neuroglia, being convinced of the mesodermal origin of the former. Hortega's belief that microglia are non-neuronal, non-astocytic, non-oligodendrocytic phagocytes was

certified by morphological and functional similarities of microglial cells with macrophages (reviewed by Ginhoux et al, 2013). Experiments using transgenic mice determined that adult microglia derive from primitive myeloid cells, which arise in the yolk sac by embryonic day E8 and seed the brain between embryonic day E8.5 and E10.5 (Ginhoux et al, 2010). A similar pattern of microglial brain colonisation is observed in the human brain where amoeboid myeloid cells are present from 4.5 gestational weeks (Verney et al, 2010).

In analogy to the distinction of microglia from bone marrow derived macrophages (BMDMs) during embryonic development, CNS resident populations are considered to represent a different compartment from the circulating monocyte pool in adulthood. The replenishment of microglia throughout adult lifetime has been an issue of great interest. Adult microglia have the ability to synthesise DNA and self-renew in the normal CNS (Lawson et al, 1992). This mechanism is considered to be the predominant source of microglia in the steady-state. Studies of a parabiotic mouse model conducted by Ajami further supported the notion of microglia self-maintenance in the adult CNS, by reporting no contribution of circulating progenitor cells to the microglial population under normal conditions, neuropathological conditions and brain irradiation regimes (Ajami et al, 2007). However, other elaborate experimental studies using blood chimeras have shown that BMDMs can give direct rise to microglia in the adult brain, although conditioning of the brain by irradiation was a pre-requisite under both physiological and pathological conditions (Mildner et al, 2007). As a general consensus, and taking into account that the majority of studies identified no or marginal contribution of BMDMs to the maintenance of microglia in the adult brain, adult microglia are a distinct compartment from circulating myeloid cells (reviewed by Ginhoux et al, 2013).

In addition to the compartmentalisation between circulating and CNS resident cells, those two populations appear to be morphologically distinguishable in the inflamed brain, at least, with the latter being larger and having more cellular processes (Yamasaki et al, 2014). Moreover, evidence arising from gene and protein expression studies suggests that the two populations also differ at the molecular level (Butovsky et al, 2014; Yamasaki et al, 2014). A recent elaborate gene microarray study describes unique molecular signatures of resident microglia, compared to monocytes that have invaded the brain and splenic monocytes, under neuroinflammatory conditions. The microglial specific signature encompasses molecules involved in transcription (c-JUN), signalling mediated by G-coupled receptors (P2ry12, CX_3CR1), cell adhesion (integrin5) and immunity (C1q of complement system) (Butovsky et al, 2014).

1.5.2 Role of microglia in brain homeostasis

Microglia constitute up to 20% of all CNS cells. One key characteristic of microglia, which also distinguishes them from other types of macrophages, is their ramified processes (Yamasaki et al, 2014). Those processes protrude from the cell body enabling them to patrol the surrounding microenvironment and communicate with neurons and other glial cells. This state of constant surveillance is often described as the resting phenotype, although microglia are highly active and motile (Nimmerjahn et al, 2005). In fact, fine microglial processes rapidly extend and retract in the intact mouse brain as revealed by two photon *in vivo* imaging (Nimmerjahn et al, 2005; Davalos et al, 2005). It has been proposed that this microglial phenotype is maintained via intercellular communication with neurons, although likely not exclusively. Cell receptors expressed on microglia such as CX_3CR1, CD45 and

CD200R are implicated in this process (Harrison et al, 1998; reviewed by Saijo and Glass, 2011).

Microglial cells contribute to brain homeostasis by supporting neuronal and glial growth and function. Microglia derived neurotrophin 3 is implicated in the postnatal development of the brain (Elkabes et al, 1996). Recently, another important functional cross-talk between microglia and neuronal activity has been reported by Parkhurst and colleagues who show that microglia regulate dendritic spine formation and elimination. Moreover, brain derived neurotrophin factor (BDNF) from microglia mediates synaptic plasticity, which is important for memory and learning in the young and adult brain (Parkhurst et al, 2013). Microglia are involved in synaptic pruning via the fractalkine receptor CX_3CR1 in the early postnatal murine brain, during the physiological process of synaptic maturation (Paolicelli et al, 2011). Moreover, microglia engulf and phagocytose neurons committed to apoptosis (Marin-Teva et al, 2004), while suppressing proinflammatory signalling that would alter brain physiology (Takahashi et al, 2005). The active role of microglial cell function in brain development and physiology is underlined by studies of genetic depletion of the microglia specific receptor CX_3CR1. Paolicelli and colleagues reported that mice deficient in CX_3CR1 had reduced microglial populations and delayed synaptic pruning, indicating that altered microglial signalling accounts for perturbations in synaptic homeostasis, and thus, increased susceptibility to developmental disorders (Paolicelli et al, 2011). Using similar approaches, Cardona and colleagues showed that $CX_3CR1^{-/-}$ homozygous mice present with increased levels of neuronal toxicity in models of both systemic and CNS inflammation (Cardona et al, 2006). Those studies pinpoint the interdependence of microglial function and brain homeostasis and stress the important contribution of the microglial response in CNS health.

Beyond their role in neuronal support, microglia are also primary effectors of the innate immune response within the CNS. In the steady state, human and rodent microglial cells express basal levels of MHCII molecules on their surface (Mittelbronn et al, 2001; Kreutzberg, 1995) the function of which is critical for antigen presentation and, therefore, initiation of an immune response (Holling et al, 2004). However, in response to pathogenic stimuli or infectious agents, microglial cells robustly upregulate MHCII molecules (Saijo et al, 2011; Saijo et al, 2013). Synergy between invading $CD4^+$ T lymphocytes and MHCII expressing microglial cells has been implicated in resistance to *C.neoformans* brain infection in mice (Aguirre and Miller, 2002). Similarly, microglia express TLRs as part of their pathogen associated molecular patterns (PAMPs) recognition system (Saijo et al, 2011; Saijo et al, 2013). Those pattern recognition receptors have the ability to induce innate responses, including inflammatory cytokine production, in response to lipids, proteins and nucleic acids. Human and murine microglia express the majority of all identified TLRs (Olson and Miller, 2004), which renders them sentinels of the brain.

1.5.3 Microglial polarisation in disease

Activated microglia orchestrate the CNS innate response to injury and infection. However, unresolved microglial activation is often associated with pathological inflammatory conditions that may lead to neurodegeneration and neoplastic diseases. In this context, clinical and preclinical studies have shown microglial infiltration of the lesioned brain for Parkinson's disease, Alzheimer's disease, multiple sclerosis and brain tumours (Saijo and Glass, 2011). Extensive research over the past few years has established microglia, like macrophages, as versatile cells that have the ability to express distinct functional programs

depending on stimuli from the microenvironment they reside in. Like TAMs, as discussed in section 1.3.2, activated microglia classification resembles the well-established M1/M2 dichotomy applied for blood and tissue resident macrophages, although not studied as extensively (Sica et al, 2006; Saijo and Glass, 2011).

Recently, a protective role for CNS homeostasis was attributed to M2 microglia by a group working on spinal cord injury. Since M2 polarised cells promote neuronal regeneration while M1 cells exhibit neurotoxic properties, the group suggests that the persistence of the M1 phenotype over the M2 of the microglial/macrophage population delays CNS repair in the injured mouse spinal cord (Kigerl et al, 2009). Similarly, a neuroprotective role was attributed to CNS derived IL-4 since mice deficient in IL-4 in the brain were more susceptible to clinically severe experimental autoimmune encephalomyelitis (EAE), a rodent model of multiple sclerosis. Microglial polarisation towards the M2 phenotype induced by the CNS derived IL-4 was responsible for the regulation of inflammation and, thus, neuroprotection in the afore-mentioned model (Ponomarev et al, 2007). However, the absence of an appropriate and well-timed M2 microglial response could lead to chronic smouldering neuroinflammation and neurodegeneration (Cherry et al, 2014). In patients with Alzheimer's disease microglial activation and increased levels of both pro-inflammatory cytokines and angiogenic growth factors are reported. Microglial mediated phagocytosis of amyloid-β is essential for plaque removal and, thus, neuroprotection. On the other hand, sustained M1 activation upon recognition of the amyloid-β plaques could exert a neurotoxic effect (Saijo and Glass, 2011). A functional link between microglial phenotype and neurodegeneration might be underscored by the strong correlation of mutations in the triggering receptor expressed on myeloid cells 2 (TREM2) gene. This gene is also implicated in the M2 cell

phenotype in mouse and human microglia, and increased risk of developing Alzheimer's disease (Jonsson et al, 2013; Guerreiro et al, 2013).

In the case of brain cancer, appropriately balanced coupling of M1 and M2 microglial activation would be beneficial both for reducing intracranial tumour burden and maintaining tissue integrity. However, human biopsies and experimental models of gliomas suggest that tumour associated microglia and macrophages primarily bear an M2 molecular signature and impaired capacity to stimulate T cell anti-tumour immunity, features which sustain neoplastic outgrowth in the brain (Saijo and Glass, 2011, Li and Graeber, 2012). The immunosuppressive brain microenvironment possibly drives microglial alternative polarisation, and M2 skewed microglia, in turn, support glioma angiogenesis and invasion via TGF-β, VEGF and MMP paracrine signalling (Li and Graeber, 2012). An elegant study by Sarkar and colleagues showed that microglia isolated from glioma patients were inefficient at reducing the formation of spheres of autologous brain initiating tumour cells, while microglia from healthy human subjects significantly reduced their sphere formation capacity (Sarkar et al, 2014). Interestingly, microglia derived MCP-1 was implicated in the reduction of tumour sphere formation, which is also considered an M1 polarisation marker in primary microglia (Chhor et al, 2013). Thus, environmental cues might educate brain resident microglia to foster cancer progression via unique molecular patterns.

Overall, it has become clear that the bipolar M1/M2 paradigm is considered oversimplified in understanding CNS pathologies *in vivo* (Perry and Holmes, 2014). Clinical studies and preclinical models of CNS diseases provide evidence of co-existence of M1 cells, M2 cells as well as intermediate phenotypes in the brain microenvironment so much so that the field is now moving away from using the M1/M2 nomenclature. Moreover, there is now a strong

view that a better defined cause-effect relationship between microglial activation states and brain diseases could yield targets for microglial re-education in a disease specific setting.

1.6 Research motivation

With the great advances in both prolonging survival and improving treatment for cancer patients comes the price of increased incidence of metastasis to the brain. Brain metastasis is a devastating complication and the currently applied modalities of chemotherapy and radiotherapy confer only a small survival advantage. Thus, there is a substantial need for better characterisation of the immune response associated with metastatic disease in the brain with the aim of identifying new therapeutic strategies. The strategy of targeting immune cells for cancer therapy has yielded encouraging results. For instance, administration of antibodies against antigens expressed on T cells that negatively regulate their activation (anti-CTLA4, anti-PD1) reduce tumour burden and significantly improve survival (Marabelle et al, 2013; Quezada and Peggs, 2013). Moreover, targeting TAMs by either inhibiting their recruitment or re-educating them towards tumour destruction reduces the growth and metastatic potential of aggressive tumours. In the context of secondary cancer to the brain, microglia and macrophages have been shown to infiltrate both human and experimental brain metastases. However, the exact role and phenotype of brain resident microglia during the progression of the disease is poorly understood. Thus, the primary aim of this thesis is to better characterise the microglial response and phenotypic heterogeneity in the early stages of metastatic outgrowth in the brain. Taking into account that microglia are effectors of the innate immune response in the brain and that harnessing microglial function has produced promising results experimentally for both

neurodegenerative and neoplastic brain disorders, the possibility of targeting microglia in the context of brain metastasis as a therapeutic strategy will be also investigated as part of this thesis.

Thus, the aims of this thesis are:

- To assess microglial activation in the early stages of brain metastasis
- To investigate the polarisation of metastasis associated microglia to the M1 or M2 like phenotype
- To develop a model of *in vivo* microglial depletion in the metastatic brain
- To assess the effect of microglial depletion in metastatic outgrowth

Chapter 2

Materials and methods

2.1 Chemicals and buffers

Sodium dihydrogen orthophosphate dihydrate, di-sodium hydrogen orthophosphate (Sorrenson's salt), sucrose, tris-hydrochloride, sodium chloride, iso-Pentane (99%), ethanol (99.8%), methanol and hydrochloric acid were obtained from Fisher Scientific (Loughborough, UK). Paraformaldehyde, l-lysine monohydrochloride, (-)-tetramisole hydrochloride (≥99%), dichloromethylenediphosphonic acid disodium salt, sodium hydroxide, hydrogen peroxidase (30 % (w/w) in H_2O solution), glutaraldehyde, acetic acid and Tween20 were obtained from Sigma-Aldrich (Gillingham, UK). Sodium metaperiodate was obtained from VWR International (Lutterworth, UK). Phosphate buffered saline (PBS) tablets were obtained from Oxoid (Basingstoke, UK). 3,3'-diaminobenzidine tetrahydrochloride hydrate (97%) (DAB) was purchased from ACROS Organics (Sigma Aldrich, UK).

The following buffers were used: TNB buffer (0.1M Tris-HCL pH 7.5, 0.15M NaCl, 0.5% Blocking reagent Perkin Elmer); Citrate buffer (10mM sodium citrate, 0.05% Tween20, pH 6); PLP_{light} (75mM l-Lysine monohydrochloride, 10mM Sorrenson's salt, 2% w/v PFA, 1 mM sodium metaperiodate in phosphate buffer, pH 7.2).

2.2 Cell lines and tissue culture

2.2.1 Cell lines

The 4T1 cell line is a murine epithelial mammary carcinoma originally derived from a spontaneously arising mammary tumour in a BALB/c mouse (Dexter et al, 1978). 4T1 cells transfected with a GFP expressing vector were routinely maintained in Dulbecco's

Modified Eagle's Medium (DMEM, Invitrogen, UK) supplemented with 10% fetal bovine serum (FBS, Labtech, International, UK) and 1% L-glutamine (PAA, UK). Those cells were kindly provided by Prof. Ruth Muschel's laboratory (University of Oxford, UK).

EO771 cells are murine mammary carcinoma cells isolated from a spontaneous tumour from a C57BL/6 mouse (Sugiura and Stock, 1952). EO771 cells transfected with a GFP expressing vector were routinely maintained in Roswell Park Memorial Institute (RPMI) medium supplemented with 20% FBS (Labtech, International, UK), 1% L-glutamine (PAA, UK), 1x non-essential animo acids (Gibco, UK) and 1mM sodium pyruvate (Sigma-Aldrich, UK).

B16F10 are murine melanoma cells derived from the C57BL/6 B16F melanoma cells (Raz et al, 1980). B16F10 transfected with a GFP expressing vector were routinely maintained in DMEM medium (Invitrogen, UK) supplemented with 10% FBS (Labtech, International, UK), 1% L-glutamine (PAA, UK), 1x non-essential animo acids (Gibco, UK) and 1mM sodium pyruvate (Sigma-Aldrich, UK).

LLC cells, also referred to as Lewis lung carcinoma cells, originated from a spontaneous lung carcinoma of a C57BL/6 mouse (Bertram and Janik, 1980). Cells transfected with a GFP expressing vector were routinely maintained in DMEM medium (Invitrogen, UK) supplemented with 10% FBS (Labtech, International, UK) and 1% L-glutamine (PAA, UK).

The microglial BV2 cell line, derived from the brain of a C57BL/6 mouse, was routinely maintained in DMEM medium (Invitrogen, UK) supplemented with 10% FBS ((Labtech, International, UK) and 1% L-glutamine (PAA, UK) and used as a surrogate for primary microglia. The murine macrophage-like cell line RAW264.7, derived from ascites of a BALB/c mouse, was routinely maintained in DMEM medium (Invitrogen, UK)

supplemented with 10% FBS (Labtech, International, UK) and 1% L-glutamine (PAA, UK). Both BV2 and RAW 264.7 cell lines were kindly provided by Dr Wang from Prof. Xin Lu's laboratory (University of Oxford, UK).

2.2.2 Tissue culture

All cell lines were grown as monolayers in ventilated flasks (Corning Life Sciences, UK) in an incubator at 37˚C and 5% CO_2 with a humidified atmosphere. Cells were sub-cultured to new flasks when confluency reached 80-90% using 0.25% trypsin-EDTA solution (Sigma Aldrich, UK) and treatment for 3-5 mins. All cell lines were tested for mycoplasma infection using the MycoAlert Detection Kit (Lonza, Rockland Inc) according to the manufacturer's instructions.

2.3 Cell treatments

4T1-GFP cells were treated with dichloromethylenediphosphonic acid disodium salt ($CH_2O_6Cl_2Na_2P_2$), also known as clodronate salt. Clodronate salt was suspended in ddH_20 and its pH was adjusted to 7 using sodium hydrogen carbonate (Fisher Scientific, UK). Cells were treated with 2.5 mg/ml, 5mg/ml and 7.5 mg/ml clodronate in culture medium for 6 or 24 hours. At the end of the experiment cells were subjected to a tetrazolium based (MTT) viability assay (TL Riss et al, 2015; section 2.4).

In vitro cell polarisation of BV2 microglia cells and RAW264.7 macrophage cells was induced by treatment with LPS or IL-4. Equal numbers of cells were seeded onto 12 or 96 well plates (Greiner Bio-one, CellStar). Cells were treated with 100ng/ml LPS (E.coli

derived, 0111:B4) (Sigma-Aldrich, UK) or 20ng/ml murine recombinant IL-4 (Peprotech, UK) in culture medium for polarisation to the M1 or M2 phenotype respectively, or left untreated for the unpolarised control phenotype. At the end of the experiment, cells were fixed in 4% PFA (in PBS, pH 7.2) for immunofluorescence staining.

4T1-GFP cells, unpolarised or poralised BV2 and RAW 264.7cells were treated with mannosylated control (PBS) or clodronate (10mg/ml) liposomes (Encapsula Nanosciences, USA). 4T1-GFP, BV2 and RAW264.7 cells were seeded onto 96 well plates and when cell confluency reached 60-70%, cells were treated with mannosylated control or clodronate liposomes diluted 1:50 or 1:100 in culture medium for 6 or 24 hours. Alternatively, BV2 and RAW 264.7 cells seeded onto 96 well plates were treated with IL-4 (20ng/ml) or LPS (100ng/ml) for polarisation when cell confluency reached 40-50%. 24 hours after treatment with the polarising agents, cells were treated with mannosylated control or clodronate liposomes diluted 1:50 in culture medium for 24 or 48 hours. At the end of the experiment cells were subjected to the MTT viability assay.

2.4 MTT cell viability assay

Colorimetric MTT assays were performed in order to assess the effect of the mannosylated liposomes on the viability of the cells. MTT assays are robust and reliable in measuring cell metabolic activity and thus cell viability (TL Riss et al, 2015). The principle of this assay lies in the intracellular reduction of the yellow MTT tetrazolium (3-(4,5-dimethylthiazol-2-yl)-2,5-diphenyltetrazolium bromide) to an insoluble violet precipitate (formasan) by dehydrogenases and reducing agents, most likely NADH (Figure 2.1). The amount of formasan is directly proportional to the activity of the enzymes and

thus indicative of cell viability. BV2, RAW 264.7 and 4T1-GFP cells treated appropriately were subjected to the MTT assay (CellTiter 96® Non-Radioactive Cell Proliferation Assay; Promega, UK) according to the manufacturer's instructions. Briefly, 15µl of MTT dye solution was added per well in the dark. Plates were incubated at 37°C in a humidified, 5% CO_2 atmosphere for 3-4 hours, depending on the cell line. After the development of the violet formasan product, 100µl of solubilisation/stop solution was added per well and plates were left shaking on a platform for an hour at room temperature. Absorbance was recorded at 570 nm wavelength using a 96-well plate reader (Tecan Infinite® Pro, Switzerland).

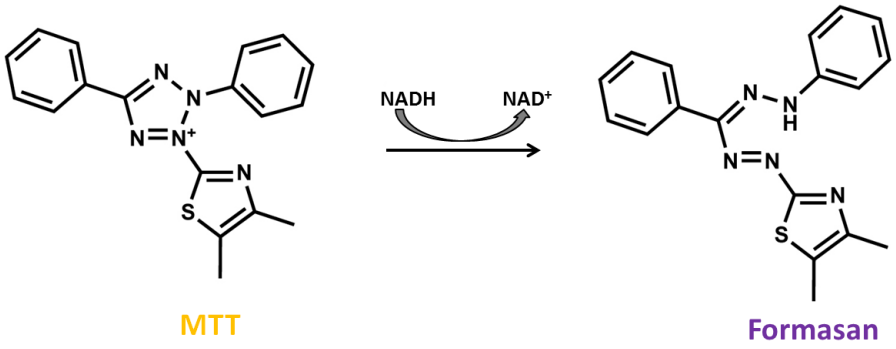


Figure 2.1: Schematic of the enzymatic reaction of the MTT assay. Yellow tetrazolium (3-(4,5-dimethylthiazol-2-yl)-2,5-diphenyltetrazolium bromide) can be converted to an insoluble violet precipitate (formasan) in viable cells by the action of dehydrogenases.

2.5 *In vivo* procedures

Animal procedures were carried out in accordance with the UK Animals (Scientific Procedures) Act 1986 and with local ethical committee approval. All mice used were housed in individually ventilated cages with food and water provided *ad libitum.* BALB/c

mice were purchased by Charles River Laboratories (Kent, UK). LYSM/LYSK mice (C57Bl/6 background) were kindly provided by Dr. Xudong Liao (Case Western Reserve University School of Medicine, Cleveland) and bred at the animal facility of the Department of Biomedical sciences (University of Oxford, UK).

2.5.1 Experimental brain metastasis

2.5.1.1 Tumour cell injections

For this thesis, experimental brain metastases were induced by intracerebral injection of tumour cells. More specifically, tumour cells (at 80-90% confluency) were trypsinised as described in section 2.2.2 and resuspended in pre-warmed sterile PBS. Number of viable cells was calculated using Nucleocounter NC-100 (Chemometec, UK) or Countess II (Invitrogen, UK) as per manufacturer's instructions and cells were diluted at appropriate concentrations. Mice were anaesthetised with 3-4% isoflurane (Abbot, UK) in 70:30 N_2O:O_2 (flow rate 4L/min), their scalps shaved and then placed on a stereotactic frame (Stoetling Co., USA). Under general anaesthesia (2% isoflurane), a skin incision was made and the skull was exposed. Using a drill, a small hole was drilled at the injection site (coordinates +0.5mm, 1.9 mm (lateral) relative to Bregma). Tumour cells were loaded on a glass microcapillary (Clark Electromedical Instruments, UK) 70µm wide in diameter and injected into the left striatum (2.8mm deep). To avoid cells tracking up in the capillary, cells were allowed to settle in the brain for 5 minutes. Capillaries were then retracted 20% before being fully retracted from the brain 3 minutes later. After surgery, the skin incision was sutured (Mersilk, Ethicon, Germany) and animals were allowed to recover.

2.5.1.2 Mouse models of brain metastasis

All mouse models used for this thesis are summarised in Table 2.1. Briefly, for the 4T1-GFP intracerebral model, 6-9 weeks old female BALB/c mice were injected with $5x10^3$ 4T1-GFP cells in 0.5µl PBS. For the LYS intracerebral models, 9-12 weeks old control (LYSM) or knock-out (LYSK) mice were used. More specifically, female LYS mice were injected with $5x10^2$ EO771-GFP cells in 0.5µl PBS and male LYS mice were injected with $2x10^3$ B16F10-GFP cells or $2x10^3$ LLC-GFP cells in 0.5µl PBS. Intracerebral injections of vehicle (sterile PBS) were performed as controls, when necessary.

intracerebral model	Strain	Cells (in 0.5µl PBS)	Timepoints (days)
4T1-GFP	BALB/c (female, 6-9 weeks old)	$5x10^3$	7, 10, 14, 21, 28
EO771-GFP	LYS (female, 9-12 weeks old)	$5x10^2$	14
B16F10-GFP	LYS (male, 9-12 weeks old)	$2x10^3$	14
LLC-GFP	LYS (male, 9-12 weeks old)	$2x10^3$	14

Table 2.1: Mouse models of brain metastasis. Murine cell lines and number of cells (based on the literature/experiments performed by colleagues) used for each metastatic model are listed in this table. Mouse strain and timepoints for each model are also indicated.

2.5.2 Model of CNS inflammation

Animal procedures and intracerebral injections were carried out as described in sections 2.5 and 2.5.1. Briefly, murine recombinant IL-4 (Peprotech, UK) was reconstituted in sterile ddH_2O at final concentration of 200ng/µl. 100ng of IL-4 were intracerebrally injected using a calibrated glass microcapillary 50µm wide in diameter. Animals were sacrificed at 6, 24, 48 or 72 hours after cytokine injection.

2.5.3 *In vivo* depletion of microglia

Animal procedures and intracerebral injections were carried out as described in sections 2.5 and 2.5.1. Briefly, mannosylated control (PBS) or clodronate (5mg/ml or 10mg/ml) liposomes were gently rocked to yield a homogeneous suspension before intracerebral injection using calibrated glass microcapillaries 50µm wide in diameter. Intracerebral injection of mannosylated liposomes was performed on naïve, tumour bearing or inflamed brains. In the cases of tumour bearing or inflamed brains, injection of liposomes was performed using the same co-ordinates as for the tumour cell or cytokine injection, respectively. Animals were sacrificed either 6 hours or 3, 9 and 16 days after liposome injection.

2.5.4 Injection of free clodronate

Animal procedures and intracerebral injections were carried out as described in sections 2.5 and 2.5.1. Briefly, 0.5µg or 4µg of clodronate salt (in ddH_20, pH 7) were intracerebrally injected using calibrated glass microcapillaries 50µm wide in diameter. Animals were sacrificed 9 days after clodronate injection.

2.6 Brain harvest

At the end of each experiment (Table 2.1; sections 2.5.2, 2.5.3, 2.5.4), animals were transcardially perfusion-fixed under terminal anaesthesia using ice cold 0.9% saline containing heparin (10.000 units/ml) followed by PLP_{light} buffer containing 0.025% w/v glutaraldehyde. Brains were removed from the scull and post fixed in PLP_{light} for 4-6

hours. Brains were then cryoprotected in 30% sucrose (w/v in dH_2O) for 48-72 hours, until frozen in OCT (Pyramid Innovation) using isopentane. Frozen tissue was stored at -20˚C until further use.

2.7 Lung/Liver harvest

In some cases, livers and lungs of experimental animals were also harvested for immunostaining. In this case, animals were transcardially perfusion-fixed under terminal anaesthesia and organs were post fixed in PLP_{light} and cryoprotected in sucrose, as previously described in section 2.6.

2.8 Immunohistochemistry

Immunohistochemistry (IHC) was performed on 10-20µm thick tissue sections mounted on glass slides (Superforst Plus, Menzel Gläzer, Braunschweig, Germany). Initially, slides were allowed to come to room temperature before rehydration in PBS. When necessary, antigen retrieval was performed using sodium citrate buffer containing 0.1% Tween20 (pH 6.0). Slides were microwaved twice in citrate buffer for 5 mins. Subsequently tissue was permeabilised in PBS containing 0.1% Tween20 (v/v) for 15 mins and then quenched for endogenous peroxidases for 20 min with 1% H_2O_2 in methanol. Tissue was washed three times in PBS and blocked for non-specific antibody binding in 10% serum (in PBS) for 1 hour at room temperature (Table 2.2). Primary antibodies were incubated in PBS Tween20 (0.05%) containing 1% serum overnight at 4˚C (Table 2.2). The next day, slides were washed three times in PBS (0.05% Tween20) and subsequently incubated with

biotinylated secondary antibody for 1 h at room temperature (Table 2.2). Slides were washed three times in PBS Tween20 (0.05%) followed by incubation with avidin/biotin complex-horseradish peroxidase (HRP) system (VECTASTAIN Elite ABC Kit Standard, Vector Laboratories, UK). Peroxidase was detected using 3,3'-diaminobenzidine (DAB). Slides were then incubated in 0.05% acetic acid (v/v in dH_2O) followed by counterstaining with 0.5% cresyl violet acetate (w/v in dH_2O) (ACROS Organics, UK). Tissue was dehydrated using increasing concentration of ethanol, cleared in xylene and mounted in DPX mountant (Fisher Scientific, UK).

1^{ary} antibody	**2^{ary} antibody (biotinylated IgG)**	**Blocking Serum**	**Antigen retrieval**
Iba1 (Abcam ab5076) 1:500	horse anti-goat (1:200)	Horse	-
iNOS (M-19) (SantaCruz sc650) 1:600	goat anti-rabbit (1:200)	Goat	-
Arg1(Novus Biologicals NBP1-54621) 1:300	goat anti-rabbit (1:200)	Goat	-
MRC1 (AbD Serotec MCA2235) 1:300	rabbit anti-rat (mouse absorbed) (1:200)	Rabbit	-
COX2 (Abcam ab15191) 1:300	goat anti-rabbit (1:200)	Goat	-
CD31 (R&D, AF3628) 1:300	horse anti-goat (1:200)	Horse	-
CC3 (Asp175) (Cell Signaling Technology 9661) 1:300	goat anti-rabbit (1:200)	Goat	+

Table 2.2: Antibodies used for immunohistochemistry. Primary antibodies, suppliers and concentrations are listed. All secondary antibodies and serums were supplied from Vector Laboratories (UK).

2.9 Immunohistochemical scoring

Immunostained slides were imaged on ScanScope CS slide scanner (Aperio, Vista, CA, USA) and analysed using ImageScope (Aperio, USA). Quantitative analysis of the volumes of metastatic lesions and microglial infiltration was performed by manual demarcation of the areas of interest. More specifically, tumours were defined as cresyl violet positive foci and microglial infiltration area was defined by the outer limit of reactive Iba1^{+} cells (Figure 2.2). For this analysis, areas of interest on brain sections 50 µm apart spanning the metastatic lesions were included. Respective volumes were calculated by multiplying areas with the thickness of tissue sections and number of sections omitted in between.

Quantitation of DAB staining was performed using the Positive Pixel Count Algorithm (Aperio, USA). This algorithm classifies pixels of the scanned immunostained tissue into weak, positive and strong positive depending on the intensity of the DAB. Positive and strong positive pixels within the areas of interest were included for the analysis while weak pixels were considered as background. Quantitation was expressed as number of pixels or converted to area (µm^2) of immunostaining.

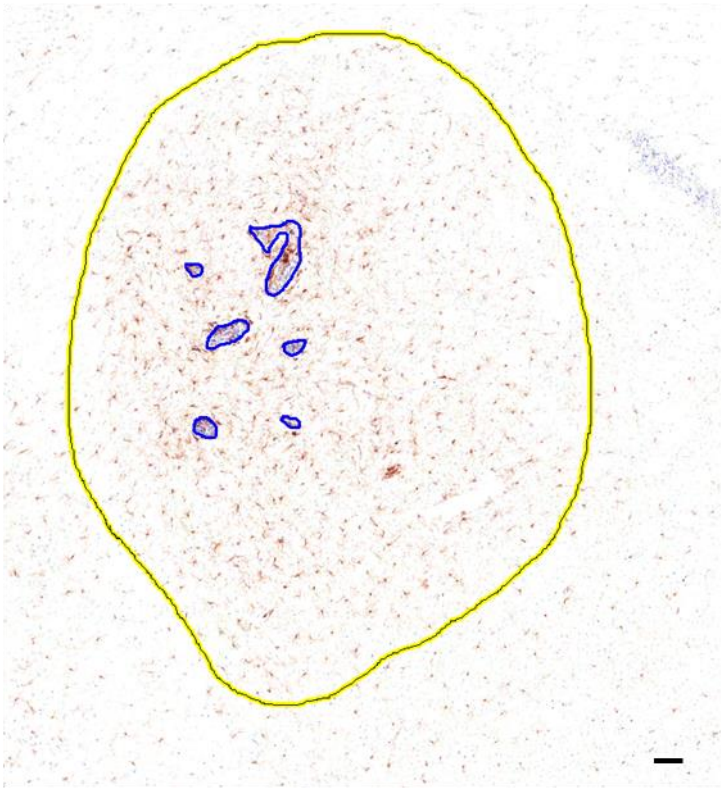


Figure 2.2: Demarcation of areas of interest for quantitation of tumour and microglial volumes. Representative IHC image stained for Iba1 and scanned on Aperio Scanner. Tumour foci (marked in blue) and microglial infiltration area (marked in yellow) were demarcated manually using ImageScope. Scale bar 50 µm

2.10 Double immunohistochemistry

Immunohistochemistry to detect multiple antigens on the same section has been described (van der Loos, 2008). Visual or spectral separation of two or more chromogens is possible, although colocalisation of multiple antigens might be challenging. We employed double IHC approaches to detect double labelled cells.

2.10.1 Sequential HRP and alkaline phosphatase double staining

Tissue of interest was initially stained for a single antigen using the HRP DAB protocol as described in section 2.8. Briefly, sections were permeabilised in PBS Tween20 (0.1%) and

endogenous peroxidase activity was quenched in 1% H_2O_2 (in methanol). Sections were incubated in 10% horse serum (in PBS) for 1 hour at room temperature to block non-specific antibody binding. Sections were then incubated with primary antibody (goat a-mouse Iba1, 1:500) in PBS (0.1% Tween20, 1% horse serum) overnight at 4˚C. The next day, appropriate biotinylated secondary antibody (horse a-goat, 1:200) was added for 1 h at room temperature followed by incubation with avidin/biotin complex HRP system (Vector Laboratories, UK) and detection with DAB. Before proceeding with the second immunostain, slides were washed in PBS (0.05% Tween20) three times, incubated with the streptavidin/biotin blocking kit (Vector Laboratories, UK) to block biotin and with 10% goat serum (in PBS) for 1 hour at room temperature to block non-specific antibody binding. The second primary antibody (rabbit a-mouse Arg1 (H-52) sc 20150, 1:50) was diluted in PBS (0.05% Tween20, 1% goat serum) and added on sections overnight at 4˚C. The day after, sections were washed three times in PBS (0.05% Tween20) and the appropriate biotinylated secondary antibody (goat a-rabbit, 1:200) was added for 1 h at room temperature. The second antigen of interest was detected using the avidin/biotin complex phosphatase system (VECTASTAIN ABC-Alkaline Phosphatase Standard) (Vector Laboratories, UK) and the Vector Red substrate (Vector Laboratories, UK). Endogenous alkaline phosphatase activity was quenched prior to the addition of the Red substrate by incubation of the sections with 2mM levamisole (in PBS). Slides were then incubated in 0.05% acetic acid (v/v in dH_2O) followed by counterstaining with 0.5% cresyl violet acetate (w/v in dH_2O) (ACROS Organics, UK). Tissue was dehydrated using increasing concentration of ethanol, cleared in xylene and mounted in DPX mountant (Fisher Scientific, UK). Double IHC protocol is summarised in Table 2.3.

2.10.2 Sequential double HRP staining

An approach to detect double labelled cells using sequential HRP stains was also employed. Tissue of interest was initially stained for a single antigen using the HRP DAB protocol as described in chapter 2.8. Briefly, sections were permeabilised in PBS Tween20 (0.1%) and endogenous peroxidase activity was quenched in 1% H_2O_2 (in methanol). Sections were incubated in 10% rabbit serum for 1 hour at room temperature to block non-specific antibody binding. Sections were incubated with primary antibody (rat a-mouse MRC1, 1:300) in PBS (0.1% Tween20, 1% rabbit serum) overnight at 4˚C. The next day, appropriate biotinylated secondary antibody (rabbit a-rat, 1:200) was added for 1 h at room temperature followed by incubation with avidin/biotin complex HRP system (Vector Laboratories, UK) and detection with DAB. Before proceeding with the second immunostain, slides were washed in PBS (0.05% Tween20) three times and peroxidase activity was quenched in 1% H_2O_2 (in methanol). Then biotin was blocked using the streptavidin/biotin blocking kit (Vector Laboratories, UK) and non-specific antibody binding in 10% horse serum for 1 hour at room temperature. The second primary antibody (goat a-mouse Iba1, 1:500) was appropriately diluted in PBS (0.1% Tween20, 1% horse serum) and added on sections overnight at 4˚C. The day after, sections were washed three times in PBS (Tween20 0.05%) and the appropriate biotinylated secondary antibody (horse a-goat, 1:200) was added for 1 h at room temperature. The second antigen of interest was detected using the avidin/biotin complex HRP system (Vector Laboratories, UK) and the Vector NovaRed substrate (Vector Laboratories, UK). Slides were then incubated in 0.05% acetic acid (v/v in dH_2O) followed by counterstaining with 1% cresyl violet acetate (ACROS Organics, UK). Tissue was dehydrated using increasing

concentration of ethanol, cleared in xylene and mounted in DPX mountant (Fisher Scientific, UK). Double HRP protocol is summarised in Table 2.3

1st immunostain		**2nd immunostain**			
HRP(**DAB** or **NovaRed**)		AP(**Red**)		HRP(**DAB** or **NovaRed**)	
1ary antibody	2ary antibody (biotinylated IgG)	1ary antibody	2ary antibody (biotinylated IgG)	1ary antibody	2ary antibody (biotinylated IgG)
Iba1 (ab5076) 1:500	horse a-goat (1:200)	**Arg1** (H-52 sc20150) 1:50	goat a-rabbit (1:200)	--	--
MRC1 (MCA2235) 1:300	rabbit anti-rat (mouse absorbed) (1:200)	--	--	**Iba1** (ab5076) 1:500	horse a-goat (1:200)
MRC1 (MCA2235) 1:300	rabbit anti-rat (mouse absorbed) (1:200)	--	--	**Iba1** (ab5076) 1:500	horse a-goat (1:200)

Table 2.3: Antibody, enzyme and substrate combinations for double immunohistochemistry. Primary antibodies and chromogenic substrates used are colour coded while experimental combinations of antibodies and enzyme/substrate are illustrated as highlighted table rows

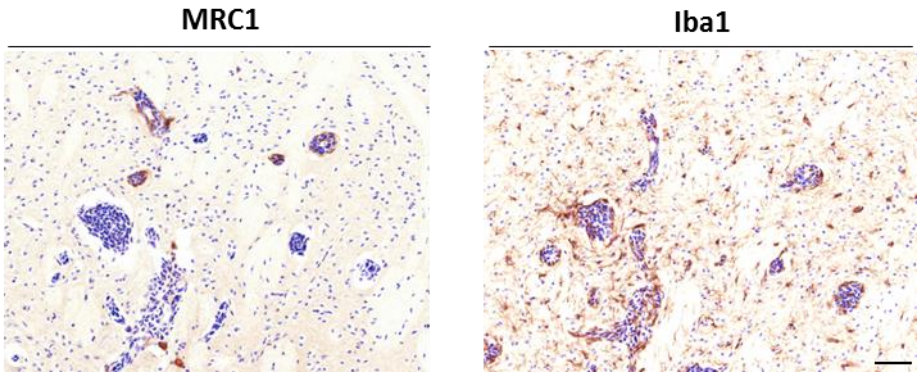
2.11 Matlab co-registration of sequential immunostained brain sections

An in-house Matlab based approach to co-register immunostains on sequential sections was developed [the Matlab code was written by Dr. Danny Allen (University of Oxford, UK)]. 10 µm thick sequential brain sections from mice bearing 4T1 metastases were

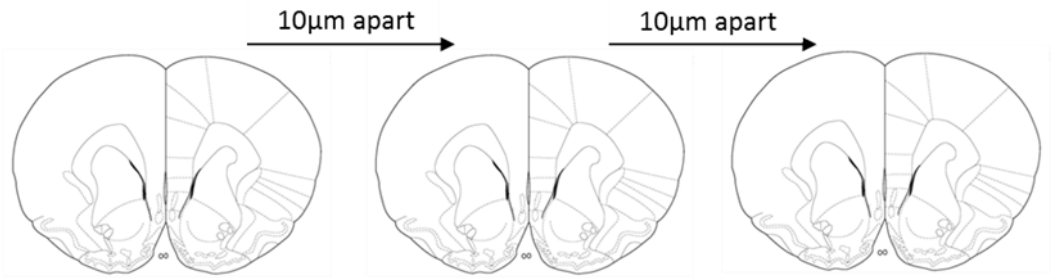
stained for different biomarkers and counterstained with cresyl violet. Since each section is 10 µm apart from the next one, the location and morphology of the tumours share high degree of similarity across the two sections (Figure 2.3 A). Thus, co-registration of two 10 µm thick sequential sections will essentially produce a single 20 µm thick immunostained section.

Brain sections were stained for microglia (Iba1), M1 markers (iNOS, COX2) and M2 markers (Arg1, MRC1) following the pattern: M1 marker, microglia, M2 marker (Figure 2.3 B). Slides were scanned on ScanScope scanner at 20x or 40x. On Matlab, sequential IHC images were co-registered by choosing points that correspond to the same areas on both images based on metastatic lesion and brain morphology (corpus callosum, ventricle) (Figure 2.3Ci). Co-registered images were subsequently thresholded using Fiji (ImageJ). Those images were then merged into a single image using Matlab. The Matlab generated images show the colocalisation of Iba1 with either polarisation marker in white and immunostained pixels for the polarisation markers which did not colocalise with Iba1 pixels on the sequential section in red (Figure 2.3 Cii).

A

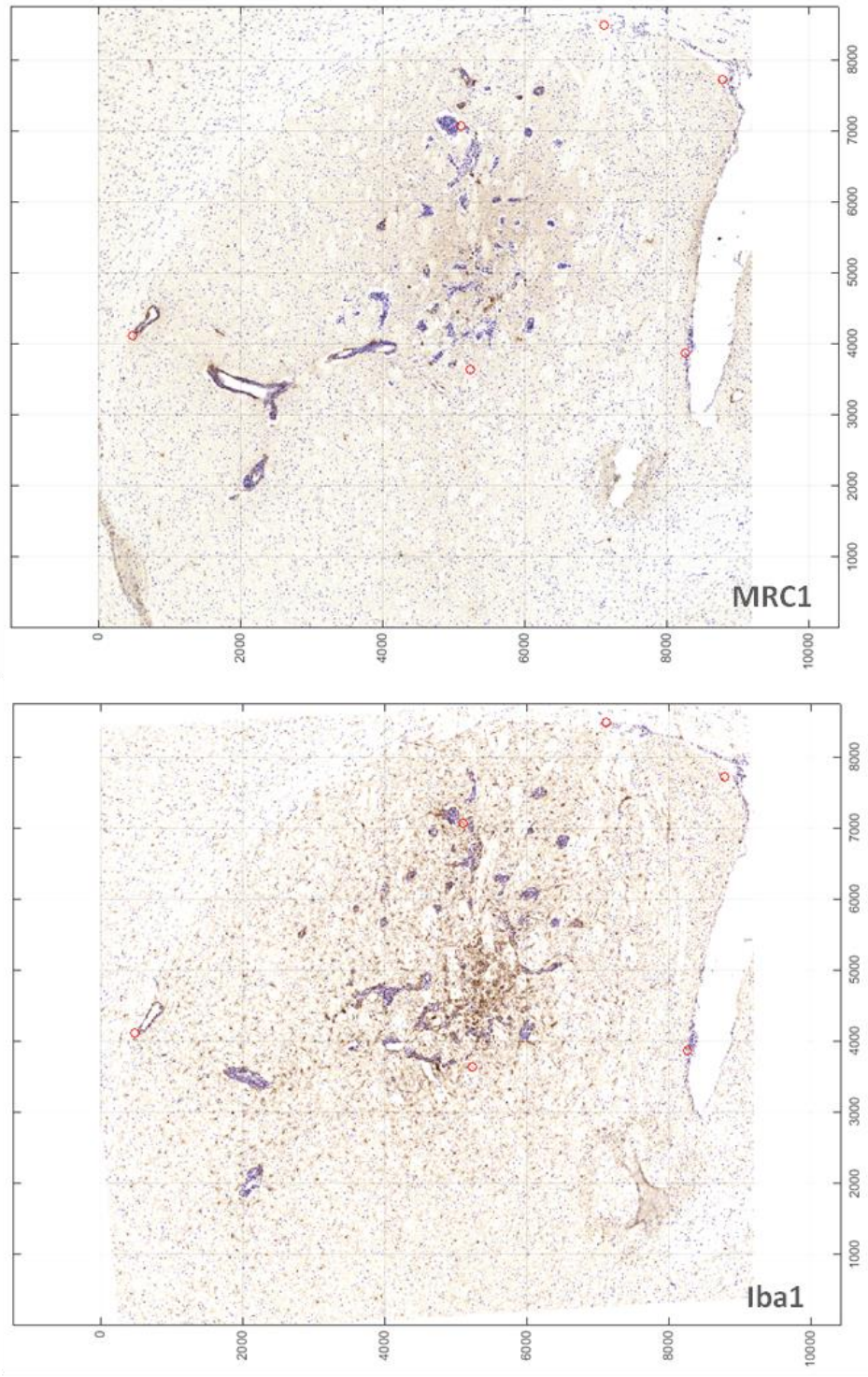

MRC1
Iba1

B


10µm apart
10µm apart
Section A: M1 marker
Section B: Microglia marker
Section C: M2 marker

c

i


MRC1
Iba1
0
2000
4000
6000
8000
10000
1000
2000
3000
4000
5000
6000
7000
8000

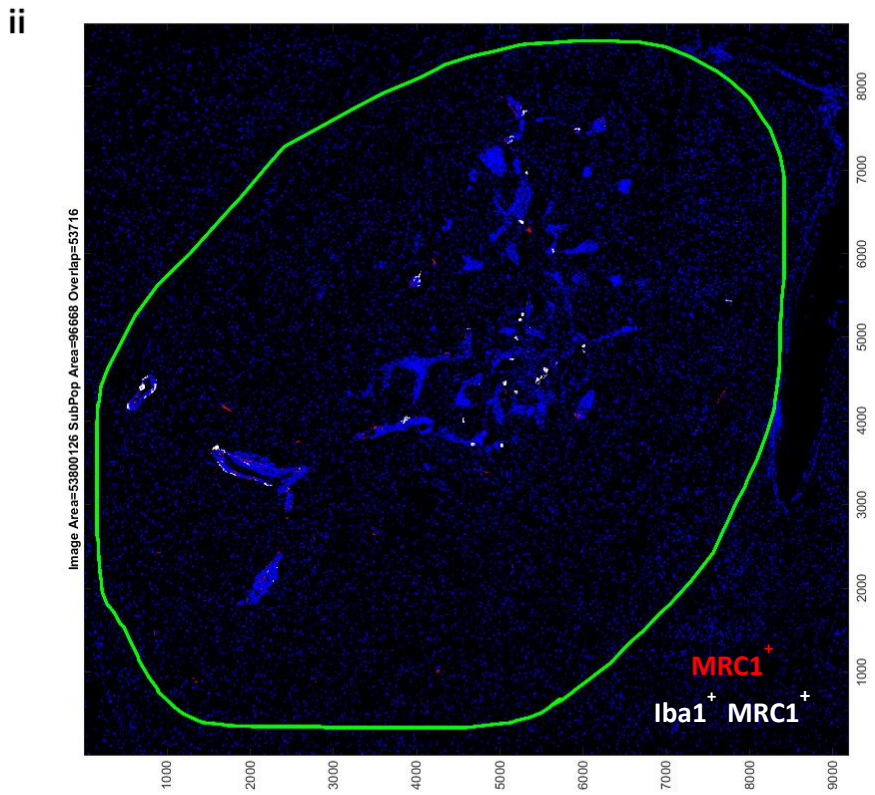


Figure 2.3: Matlab co-registration of sequential immunostained brain sections. Representative IHC images (A) of two sequential 10µm brain sections immunostained for MRC1 and Iba1 showing similar tumour morphology. In (B) is shown a schematic representation of the experimental strategy used to stain sequential 10 µm thick sections for different markers. An example of striatal regions from two sequential immunostained sections (Ci) showing points co-registration is based on (red circles). The Matlab generated image (Cii) shows tumours in blue, co-registered pixels in white and MRC1 pixels not co-registered with Iba1 in red.

2.12 Immunofluorescence

2.12.1 Immunofluorescence on tissue sections

Immunofluorescent detection of antigens was performed on 10-20 µm thick tissue sections mounted on glass slides (Superforst Plus, Menzel Gläzer, Braunschweig, Germany). Briefly, tissue was permeabilised with PBS Tween20 (0.1%), endogenous

peroxidase activity was quenched in 1% H_2O_2 (in PBS) for 20 minutes. Sections were blocked for endogenous biotin using the streptavidin/biotin blocking kit (Vector Laboratories, UK) and for non-specific antibody binding in TNB buffer (PerkinElmer, UK) for 1 hour in a humidified chamber. Appropriate primary antibodies were applied to the tissue sections overnight at 4°C in a humidified chamber (Table 2.4). Next day, tissue sections were washed three times in PBS (0.05% Tween20) and appropriate fluorophore conjugated secondary antibodies were applied on the sections for an hour at room temperature. Alternatively, biotinylated secondary antibodies were applied on sections for 1 hour at room temperature before the addition of streptavidin conjugated fluorophores for an additional hour (Table 2.4).

In order to amplify the weak signals, amplification was performed using the TSA Biotin System (PerkinElmer LAS, UK). Briefly, after the overnight incubation with primary antibodies only the biotinylated secondary antibody for the antigen whose signal was to be amplified was added onto the sections. After incubation for an hour at room temperature, streptavidin–HRP (1:200 in TNB buffer) was applied to the tissue for 30 minutes followed by an 8 minute incubation with biotinylated TSA (1:100 in amplification buffer). Fluorophore conjugated reagents were used as the final step for the protocol; streptavidin conjugated for the signal to be amplified and appropriate species for the other antigens.

In the case of double immunostaining using goat and rabbit primary antibodies, a sequential protocol was followed in order to avoid cross reactivity of species. Briefly, both primary antibodies were probed overnight at 4°C in a humidified chamber. The following day, a fluorescent a-goat secondary antibody was added on the sections for an hour at

room temperature. After washing the sections three times in PBS (0.05% Tween20), we proceeded with the second immunostain using biotinylated a-rabbit secondary and streptavidin conjugated fluorophore, as described above.

Cell nuclei were stained with DAPI (Vector Laboratories, UK) when required. All slides were mounted using Vectashield Mounting Medium (Vector Laboratories, UK) and imaged using Zeiss 710 or Leica SP8 confocal microscope.

Quantification of co-localisation of fluorescence was performed using an ImageJ plugin kindly provided by Dr.Vasiliki Economopoulos (Prof. Niki Sibson's group, University of Oxford, UK).

1ary antibody	2ary biotinylated antibody (1:100)	2ary fluorescent antibody (1:100)	Streptavidin fluorophore (1:100)	amplification
Iba1 (Abcam ab5076) 1:100	--	a-goat TexasRed or a-goat Dylight 594	--	--
iNOS (M-20) (sc651) 1:100	a-rabbit	--	AMCA	+
Arg1(H-52 sc20150) 1:100	a-rabbit	--	AMCA	+
MRC1 (AbD MCA2235) 1:100	a-rat	a-rat TexasRed	AMCA	--
GFAP (Invitrogen 13-0300 1:200		a-rat TexasRed	Dylight 488	--
NeuN(60) (MAB377) 1:100	a-mouse		Dylight 488	--
KLF4 (NBP2-24749) 1:200	a-rabbit		AMCA	+
CD31(R&D, AF3628) 1:100	a-goat	a-goat TexasRed	Dylight 488	--
CC3 (Asp175) (CST 9661) 1:100	a-rabbit		AMCA	--
GFP (abcam 13970) 1:100	--	a-chicken CF^{TM}488A (Sigma-Aldrich SAB4600031)		--

Table 2.4: List of antibodies used for fluorescent staining. Primary antibodies, suppliers and concentrations are listed. All secondary antibodies and streptavidin fluorophores were supplied from Vector Laboratories (UK), unless stated otherwise.

2.12.2 Immunofluorescence on cells

Cells grown on coverslips and treated appropriately (section 2.3) were fixed in 4% PFA (in PBS, pH7.2) for 10 mins and washed in PBS twice. Cells were permeabilised with PBS Tween20 (0.1%) and blocked for endogenous biotin using the streptavidin/biotin blocking kit (Vector Laboratories, UK). Then, cells were incubated with TNB buffer (PerkinElmer) for 1 hour in a humidified chamber to block non-specific antibody binding. Appropriate primary antibodies [1:100 a-mouse F4/80 Biotin (eBioscience, 13-4801-81), 1:100 a-rat MRC1 (AbD MCA2235)] were applied to the cells overnight at 4°C in a humidified chamber. Next day, cells were washed three times in PBS (0.05% Tween20) and appropriate fluorophore conjugated secondary antibodies (1:100 DyLight 488 Streptavidin antibody, a-rat Texas Red antibody from Vector Laboratories) were applied on the cells for an hour at room temperature. Cell nuclei were counterstain with DAPI (Vector Laboratories, UK).

Chapter 3

Microglial infiltration in an experimental model of breast cancer brain metastasis

3.1 Introduction

As already highlighted in the main introduction, the exact role of the mononuclear phagocytic system, that is to say both resident microglia and peripheral monocytes, has not been comprehensively studied in the context of metastatic cancer to the brain. Histological analysis of autopsy samples from patients with brain metastases suggests that microglia, rather than lymphocytes, are the major immune population activated around the metastatic foci. HLA-DR$^+$ microglia/macrophages infiltrate the intracranial metastatic lesions in the cases of breast, melanoma, small cell lung and non-small cell lung cancers (Berghoff et al, 2013). The histological study of another cohort of patients with breast cancer brain metastasis revealed the presence and close association of CD68$^+$ microglia/macrophages with GFAP expressing astrocytes between clusters of carcinoma cells (Fitzgerald et al, 2008).

Although information derived from clinical samples is of paramount importance for the identification of biomarkers and therapeutic targets, the necessity of studying the metastatic disease at its early stages remains. In the pre-clinical setting, only a few studies have been conducted to investigate the role of peripheral immune cells in brain metastasis. Co-culture of breast cancer cell lines MCF-7 and 410.4 with murine bone marrow derived monocytes has been shown to enhance their invasiveness. Treatment of the co-cultures with an anti-CSF1 antibody, which selectively confers cytotoxicity on myeloid cells, decreased cancer cells' migration nearly to basal levels (Rietkotter et al, 2015). Liu and colleagues employed an *in vivo* mouse model which bears the primary 4T1 mammary cancer, and thus accurately recapitulates the clinical scenario, to assess the contribution of circulating macrophages in the metastasis of 4T1 cells to the brain (Liu et al, 2013). Interestingly, they found that bone marrow derived CD11b$^+$Gr1$^+$ myeloid cells colonise the brain before the migration and

extravasation of 4T1 cancer cells. Their hypothesis that those circulating cells form the pre-metastatic soil in the brain was further confirmed by a functional assay of cell blockade by systemic administration of an anti-Gr1 antibody. As expected, the antibody treatment led to decreased $CD11b^{+}Gr1^{+}$ myeloid cell infiltration of the brain and significantly fewer experimental intracranial metastases.

Microglia, the brain resident population, possibly support tumour cell colonisation as suggested by *in vitro* studies. Rietkotter et al performed the exact same experiments as mentioned above with co-cultures of breast cancer cells and primary murine microglial cells. Anti-CSF1 treatment led to decreased invasiveness of breast cancer cells, although to a lesser degree compared to the primary monocyte and cancer cell co-cultures. Using the co-culture experimental approach, and having previously shown that myeloid cells induce invasiveness of cancer cells via the JNK/Wnt5a pathway, Pukrop et al. observed that inhibition of JNK/Wnt5a signalling by inhibitory peptides significantly reduced breast cancer cell invasion induced by primary microglia (Pukrop et al, 2006; Pukrop et al, 2010). Since those studies lack critical components of the brain microenvironment, the authors performed invasion assays using murine brain slices and further corroborated their findings on the role of microglia in promoting breast cancer cell migration and invasion (Pukrop et al, 2010).

From the aforementioned studies it has emerged that macrophages and microglia play a role in modulating breast cancer cells' behaviour and migration. However, a more comprehensive study of the *in vivo* microglial response to the metastatic outgrowth of breast cancer cells in the brain is lacking. With the latest great advances in understanding macrophage and microglial plasticity and polarisation, it is particularly important to study

the metastatic disease in the brain with a focus on the heterogeneity of resident cells. Glioma-infiltrating microglia have been shown to acquire an M2 alternatively activated phenotype, which possibly accounts for their immunosuppressive effect on the progression of human and murine glioma (Li and Graeber, 2012). In experimental gliomas, tumour infiltrating microglia and macrophages upregulate their M2 molecular signatures in comparison to the M1, notably Arg1, TGFβ, MMP2 and IL-10 expression (Gabrusiewicz et al, 2011; Szulzewsky et al, 2015). However, it is still unclear whether microglia acquire similar phenotypes in the context of secondary cancer to the brain. *In vitro*, microglial cells change their morphology when primed by co-culture with breast cancer cells, but do not seem to adopt an M2 phenotype (Pukrop et al, 2010). Thus, more detailed *in vivo* studies on the functional polarisation of microglia in brain metastasis are needed.

3.2 Aims

Taking into account the aforementioned findings, the primary aims of this chapter are:

1. To determine the spatial and temporal profile of microglial activation in a mouse model of early stage breast cancer brain metastasis
2. To identify classically activated (M1) and alternatively activated (M2) microglia in the metastatic brain
3. To determine the spatial and temporal profile of M1 and M2 microglia in the early stages of breast cancer brain metastasis.

3.3 Methods

For this chapter, the syngeneic 4T1-BALB/C intracerebral model was used. Briefly, 4T1-GFP mammary carcinoma cells were intrastriatally injected to induce experimental metastases (section 2.5.1). Brains were harvested on days 7, 10, 14, 21 or 28 after tumour cell injection and perfusion-fixed. Intracranial tumour volumes were calculated by quantitation of the tumour area (cresyl violet foci) on brain sections 50 µm apart, from the start to the end of the metastatic region (section 2.9). Microglia/macrophage infiltration was assessed by Iba1 IHC using the ABC kit (section 2.8). It should be noted that by referring to microglia throughout this chapter, the mixed microglia/macrophage population is considered given that microglia and macrophages cannot be distinguished by IHC. Microglia infiltration area was quantified on brain sections every 50 µm spanning the metastatic region, as described in section 2.9. The microglial polarisation markers iNOS, COX2, MRC1 and Arg1 were assessed by IHC (table 2.2). Co-registration of sequential immunostained brain sections using Matlab was performed as described in section 2.11. Quantitation of microglial phenotypes using the Matlab method was inclusive of three representative sections from the start, core and end of the 4T1 metastatic regions (one from each site) per animal, unless otherwise stated (Figure 3.1). Immunofluorescence for iNOS and Arg1 positive microglia was performed using the TSA amplification protocol, as described in section 2.12.1.

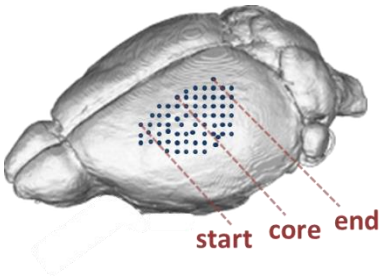


Figure 3.1: Schematic of the brain regions used for the Matlab analysis. Representation of the three distinct areas (in red) of a mouse brain bearing metastatic tumours (in blue) that were included for the Matlab analysis.

3.4 Results

3.4.1 Microglial infiltration in the metastatic brain

For my initial studies, I sought to investigate microglial infiltration in the early stages of metastatic growth in the brain both qualitatively and quantitatively. Ionized calcium binding adaptor molecule 1 (Iba1) was used as a marker of microglial cells and macrophages infiltrating the 4T1-GFP metastatic foci. I performed a 28 day timecourse study of intracerebrally injected 4T1-GFP mammary carcinoma cells and assessed tumour growth and microglial infiltration at days 7, 10, 14, 21 and 28. Initially, I confirmed that the intracranial model consistently yields progressive metastatic growth in the brain (Figure 3.2A, 3.2B). Importantly, I excluded the possibility of sustained inflammation and microglial activation caused by the experimental procedure of the intracerebral microinjection by assessing microglial activation in PBS injected animals. Minimal Iba1 upregulation was evoked in the PBS injected hemispheres at the earliest timepoint studied (day 7) as observed by Iba1 immunohistochemistry and quantitation in comparison to contralateral naïve hemispheres ($p>0.05$; Figure 3.2C).

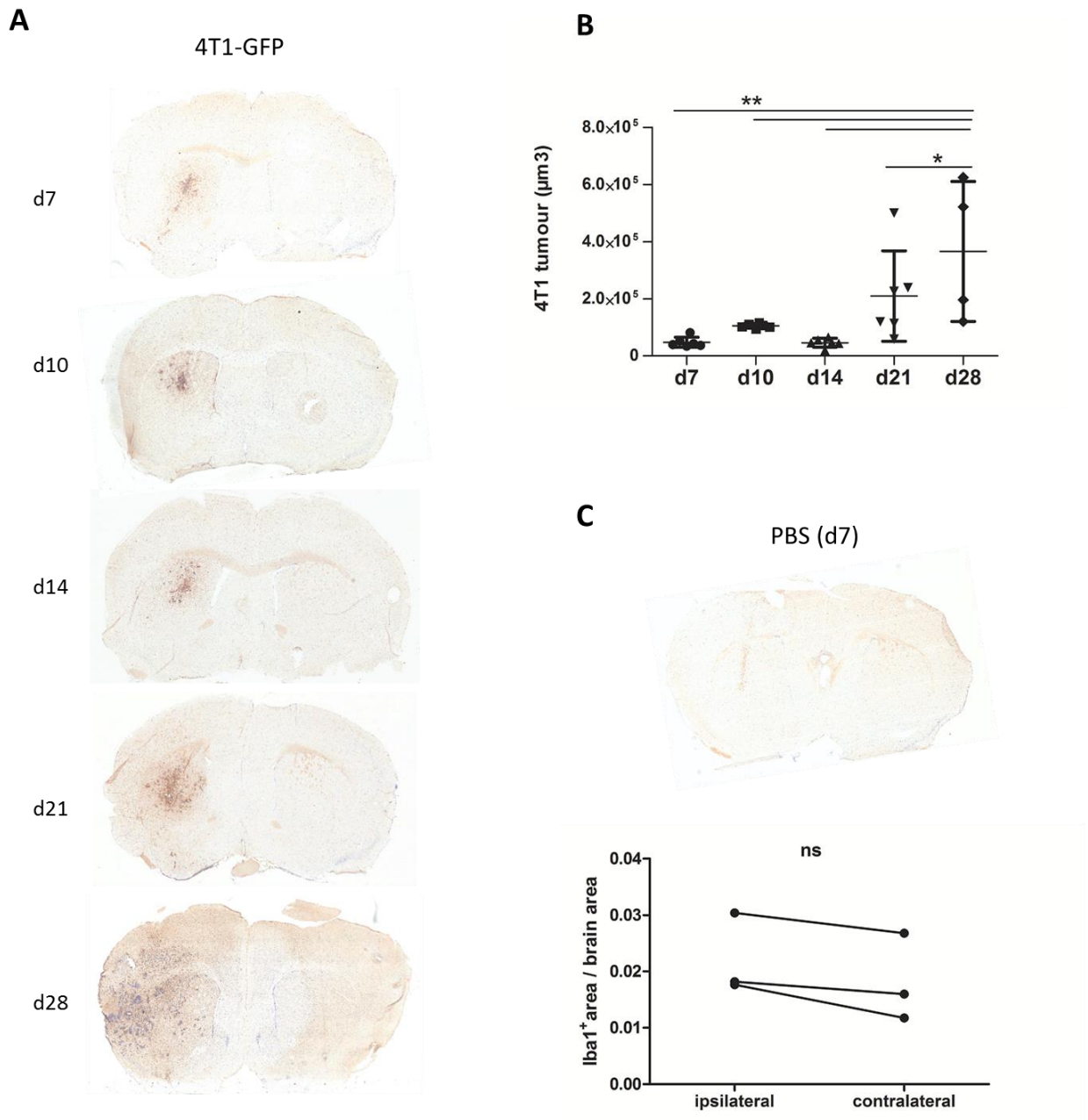
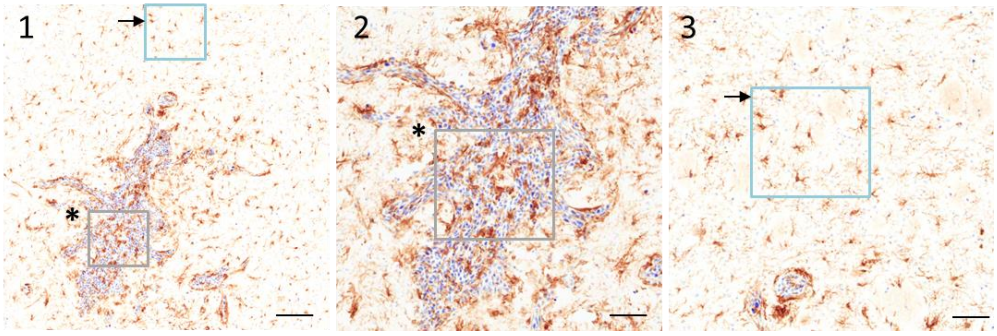


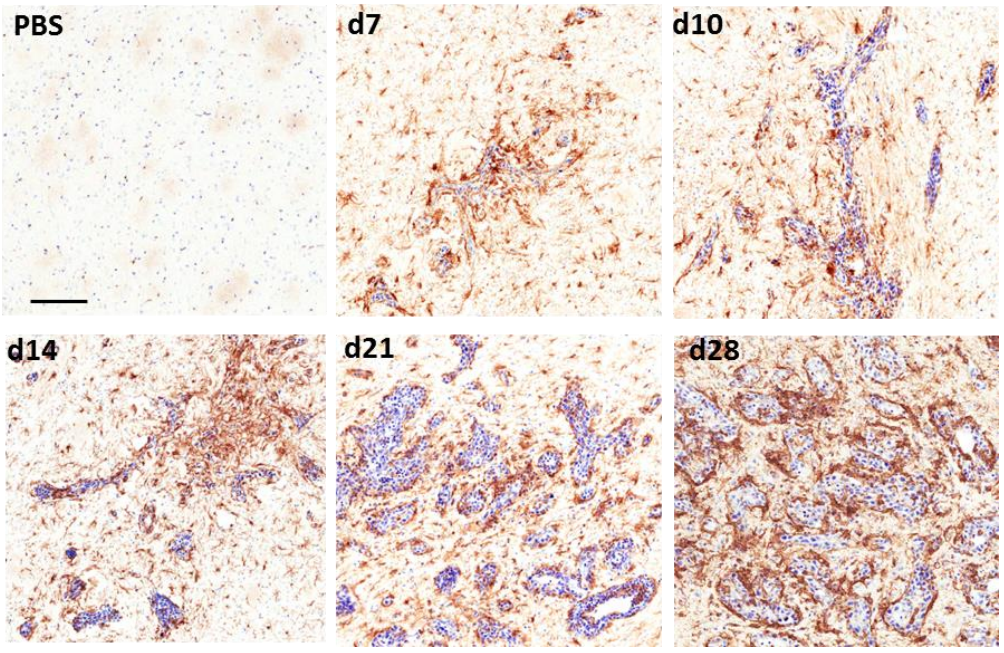
Figure 3.2: Validation of the intracerebral 4T1-GFP model. Progression of intracranial tumour growth as shown by representative images of coronal brain sections from mice injected with $5x10^3$ 4T1 cells and sacrificed at days 7, 10, 14, 21 and 28. (A) Brain sections were immunostained for the microglial marker Iba1 and counterstained with cresyl violet. (B) Quantitation of metastatic foci (cresyl violet) reveals an increase in tumour volumes over time (n=4-6; p=0.0013, one-way ANOVA with Neuman-Keuls multiple comparison test). (C) Intracerebral injection of PBS evokes minimal microglial activation at day 7 as indicated by immunostaining for Iba1 and quantitation of Iba1 expression in the ipsilateral and contralateral hemispheres (n=3, 5 sections per animal; p=0.0683, two-tailed paired t test).

Qualitatively, sustained microglial infiltration of the 4T1-GFP metastatic foci at all time points throughout the 28 day study was observed (Figure 3.3). Iba1^{+} cells were found in close vicinity to the metastatic foci as well as in the wider tumour microenvironment (Figure 3.3A1). Both ramified and amoeboid Iba1 positively stained cells were identified, suggesting that different activation states exist within the tumour microenvironment in the metastatic brain. Qualitatively, cells with amoeboid morphology that could be either microglia or perivascular macrophages (Perry and Teeling, 2013) mostly associated with the 4T1-GFP foci (Figure 3.3A2) while ramified microglia were found both close to the tumour foci and within the broader tumour microenvironment (Figure 3.3A3). Next, I quantified microglial infiltration across the 28 day timecourse by measuring the Iba1 immunostained area (described in section 2.9, Figure 3.3B). Microglial infiltration significantly increased over time (Figure 3.3C) and a strong positive correlation was evident between the Iba1 immunostained area and the volume of the 4T1-GFP lesion (Figure 3.3D).

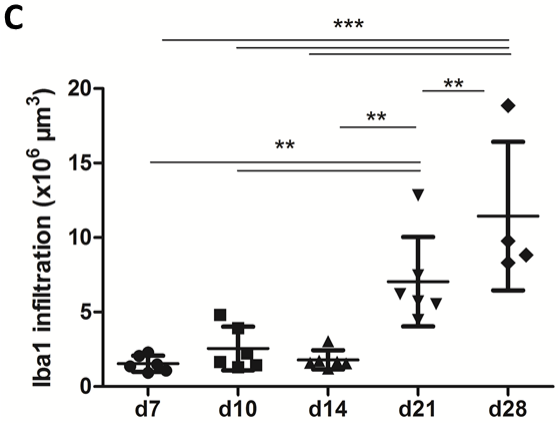
A


1
2
3
*
*

B


PBS
d7
d10
d14
d21
d28

C


***
**
**
**
Iba1 infiltration (x10^6 µm^3)
20
15
10
5
0
d7
d10
d14
d21
d28

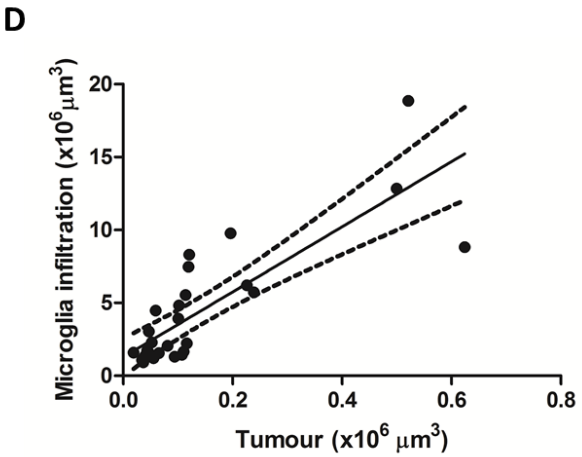
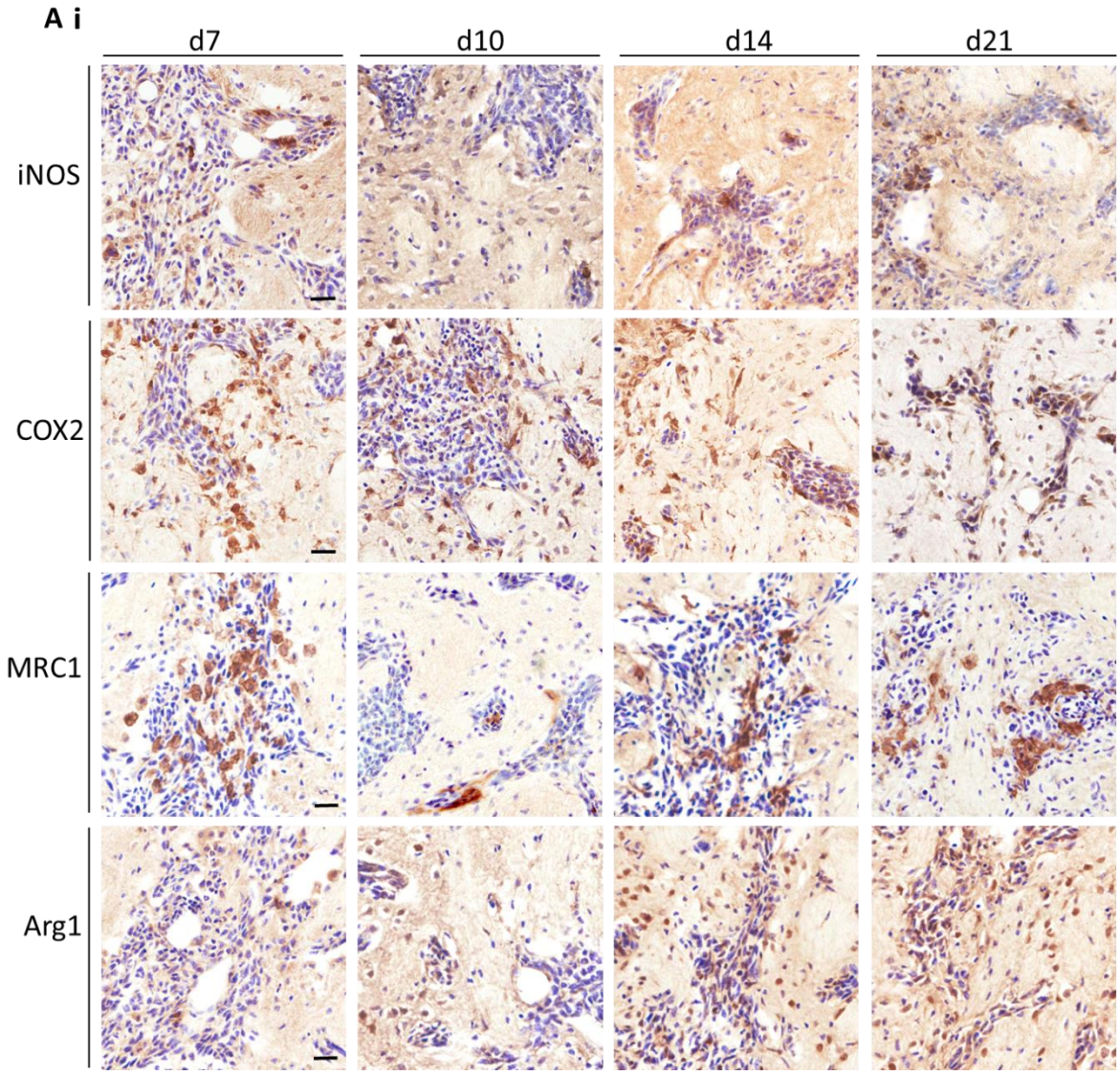


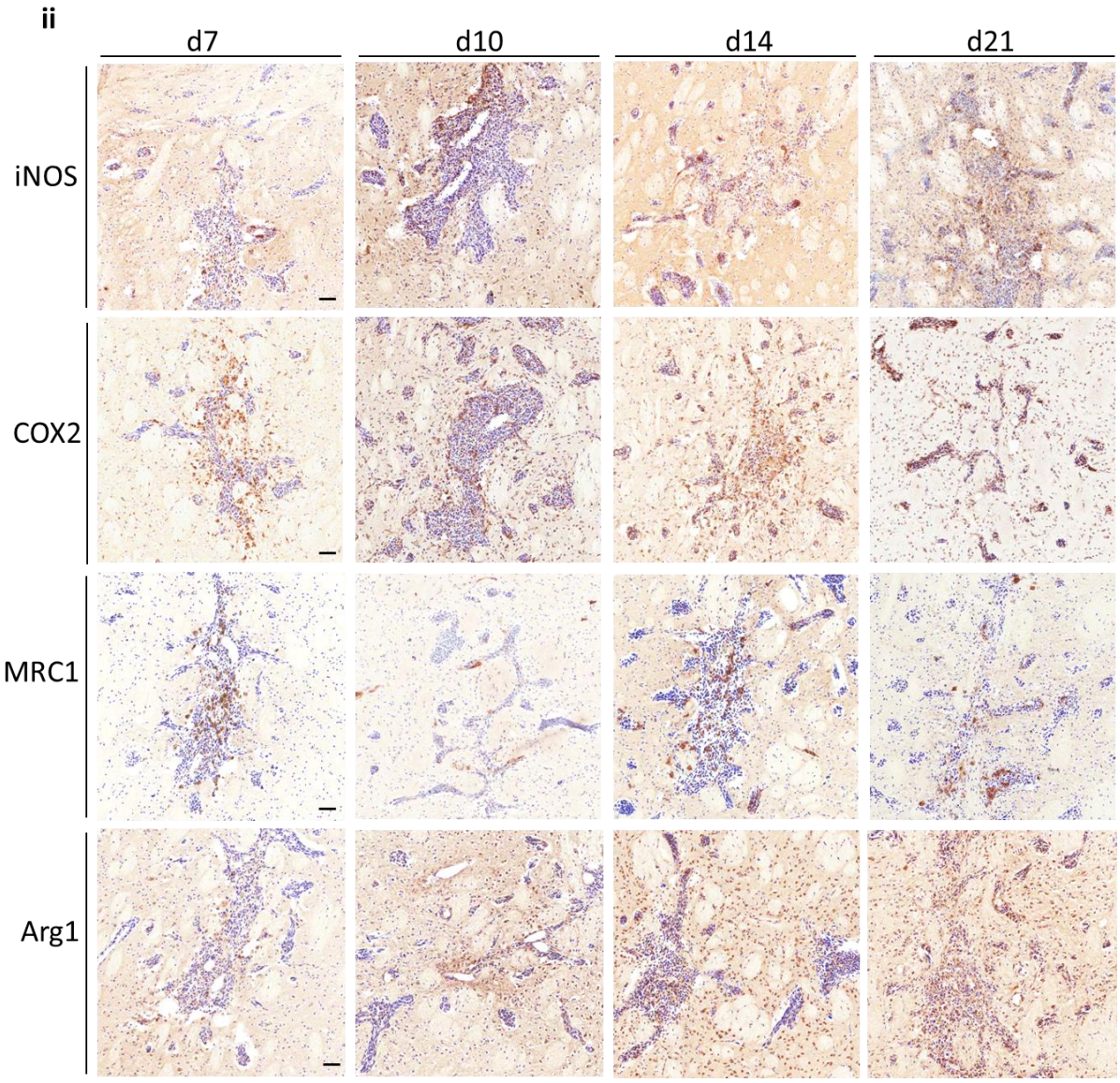
Figure 3.3: Sustained microglial infiltration during the early stages of breast cancer brain metastasis. (A) Iba1$^+$ microglial cells are detected in close association with the tumour foci (cresyl violet) and within the broader tumour microenvironment in the 4T1-GFP metastatic brains, as shown by a representative IHC image of a brain section at day 7 after intracerebral injection of 5x10^3 4T1-GFP cells (A1, scale bar 100 μm; A2 and A3 scale bars 50 μm). (B) Increased expression of Iba1 was detected at days 7, 10, 14, 21 and 28 (scale bars 100 μm). (C) Quantitation of the Iba1$^+$ immunostained area showed a significant increase over time (n=4-6; $p<0.001$, one-way ANOVA with Newman-Keuls multiple comparison test). (D) Pearson correlation plot of microglial infiltration area against tumour volume revealed a strong positive correlation ($R^2= 0.671$).

3.4.2 Expression of M1 and M2 markers in the metastatic brain

Since it is well established that microglia and macrophages can exert different functions in the tumour microenvironment depending on their molecular phenotype, I next investigated the polarisation state of the microglial population infiltrating the 4T1 metastatic foci. Initially, I assessed the expression of M1 and M2 polarisation markers in the brain during the early stages of metastatic growth by IHC. The M1 phenotype markers iNOS and COX2 were expressed in the brain at days 7, 10, 14 and 21 after intracerebral injection of 4T1-GFP cells (Figure 3.4Ai, Aii). Similarly, the M2 phenotype markers Arg1 and MRC1 were also expressed in the metastatic brain at all timepoints (Figure 3.4A). MRC1 and iNOS immunostained cells were usually in close association with the 4T1-GFP foci, while Arg1 and COX2 expression was

also detected within the broader tumour microenvironment (Figure 3.4Aii). All four markers were specifically upregulated in response to brain metastasis as indicated by the lack of expression in ipsilateral and contralateral hemispheres of mice injected intracranially with PBS as control (Figure 3.4B).




ii
d7
d10
d14
d21
iNOS
COX2
MRC1
Arg1

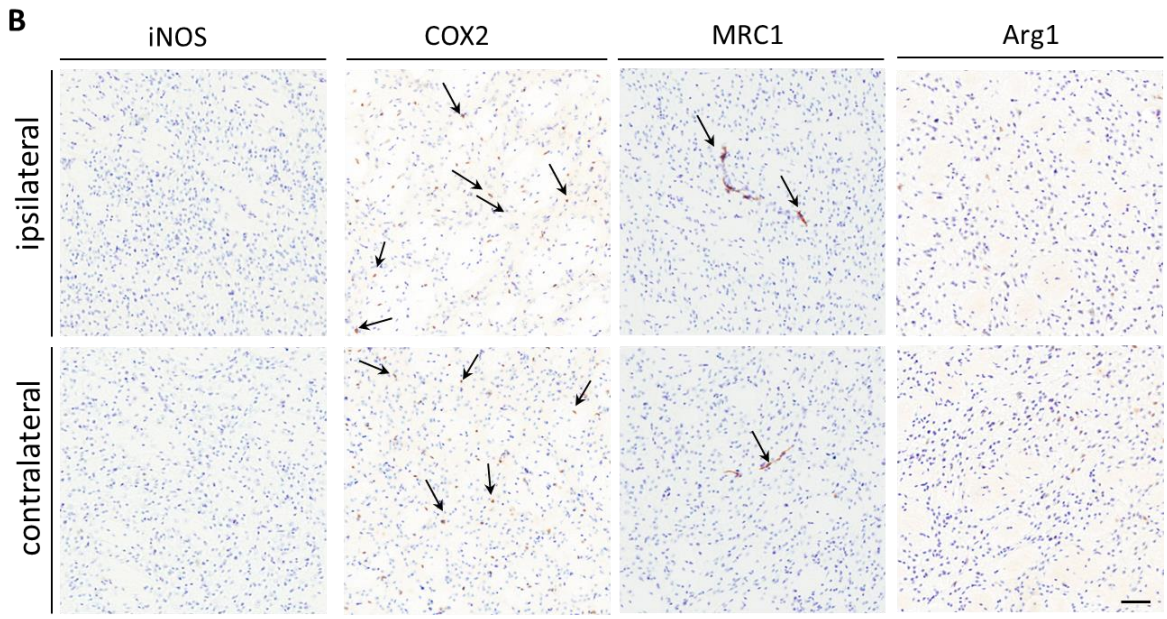


Figure 3.4: **Expression of M1 and M2 markers in the metastatic brain**. Immunohistochemical detection (A) of the M1 markers iNOS, COX2 (rows 1, 2 respectively) and the M2 markers MRC1, Arg1 (rows 3, 4 respectively) at days 7, 10, 14 and 21 after intracerebral injection of $5x10^3$ 4T1-GFP cells. Representative images at high (Ai) and low magnification (Aii). At day 7 after intracerebral injection of PBS, there is negligible expression of the M1 (iNOS, COX2) and M2 (MRC1, Arg1) markers in ipsilateral and contralateral hemispheres (B). Cresyl violet was used as counterstain. Scale bars: 20 µm (Ai), 50 µm (Aii, B).

3.4.3 M1 and M2 microglia in the metastatic brain

The polarisation markers assessed showed robust expression at all timepoints studied. However, they are not exclusively expressed by microglia and macrophages. Rather, other types of brain resident cells are sources of Arg1, iNOS and COX2. Thus, I employed double immunofluorescence to identify $Iba1^+$ microglial cells bearing an M1 or M2 phenotype. Arg1 was used as the prototype marker for alternative M2 phenotype whereas iNOS for the classical M1 phenotype. Microglia expressing Arg1 and microglia expressing iNOS were identified in the murine metastatic brain at days 7, 14 and 21 after intracerebral injection of 4T1-GFP mammary carcinoma cells (Figure 3.5). Both Arg1 and iNOS were expressed by

other cells in the tumour microenvironment, most evidently Arg1 (Figure 3.5). Classically activated M1 and alternatively activated M2 microglia were in close vicinity to the 4T1-GFP metastatic foci at days 7, 14 and 21 after intracerebral injection of the tumour cells.

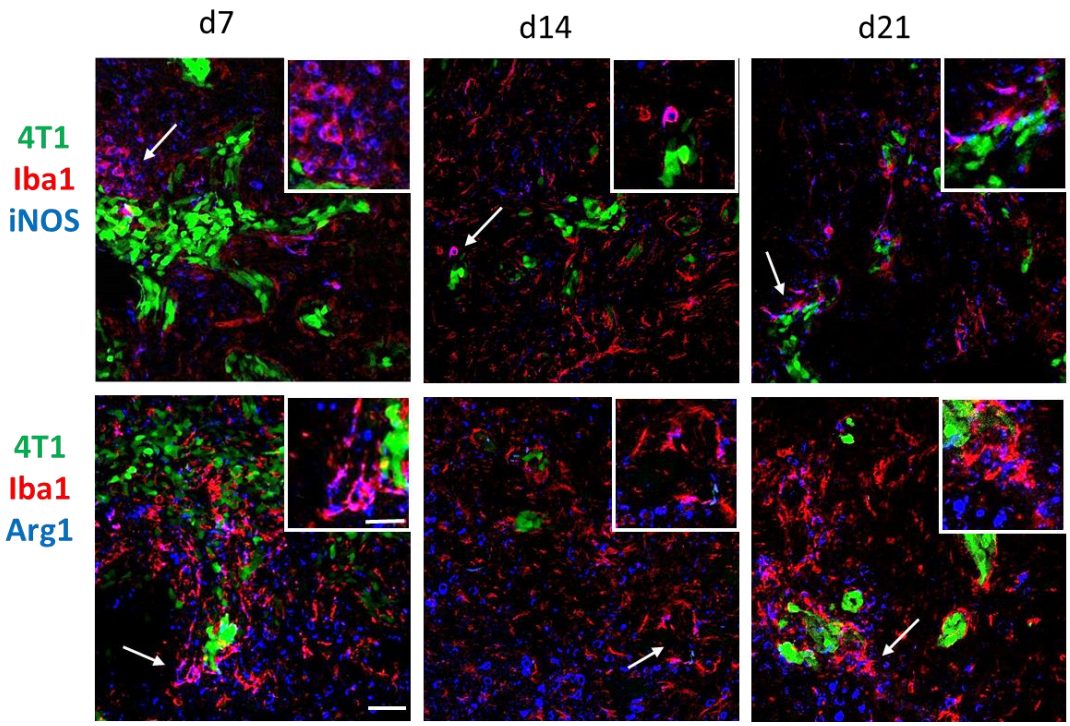
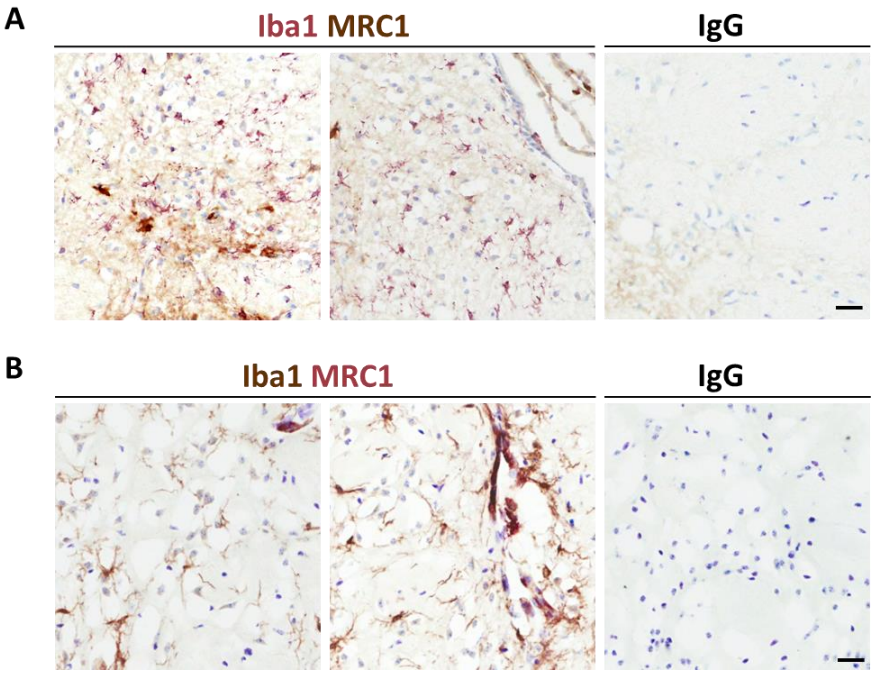


Figure 3.5: Detection of M1 and M2 microglia in the metastatic brain by immunofluorescence. Double immunofluorescent staining for the Iba1 microglia marker with iNOS for the M1 phenotype (top panel) or Arg1 for the M2 phenotype (bottom panel) at days 7, 14, 21 after intracerebral injection of $5x10^3$ 4T1-GFP cells. Iba1 was detected with Texas Red, iNOS and Arg1 signals were amplified and detected with blue AMCA. Arrows indicate co-localisation of markers. Scale bar 50 µm. Arrows show areas of co-localisation, which are shown magnified in the insets. Scale bars 20 µm (A), 50 µm (B) or 25 µm (B insets).

Double immunohistochemistry was also employed as a complementary approach to identify double labelled microglia in the murine brain. Horseradish peroxidase and alkaline phosphatase based immunodetection (as described in section 2.10) was assessed in an experimental murine model of CNS inflammation, as a proof-of-principle experiment (Figure

3.6A, B). Intracerebral injection of IL4 induces an inflammatory response with an M2 molecular signature, including upregulation of MRC1 expression. Using double IHC for Iba1 and MRC1, double labelled cells were difficult to identify, although single labelled cells for either Iba1 or MRC1 were present on the same brain section. In a similar approach, double IHC for Arg1 and Iba1 in lung tissue of naïve mice clearly showed specific individual stains on the same section, but again not evidently double labelled cells (Figure 3.6C). Owing to the lack of clarity in the results, this approach was not pursued further in the metastasis model.



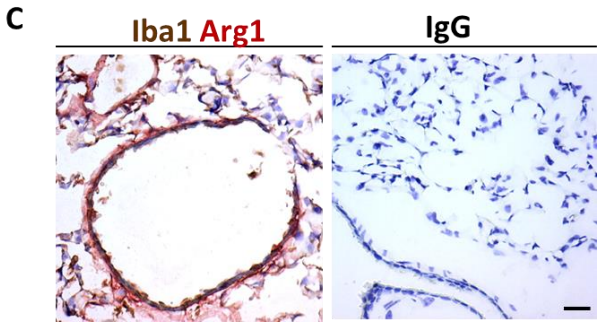


Figure 3.6: Double immunohistochemistry to identify M2 microglia and macrophages. Double HRP immunostaining (A, B) or HRP and AP immunostaining (C) in an IL-4 induced neuroinflammatory model or naïve mouse lung, respectively. Immunostaining for the microglia/macrophage marker Iba1 and the M2 phenotype markers MRC1 (A, B) or Arg1 (C) was performed using DAB and Nova Red peroxidase substrates (A, B) or Red phosphatase substrate (C). In all cases, IgG controls for both stains show no signal. Scale bar 20 µm.

Consequently, an alternative method to identify and quantify M1 and M2 microglia in the metastatic brain using IHC and Matlab was developed (described in section 2.11) and applied to our intracerebral 4T1-GFP model. Sequential 10 µm thick brain cryosections were immunostained for Iba1 and the M1 polarisation markers iNOS and COX2 (Figure 3.7A) or the M2 polarisation markers MRC1 and Arg1 (Figure 3.7B) using the peroxidase DAB protocol (section 2.8) and co-registered for pixel co-localisation.

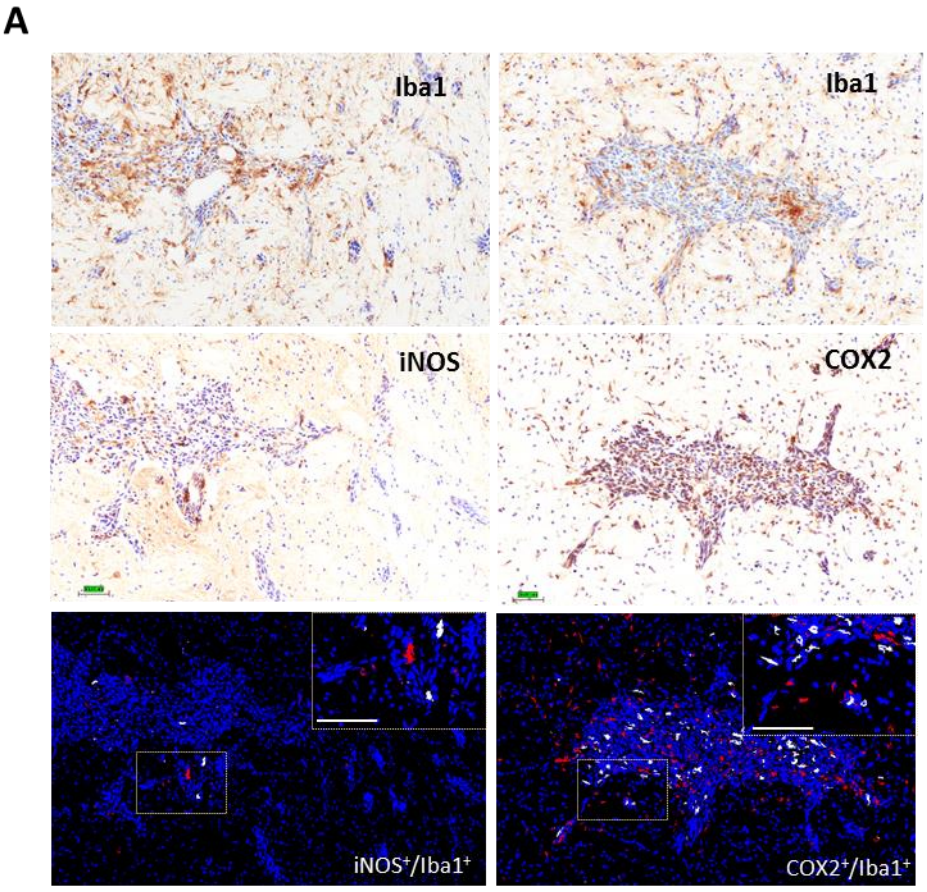
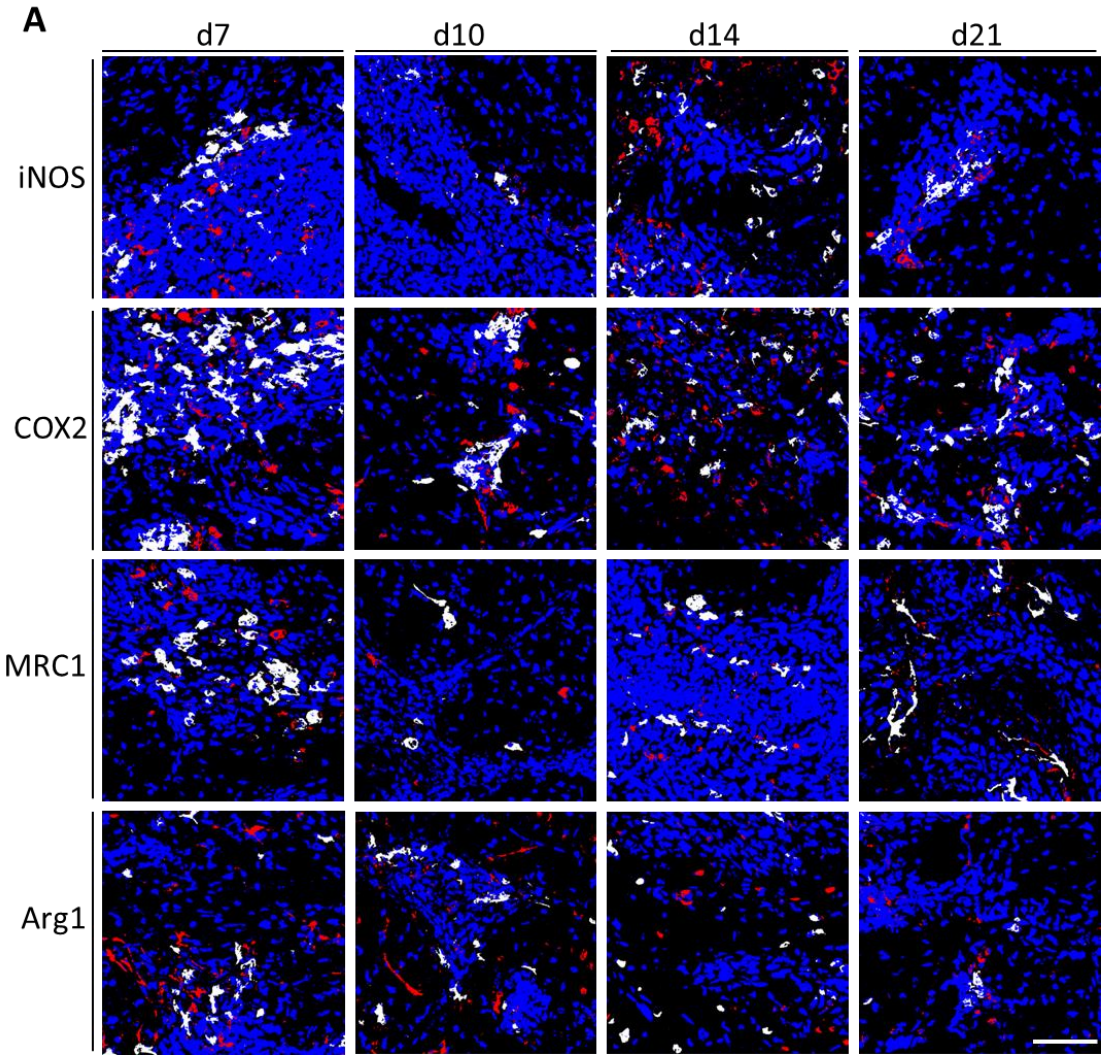

A
Iba1
Iba1
iNOS
COX2
iNOS+/Iba1+
COX2+/Iba1+
B
Iba1
Iba1
MRC1
Arg1
MRC1+/Iba1+
Arg1+/Iba1+

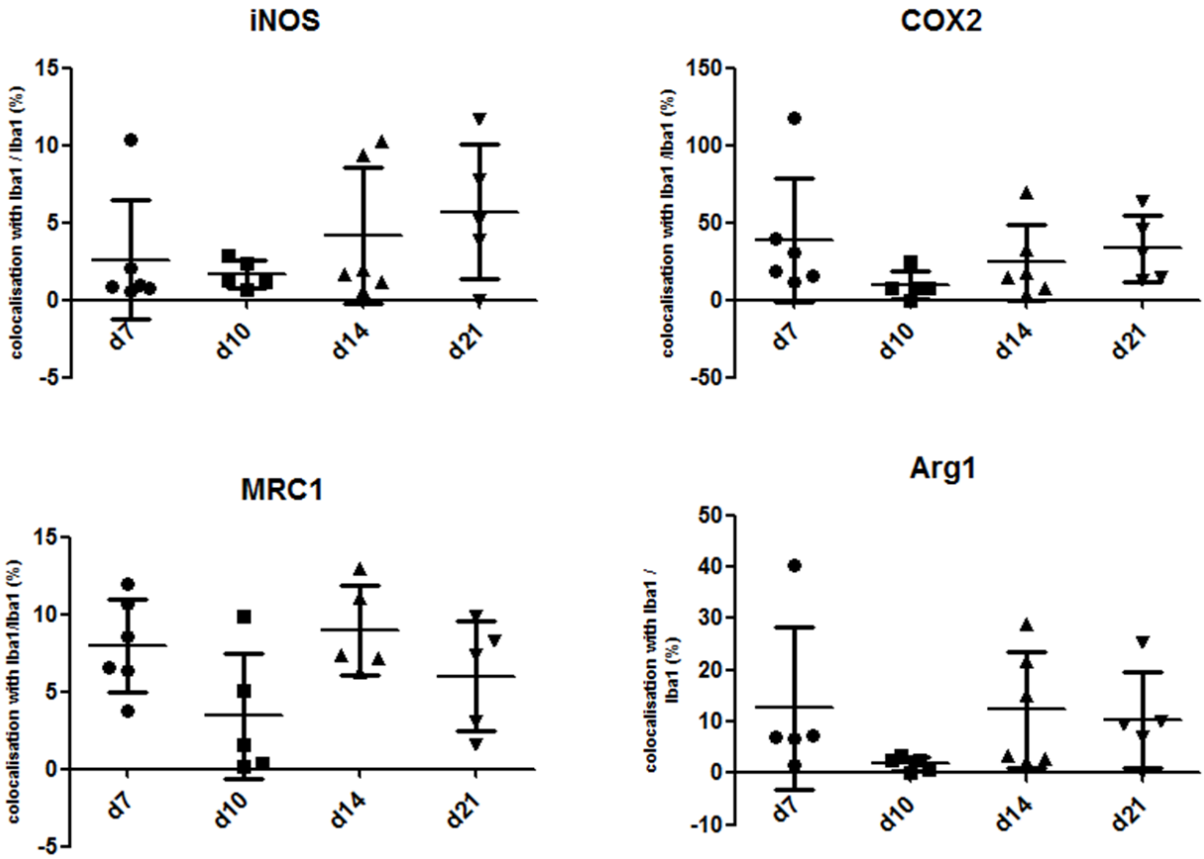
Figure 3.7: **Detection of M1 and M2 microglia in the metastatic brain using Matlab**. Iba1 immunostained sections (top panels) were co-registered with sequential sections immunostained for (A) M1 (iNOS, COX2) or (b) M2 markers (MRC1, Arg1) (middle panels). Matlab generated images (bottom panels) show co-localised pixels in white, tumours in blue, M1/M2 markers in red. Representative images from day 7 after intracerebral injection of $5x10^3$ 4T1-GFP cells. Scale bars 100 μm, 50 μm (insets).

Using the approach depicted in Figure 3.7, the spatiotemporal expression of M1 and M2 microglia during the early stages of brain metastasis was analysed (Figure 3.8A). M1 microglia were identified as $iNOS^+Iba1^+$ or $COX2^+Iba1^+$ cells while M2 microglia as $MRC1^+Iba1^+$ or $Arg1^+Iba1^+$ cells. Populations of M1 and M2 cells were found in close association with the tumour foci and within the microglial infiltration area at days 7, 10, 14 and 21 after intracerebral injection of 4T1-GFP cells (Figure 3.8A). Quantitation of the co-localisation of each marker with Iba1 within the microglial activation area and on representative sections from the start, core and end of the 4T1 tumours revealed populations of both M1 and M2 microglia without significant differences between timepoints (Figure 3.8B). Further quantitative analysis of the core of the tumours showed significant increase in $iNOS^+$ and $Arg1^+$ microglia closely associated with the metastatic tumours at day 21 ($p<0.05$; Figure 3.8C). However, at day 21, $iNOS^+$ microglia maintained similar abundance with $Arg1^+$ microglia at the core of the tumours ($p=0.1367$). Importantly, spatial analysis of the broader microglial activation area at the core of the tumours revealed high percentages of polarised microglia, both M1 and M2, in close association with the metastatic foci compared to the broader tumour microenvironment (Figure 3.8D). More than 50% of $MRC1^+$ and $iNOS^+$ microglia were associated with the 4T1 foci at days 7, 14 and 21 after intracerebral injection. COX2 expressing microglia also presented with affinity for the metastatic tumours, as 50% of $COX2^+$ cells or more were associated with 4T1 foci at all

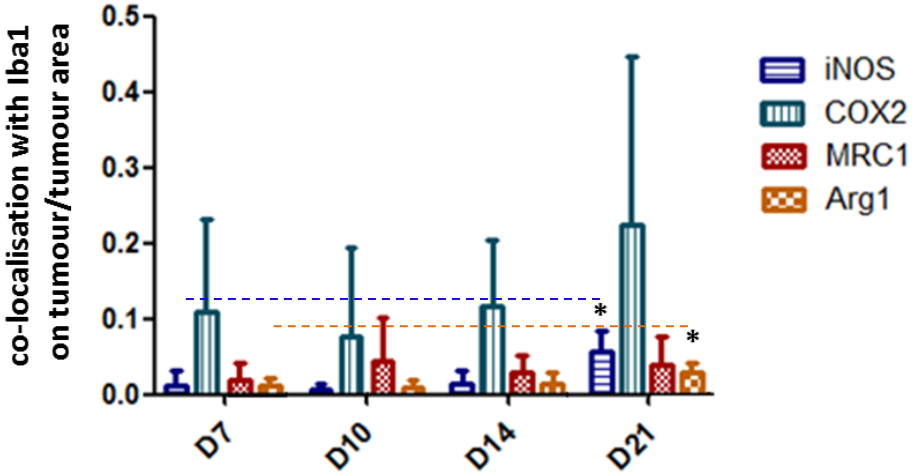
timepoints studied while Arg1^{+} M2 microglia were found both in close vicinity to the metastatic tumours and in the wider tumour microenvironment .



B


iNOS
colocalisation with Iba1 / Iba1 (%)
15
10
5
0
-5
d7
d10
d14
d21
COX2
colocalisation with Iba1 /Iba1 (%)
150
100
50
0
-50
MRC1
colocalisation with Iba1/Iba1 (%)
Arg1
colocalisation with Iba1 / Iba1 (%)
50
40
30
20
10
-10

C


co-localisation with Iba1 on tumour/tumour area
0.5
0.4
0.3
0.2
0.1
0.0
D7
D10
D14
D21
iNOS
COX2
MRC1
Arg1
*
*

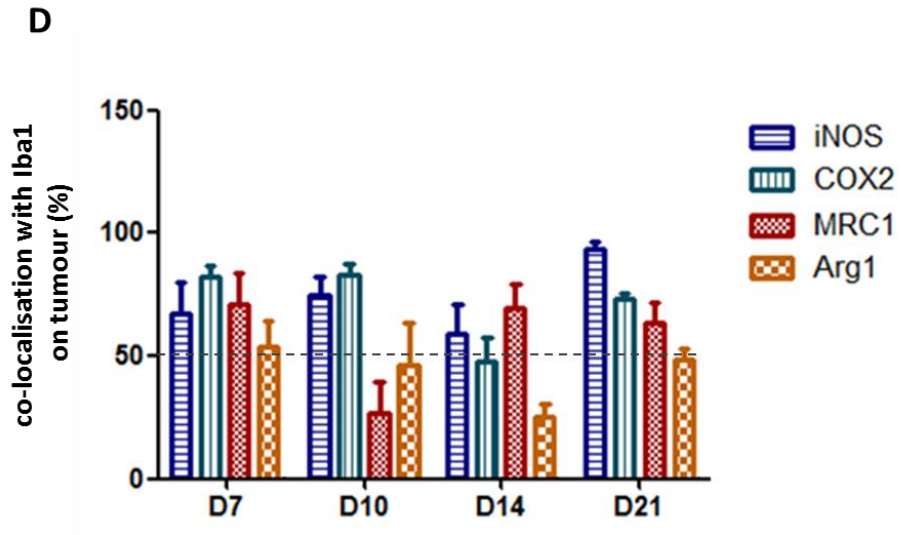


Figure 3.8: Spatiotemporal expression of M1 and M2 microglia in the metastatic brain. (A) Representative Matlab generated images of M1 ($iNOS^+$, $COX2^+$) and M2 ($MRC1^+$, $Arg1^+$) microglia ($Iba1^+$) at days 7, 10, 14 and 21 after intracerebral injection of $5x10^3$ 4T1-GFP cells (scale bar 50 µm). (B) Quantitation of co-localised pixels for M1 and M2 markers with Iba1 within the microglial activation area, normalised to total Iba1 pixels, from 3 representative brain sections spanning the metastatic region (start, core, end) (n=4-6). (C) Quantitative analysis of co-localised pixels for M1 and M2 markers with Iba1 on the tumours at the core of the metastatic regions, normalised to the tumour area ($p<0.05$ for iNOS and Arg1, one-way ANOVA with Newman-Keuls multiple comparison test between timepoints for each marker; $p=0.1367$, two tailed unpaired t-test for iNOS and Arg1 at day 21) or (D) as percentage of total co-localised pixels within the microglia activation area.

3.5 Discussion

Previous work conducted in our laboratory has demonstrated microglial activation in response to experimental breast cancer brain metastasis (O'Brien et al, 2014). In this chapter an intracerebral model of breast cancer brain metastasis was used in order to further investigate the role of microglial cells, the brain resident macrophages, in the early stages of the metastatic outgrowth. For the intracerebral model, fine glass capillaries (70 µm in diameter) were used for microinjection of cancer cells orthotopically into a defined brain area, the striatum. This model has been previously shown to elicit minimal inflammation

caused by the injection itself (DPhil thesis, Emma R. O'Brien). In addition, the data on microglial activation, as assessed by Iba1 expression, in PBS injected brains further support the suitability of the intracerebral model as a surrogate of non-invasive metastatic models. At day 7 after intracranial injection of PBS minimal microglial activation was observed, as compared to naïve contralateral hemispheres, which decreased rapidly after that timepoint (data not shown). Most importantly, the intracranial model has been shown to recapitulate the widely used intracardiac model of brain metastasis where cancer cells are injected into the left cardiac ventricle and disseminate haematogenously to the brain (Soto et al, 2014). Importantly, 4T1-GFP cells intracerebrally injected into the brain show vascular co-option and present with local invasion of the brain parenchyma (Carbonell et al, 2009). In our hands, 4T1-GFP mammary carcinoma cells intracerebrally injected also show vascular co-option and local invasion of the parenchyma, a characteristic that becomes more evident with time over a 28 day study (Figure 3.3B).

In our studies microglial cells and microglial activation were identified using an antibody against Iba1. Iba1, also known as allograft inflammatory factor 1 (AIF1), is a cell surface marker commonly used to identify microglia and macrophages. Iba1 is not expressed by neurons, astrocytes or oligodendrocytes and is thus commonly used in immunohistochemical studies to specifically detect microglial cells in mouse and rat brains (Ito et al, 1998). Iba1's involvement in membrane ruffling and phagocytotic ability of microglial cells is dependent on calcium induced cell signalling pathways (Ohsawa et al, 2000). Thus, Iba1 is often considered as a functional marker. Importantly, microglia activated by experimental facial nerve axotomy or cerebral ischemia show upregulation of Iba1 expression (Ito et al, 1998; Ito et al, 2001). In accordance with those *in vivo* studies of CNS

inflammation, I observed increased Iba1 expression in the mouse metastatic brain compared to PBS injected brains. Using DAB IHC both ramified and amoeboid Iba1$^+$ immunostained cells were evident around the 4T1-GFP metastatic foci and within the broader tumour microenvironment (Figure 3.3A). The pleomorphic nature of microglia has been reported in other experimental models of brain pathology. For instance, similar findings are described for a mouse model of cerebral ischemia, where hyper-ramified and de-ramified microglial cells comprise the inflammatory cellular milieu at the site of injury and around the site of injury, as well as post-reperfusion (Morrison and Filosa, 2013). Ramified and amoeboid microglia also infiltrate experimental gliomas (Gabrusiewicz et al, 2011). Interestingly, there appears to exist a pattern of site specific infiltration of morphologically distinct cells in experimental brain tumours. Gabrusiewicz et al observed amoeboid microglia in association with glioma cells and ramified microglia in the tumour microenvironment (Gabrusiewicz et al, 2011). In the 4T1 model of brain metastasis, amoeboid cells (microglia or perivascular macrophages as discussed above) are also associated with the tumour foci whereas ramified microglia exist within the broader tumour microenvironment. Those morphologically distinct cells may account for differential functions within the neoplastic brain since it is known that ramified and primed microglia have different transcriptional profiles (Parakalan et al, 2012). However, the potentially different molecular profiles of microglia associated with the 4T1-GFP foci and microglia within the Iba1$^+$ immunostained area were not investigated as part of this thesis.

Irrespectively of the morphology of microglia, I observed sustained microglial infiltration of the 4T1-GFP metastatic foci during a 28 day timecourse study by quantifying the Iba1$^+$ immunostained area. Although absolute numbers of cells in the lesioned brain are often

presented in the literature, quantitation of the microglial immunostained area provides a robust and accurate method of assessing the microglial response under experimental conditions (Donnelly et al, 2009). Thus, the strong positive correlation between the $Iba1^{+}$ immunostained area with the intracranial tumour burden I observed corroborates the concept that microglial cells are important effectors of the inflammatory response during the early stages of brain metastasis.

Given that microglial cells are versatile and acquire M1 and M2 phenotypes, like macrophages, we investigated the polarisation of microglia in experimental brain metastases. Using the intracerebral 4T1 metastatic model and immunohistochemical approaches, pro-inflammatory (M1) and anti-inflammatory (M2) microglial cells were identified in the metastatic brain. A Matlab based approach for co-registration of sequential IHC images was developed and used to quantify M1 and M2 microglia within the Iba1 immunostained area around the experimental 4T1 metastases. Although a similar approach for IHC co-registration has not been described in the literature, autoradiography and microscopy images from sequential tissue sections have been accurately co-registered using a method based on Matlab (Axente et al, 2011). However, co-registration of small immunostained tissue areas, for instance individual cells, rather than broader areas on sequential sections might be a limitation of the current method. Given the size of brain macrophages/microglia cell body (up to 10 μm; Perry et al, 1985) and the thickness of the brain tissue used for IHC and co-registration (10 μm), it is rational to expect that a high proportion of cells will not be captured in both adjacent immunostained sections. Thus, methods of fluorescent co-localisation of markers of the same section, as already presented

in this chapter, could be employed in order to validate the quantitative data on M1 and M2 microglia.

Temporally, $Arg1^+$ and $MRC1^+$ M2 microglia maintained their levels across the timecourse study throughout the entire metastatic region, as did $iNOS^+$ M1 cells. Although it has been clearly shown that both M1 and M2 cells exist in the metastatic brain, the possibility that microglia acquire one phenotype bearing both M1 and M2 characteristics cannot be excluded since triple immunostaining was not performed. Microglial heterogeneity in this model could be further investigated by assessing the simultaneous expression of the investigated M1 and M2 markers by individual microglial cells as well as the expression levels of M1 and M2 markers by microglia using PCR of flow cytometry. To our knowledge, there is only one paper recently published examining the polarisation of metastasis associated macrophages in the murine brain (Rippaus et al, 2016). Using flow cytometry on dissociated tissue bearing parenchymal 4T1 metastases, Rippaus and colleagues identify M2 cells as MRC1 and Arg1 positive cells and M1 cells using iNOS as biomarker. The authors describe expression of both M1 and M2 markers similarly to what we observed for microglia in the 4T1 metastatic region using the IHC/Matlab method (Figure 3.8B). Overall, low abundance of both M1 and M2 microglia was observed at the timepoints studied. A decrease in microglial polarisation, evident at day 10, indicates that further analysis at later timepoints, for example at day 28 of the intracerebral 4T1 model when microglial activation is evidently robust, is warranted to provide more insights into the dynamics of the microglial phenotypes in response to brain metastasis.

COX2 was also used as another biomarker for the M1 phenotype since COX2 is upregulated in M1 polarised cells (Martinez et al, 2006; Murray and Wynn, 2011; Chhor et al, 2013).

$COX2^+$ microglia outnumber $iNOS^+$ and M2 microglia by at least 3 fold. Although COX2 appears to be a robust polarisation marker in the metastatic brain, it should be noted that COX2 is expressed at basal levels in the striatum of sham operated (Figure 3.4B) and naïve animals (Font-Nieves et al, 2012). COX2 is considered to be the inducible form of the COX isoenzymes, however it is expressed at low abundance in the rat brain by microglia and astrocytes (Strauss et al, 2000; Font-Nieves et al, 2012). Unlike COX2, there was almost undetectable expression of Arg1, iNOS and MRC1 by immunohistochemistry in the striatum of sham injected or naïve brains. In support of our findings, undetectable levels of Arg1 and MRC1 proteins in the striatum of mice injected with saline intracerebroventricularly have been previously reported (Pepe et al, 2014).

Spatially, no obvious site-specific infiltration of M1 and M2 microglial cells was evident in the metastatic brain. For instance, Turtzo and colleagues reported a pattern of M1 and M2 microglia/macrophage infiltration after experimental brain traumatic injury. According to their studies, M1 cells were located in the necrotic area of the lesion, while M2 cells surrounded the lesion (Turtzo et al, 2014). Clinical specimens of NSCLC biopsies also revealed a pattern of M1 and M2 macrophage infiltration, with the former predominantly found in the adjacent non-tumour tissue, while the latter population correlated with the tumour tissue (Almatroodi et al, 2016). In our model, M1 and M2 cells were located both in close vicinity to the metastatic foci and within the broader tumour microenvironment. However, analysis of the core of the tumours, where the number of metastatic foci is higher than the edges, revealed that $iNOS^+$ microglia presented with higher affinity for the metastatic tumours compared to $Arg1^+$ microglia. $Arg1^+$ cells are anti-inflammatory and trophic for tumours. Since both $iNOS^+$ and $Arg1^+$ microglia significantly increase at the latest timepoint,

the finding that $Arg1^+$ microglia are also present within the wider tumour microenvironment and not only in close vicinity to the tumours, like $iNOS^+$ cells, might explain the spread and progression of micrometastases in our model.

In conclusion, using the intracerebral breast cancer brain metastasis 4T1 model I observed sustained microglial infiltration of the 4T1 tumour foci at the early stages of metastatic outgrowth in the brain. Moreover, using iNOS or COX2 to identify M1, and Arg1 or MRC1 to identify M2 microglia, respectively, I identified pro-inflammatory and anti-inflammatory microglial cells within the tumour microenvironment and in close association with the metastatic foci. Although I did not perform triple immunostaining to identify microglial cells bearing both M1 and M2 pheontypes in the metastatic brain, I believe this might be a plausible scenario given that microglial and macrophage polarisation consists of a dynamic equilibrium *in vivo* (Sica and Mantovani, 2012, Gabrusiewicz et al, 2016). Importantly, microglia were not significantly skewed to either phenotype in brain metastasis. Expression of both pro-inflammatory M1 and anti-inflammatory M2 profiles by microglia was evident in the early stages of metastatic outgrowth, which might account for tumour progression. My findings corroborate our hypothesis that microglia are important effectors of the inflammatory response to brain metastasis.

Chapter 4

In vivo depletion of MRC1^{+} microglia in the mouse metastatic brain

4.1 Introduction

As cellular effectors of inflammation and innate immunity, macrophages and microglia are thought to be important modulators of disease progression (Wynn et al, 2013). Macrophage depletion from the complex *in vivo* environment can be challenging but its application in pre-clinical rodent models has shed light on the biology of numerous diseases including cancer, cardiovascular and neurological conditions. Commonly used approaches involve genetic targeting of the myeloid specific promoters, such as CD11b. For instance, systemic depletion of macrophages has been reported in a mouse strain of CD11b promoter mediated expression of the human diphtheria toxin receptor (designated CD11b-DTR) upon administration of the toxin. Murine cells are naturally resistant to the toxin, thus this method allows selective targeting of CD11b positive cells (Cailhier et al, 2005). Inducible depletion of myeloid cells and macrophages using the CD11b-DTR system has been successfully employed in preclinical cancer models and provided mechanistic knowledge about their contribution to primary and metastatic cancer development (Qian et al, 2009; Liu et al, 2011; Lim et al, 2015). Similarly, macrophage and microglial depletion has been achieved in transgenic mice expressing the herpes simplex virus thymidine kinase under the control of the CD11b promoter (CD11b-TK). In those mice, myeloid specific depletion is possible by administration of ganciclovir (Gowing et al, 2006). Researchers have employed the CD11b-TK-ganciclovir model to deplete microglia and macrophages in experimental models of glioma and ischemic stroke (Galarneau et al, 2007; Lalancette-Hébert et al, 2007).

In recent years, another tailored method for systemic and region specific *in vivo* macrophage depletion that does not require time consuming genetic manipulation and

breeding of mice has been used to unravel macrophage function in disease (Van Rooijen and Hendrikx, 2010). First introduced by Van Rooijen, the clodronate liposome method exploits the unique phagocytotic ability of macrophages and macrophage-like cells (Van Rooijen and Van Nieuwmegen, 1984). Clodronate is a non-nitrogenous bisphosphonate drug known to induce cell apoptosis through its conversion to a non-hydrolysable ATP-like metabolite (AppCCl2p) and, thus, interference with ATP dependent cell metabolism (Lehenkari et al, 2002). Liposome encapsulated clodronate can be delivered intracellularly via endocytosis. Inside the cells, the liposomes' lipid bilayers are disrupted by the action of lysosomal phospholipases and released clodronate is metabolised to its cytotoxic analogue (Figure 4.1) (Van Rooijen et al, 1996). Thus, cell apoptosis is induced selectively and rapidly. This macrophage "suicide" approach has been used in *in vivo* models of cancer and other inflammation related conditions (Allavena and Mantovani, 2012; Van Rooijen and Henrikx, 2002). For instance, macrophage depletion with clodronate liposomes reduced tumour burden in a mouse model of chemically induced lung adenocarcinoma (Fritz et al, 2014). Similarly, another team observed reduced breast cancer cell growth and metastatic potential in mice treated with clodronate liposomes (Qian et al, 2009).

Following the unravelling of the phenotypic and functional diversity of distinct macrophage subsets, approaches to specifically target cell subpopulations have been a hot topic of research lately. Elaborate experimental methods, based on the aforementioned genetic and suicide techniques, have been described in the literature for *in vivo* and cell subset specific depletion. For example, Coffelt and colleagues describe the depletion of Tie2 positive macrophages in Tie2-thymidine kinase transgenic mice upon ganciclovir administration and its effect on various tumour models (Coffelt et al, 2011). In

a mouse model of endotoxemic lung injury, depletion of CD206 positive cells was achieved by administration of the diphtheria toxin in CD206-DTR transgenic mice (Kambara et al, 2015). CD206 or MRC1 is a phenotypic marker of M2 polarised cells, thus the authors describe M2 macrophage depletion in experimental lung injury and show increased neutrophil infiltration and exaggerated lung inflammation upon M2 macrophage depletion. *In vivo* targeting of M2 cells has been recently described in an experimental model of brain pathology using the clodronate liposome method. Miron and colleagues employed the mannosylated version of clodronate liposomes, that is to say mannose coated liposomes, to specifically deplete MRC1 positive M2 microglia and macrophages in mouse brains (Miron et al, 2013).

In the tumour microenvironment, macrophages acquire an alternative pro-tumourigenic phenotype (the M2) which promotes tumour expansion and invasion (Sica et al, 2006). Thus, tumour associated M2 macrophages could be promising targets for anticancer strategies. However, to our knowledge specific depletion of M2 cells in preclinical cancer models has not been reported. One study reports M2 macrophage depletion using clodronate liposomes, although this correlation is probably due to the strong M2 polarisation of tumour associated macrophages in the relevant cutaneous T-cell lymphoma model (Wu et al, 2014). Given that both M1 and M2 microglia are evident in our preclinical model of breast cancer brain metastasis and that the exact role of M2 cells in the brain microenvironment is not well studied, the overall aim of this chapter was to determine the effect of M2 cell depletion in the metastatic brain employing the mannosylated clodronate liposome method (Figure 4.1).

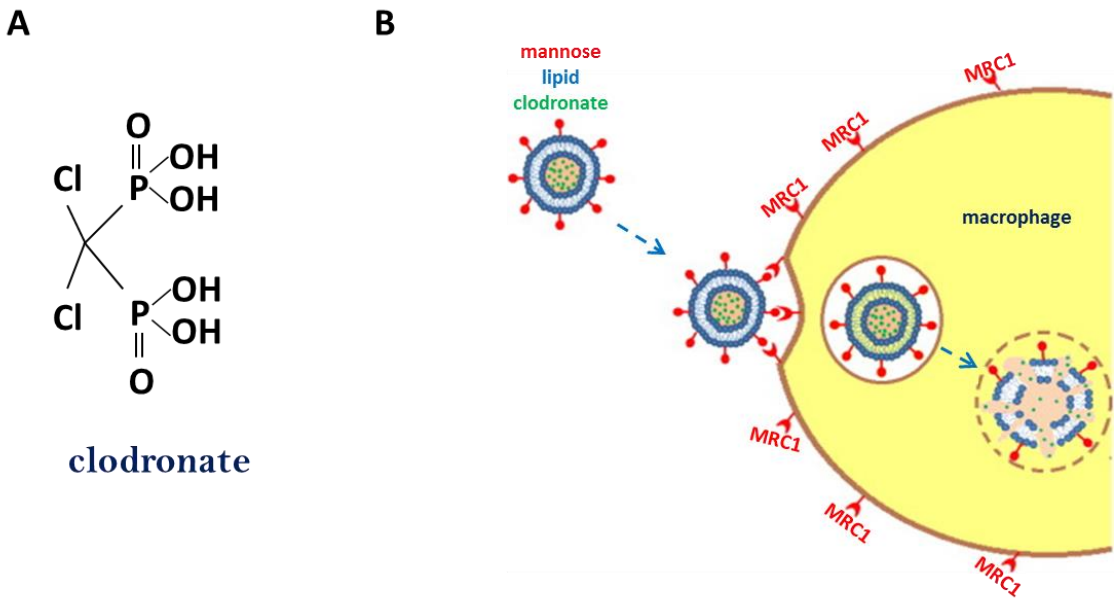


Figure 4.1: The clodronate liposome approach for macrophage depletion. (A) The chemical structure of the bisphosphonate clodronate. (B) Schematic representation of the macrophage suicide approach in the case on mannose receptor (MRC1) targeted clodronate liposomes (Adapted from Eloy et al, 2014).

4.2 Aims

Principal aims of this chapter are the following:

1. To determine the effect of mannosylated clodronate liposomes on 4T1 and microglial/macrophage cells *in vitro*
2. To validate the *in vivo* depletion of $MRC1^+$ cells in an IL-4 induced CNS inflammation model
3. To validate the *in vivo* depletion of $MRC1^+$ microglia in the intracerebral 4T1-GFP brain metastasis model and assess its effect on tumour burden.

4.3 Methods

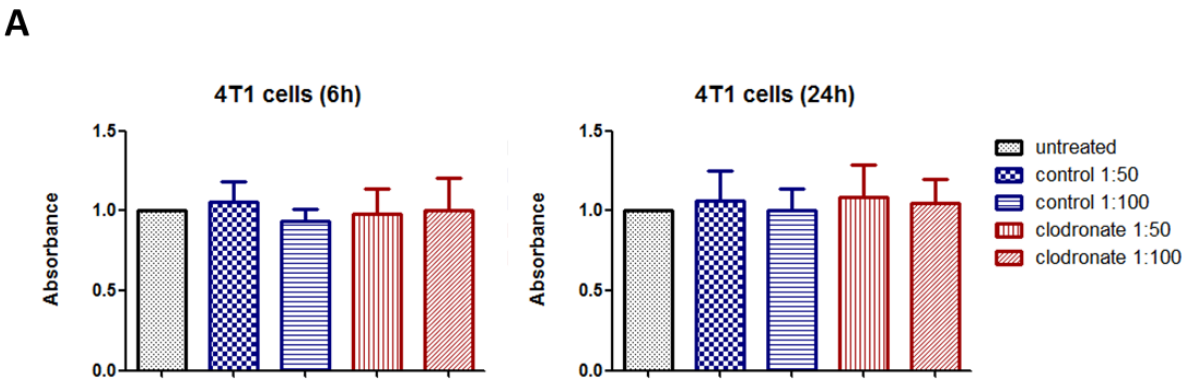
For the in vitro experiments, the RAW264.7 and BV2 cell lines were used. M1 or M2 polarisation was induced by LPS or IL-4 treatment, respectively (section 2.3). Unpolarised or polarised cells were incubated with mannosylated control or clodronate containing liposomes diluted in culture medium. MTT viability assays were performed on cells appropriately treated as described in section 2.4. Immunocytochemistry was performed on fixed cells appropriately treated using anti-F4/80, anti-MRC1 or anti-iNOS antibodies (section 2.12.2). Control liposomes were visualised under the fluorescent microscope by the lipid-incorporated DiD dye.

The M2 neuroinflammatory mouse model was induced by intrastriatal injection of murine IL-4. For experimental brain metastasis, we used the syngeneic 4T1-BALB/c intracerebral model which was described in Chapters 2 and 3. Mannosylated liposomes were injected undiluted intracerebrally in IL-4 challenged, 4T1-GFP challenged or naïve brains. Iba1, MRC1, CC3 and CD31 expression were assessed by IHC using the ABC kit (section 2.8). Quantitation of the markers across the IL-4 or 4T1-GFP regions was performed using the positive pixel count algorithm. Intracranial tumour volumes were calculated by quantitation of the area of tumour foci (cresyl violet) on every section 50 μm apart spanning the 4T1 metastatic region. Immunofluorescence was performed using antibodies against Iba1, MRC1, GFP, CD31, NeuN, GFAP, CC3 (section 2.12.1). Finally, it should be noted that by referring to microglia throughout this chapter, the mixed microglia/macrophage population is considered given that microglia and macrophages cannot be distinguished by IHC.

4.4 Results

4.4.1 Effect of mannosylated liposomes on cell viability *in vitro*

Initially, the effect of mannosylated control and clodronate liposomes on the metabolic activity of 4T1-GFP tumour cells, as measured by the reduction of tetrazolium dye (MTT assay), was investigated. The presence of control liposomes at a low or high concentration (1:100 or 1:50 dilution, respectively) in the culture medium did not confer any change in the viability of 4T1-GFP mammary carcinoma cells after 6 and 24 hours of treatment (Figure 4.2A, blue bars). Similarly, 4T1-GFP cells did not present with altered metabolic activity upon treatment with the mannosylated clodronate liposomes (10mg/ml), even 24 hours into treatment at a high concentration (1:50 dilution) (Figure 4.2A, red bars). In support of our findings, 4T1-GFP cells do not express the mannose receptor MRC1, whilst microglia BV2 cells do (Figure 4.2 B)



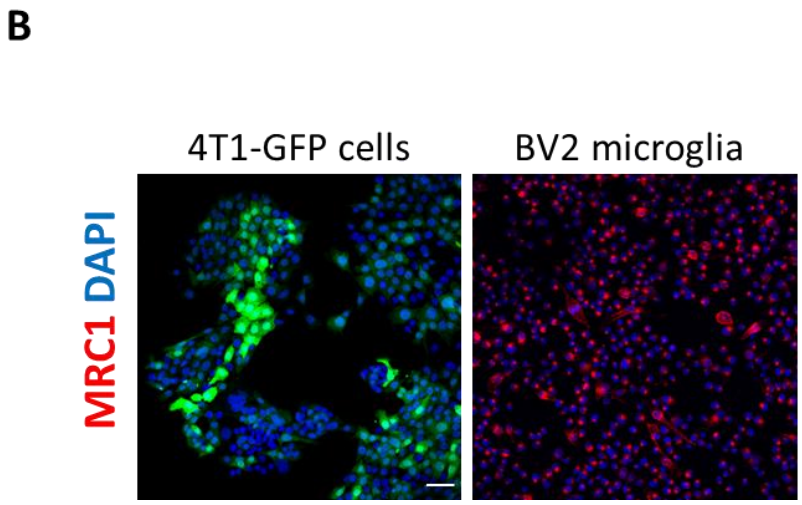


Figure 4.2: **Mannosylated liposomes do not affect viability of 4T1-GFP tumours cells *in vitro*.** Formasan absorbance (A) as a measure of viability of 4T1-GFP cells treated with mannosylated control (blue bars) or clodronate (red bars) liposomes at a high (1:50) and low (1:100) concentration for 6 hours and 24 hours (n=3; p>0.05, one-way ANOVA). Absorbances of untreated cells are normalised to 1. Immunocytochemistry (B) for MRC1 expression (Texas Red) on 4T1-GFP and BV2 cells with DAPI as counterstain. Scale bar 50 µm.

Similar experiments were performed using BV2 microglial cells and RAW264.7 macrophages. Treatment of BV2 and RAW264.7 cells with mannosylated control liposomes for 6 and 24 hours confered no significant changes in their viability as assessed by the MTT assay (Figure 4.3A, B; blue bars). Mannosylated clodronate liposomes did not change the viability of BV2 or RAW264.7 cells after 6hours of treatment (Figure 4.3A, B; red bars). However, a statistically significant decrease in formazan absorbance, and thus cell viability, was observed for both cell lines after 24 hours of treatment with high and low concentrations (1:50 and 1:100 dilution, respectively) of clodronate liposomes compared to untreated cells or cells treated with control liposomes (Figure 4.3A, B; red bars).

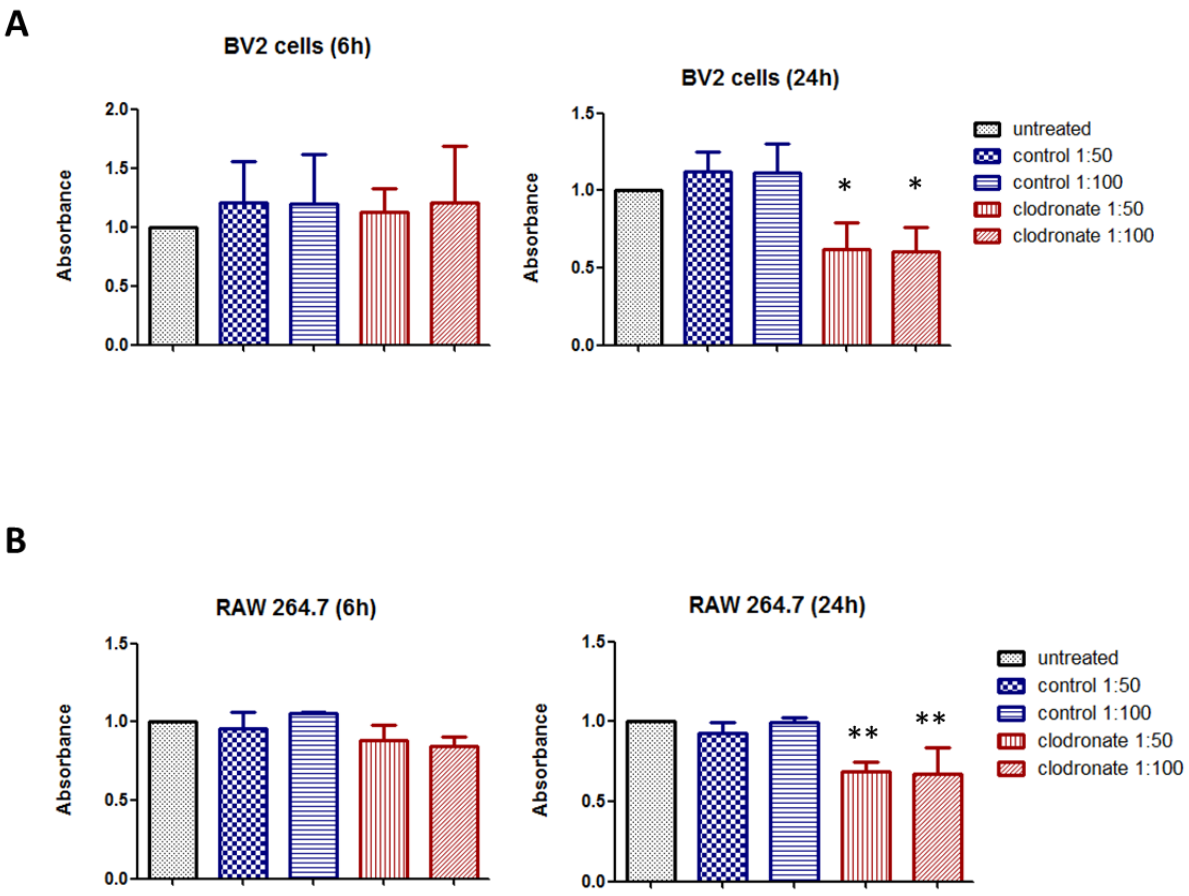
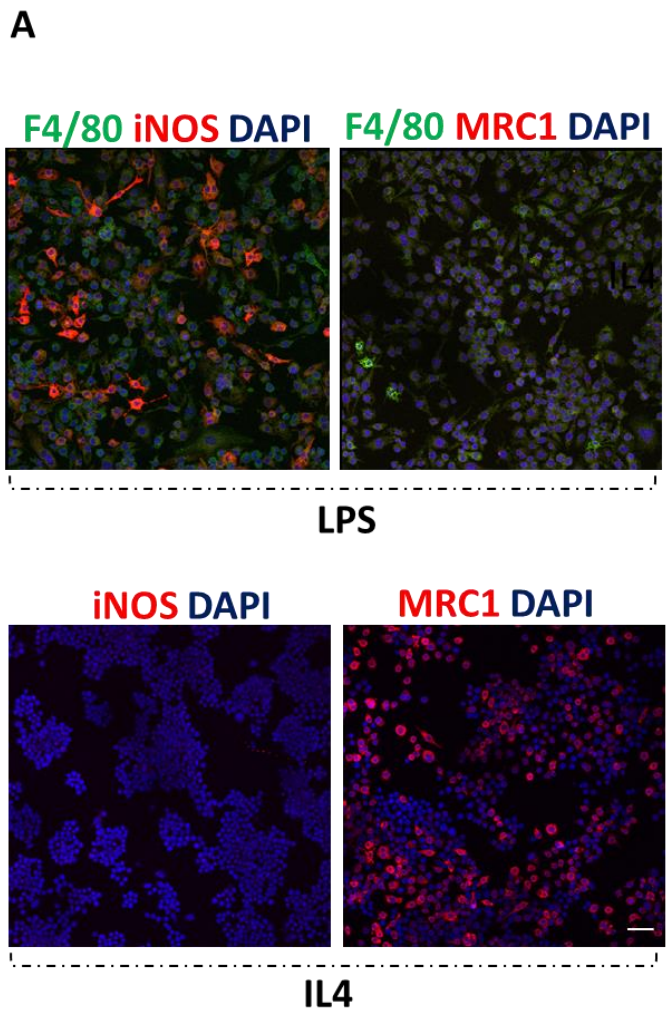


Figure 4.3: Mannosylated clodronate liposomes decrease viability of BV2 microglia and RAW264.7 macrophages *in vitro*. Formasan absorbance as a measure of viability of BV2 (A) and RAW246.7 (B) cells treated with mannosylated control (blue bars) or clodronate (red bars) liposomes at a high and low concentration (1:50 and 1:100 in culture medium, respectively) for 6 and 24 hours (n=3; $p<0.05$, one-way ANOVA with Dunnett's multiple comparison test). Absorbances of untreated cells are normalised to 1.

Next, I sought to determine the specificity of the mannose receptor targeted liposomes for *in vitro* polarised microglial cells and macrophages. BV2 and RAW264.7 cells were polarised to the classical M1 or alternative M2 phenotype by a 24 hour treatment with LPS (100ng/ml in culture medium) or IL-4 (20ng/ml in culture medium), respectively. As a confrimation of the cellular polarisation regimes widely used, iNOS and MRC1 expression was examined qualitatively by immunocytochemistry on LPS and IL-4 treated RAW264.7

cells. (Figure 4.4A). As expected, iNOS was induced by LPS treatment but not by IL-4 while MRC1 was evidenlty expressed by IL-4 treated cells but minimally by the LPS treated counterparts. On a similar setting, a single experiment performed in quadruplicates showed that IL-4 treated BV2 cells present with increased expression of MRC1 compared to LPS treated cells, which maintain nearly basal expression levels (Figure 4.4B).



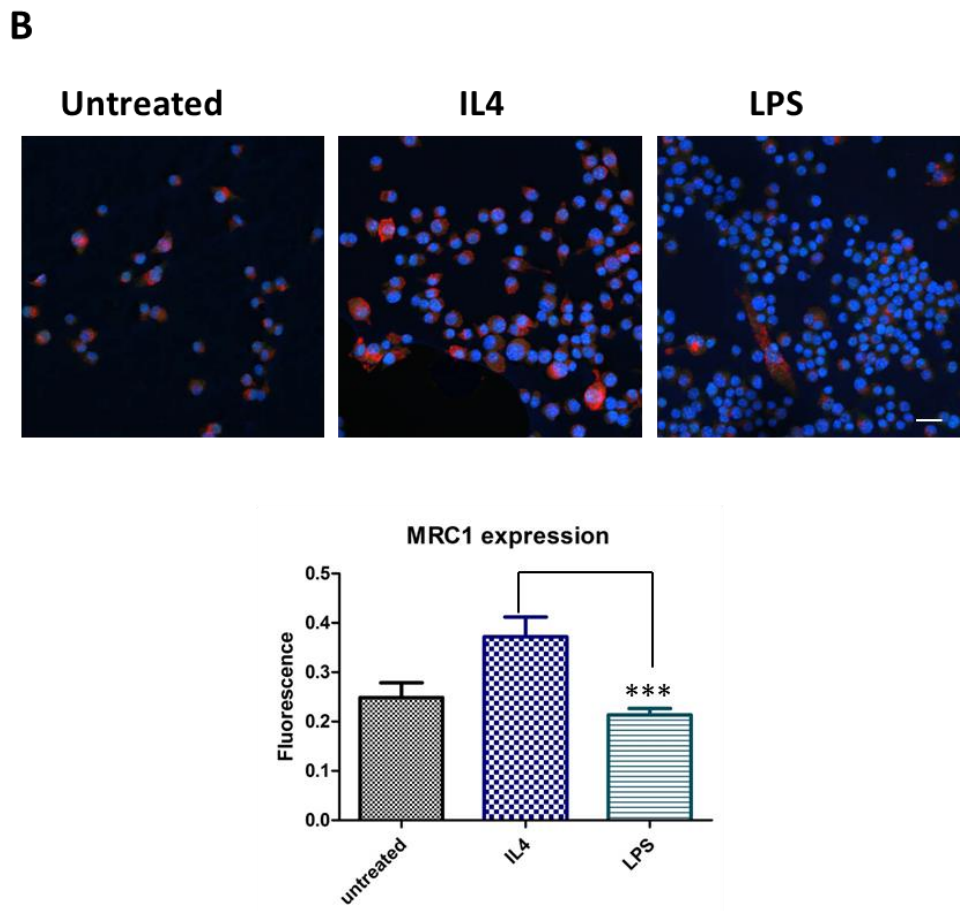
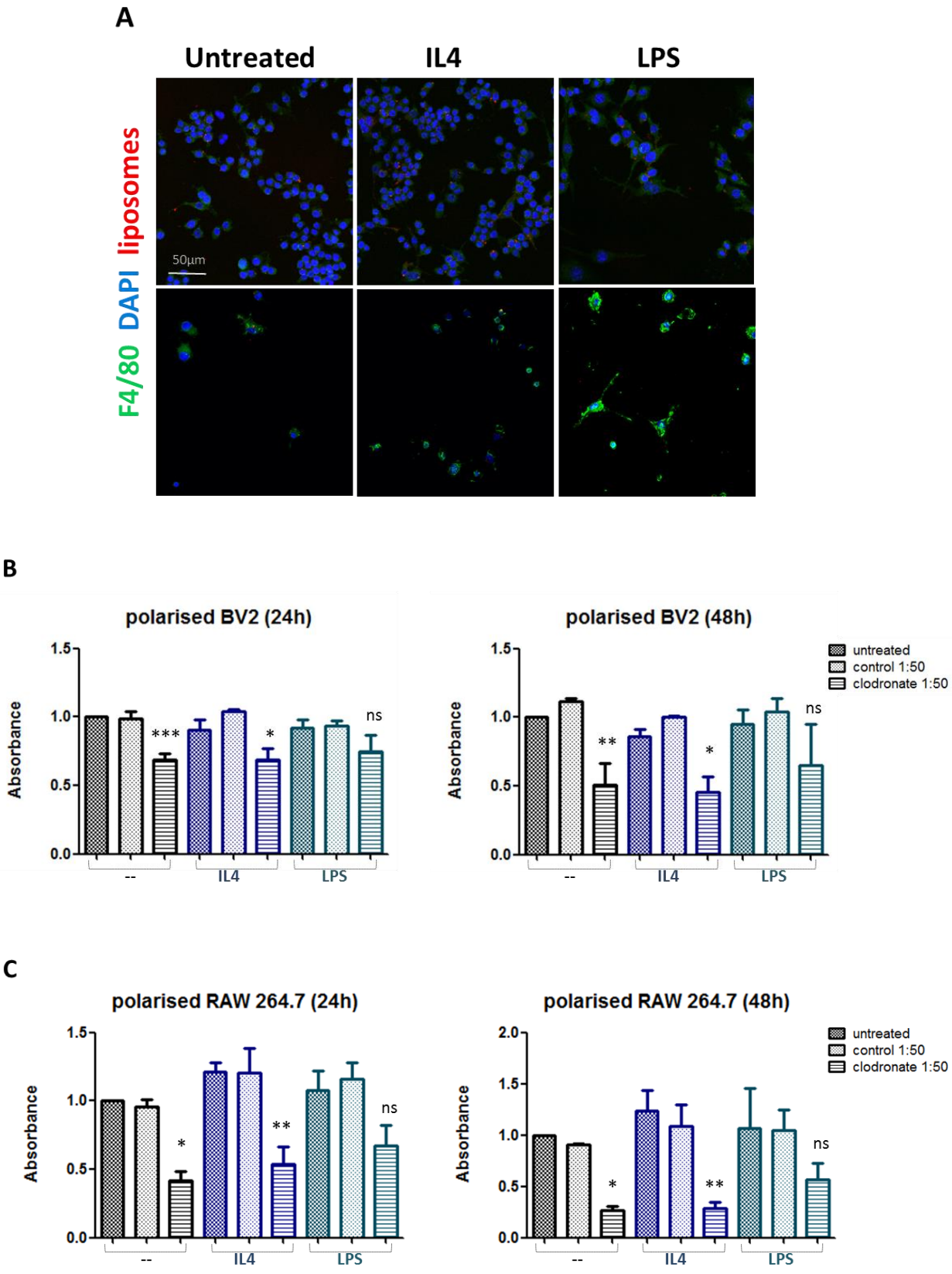


Figure 4.4: *In vitro* polarisation of microglia/macrophages. Immunocytochemistry for iNOS (M1 marker) and MRC1 (M2 marker) (A) on RAW264.7 cells treated with LPS or IL4 (24 hours) for polarisation. Immunocytochemistry for and quantitation of MRC1 expression (B) on untreated or polarised BV2 cells (one experiment performed in quadruplicates; red fluorescence was normalised to DAPI intensity; p=0.0025 for untreated and IL4, p=0.0003 for IL4 and LPS with two tailed unpaired t-test). Scale bar 50 µm

Mannosylated control liposome uptake by unpolarised and polarised cells was qualitatively confirmed by fluorescence (since control liposomes are DiD positive) at 6 hours of incubation (Figure 4.5A). Unstimulated and polarised cells were subsequenlty treated with mannosylated control or clodronate liposomes (1:50 dilution) for 24 or 48 hours and their viability assessed with the MTT assay. Mannosylated control liposomes did not affect the viability of unstimulated, M1 polarised or M2 polarised cells of either cell line at 24 and 48 hours of treatment (Figure 4.5). Importantly, 24 and 48 hours

treatment of unstimulated BV2 and RAW264.7 cells with 1:50 mannosylated clodronate liposomes significantly reduced their viability (Figure 4.5B, C) as expected based on our previous experiments in which cell viability decreases upon mannosylated clodronate liposome treatment (Figure 4.3). M2 polarisation of BV2 and RAW264.7 cells sustained the significant decrease in cell viability upon treatment with mannosylated clodronate liposomes for both 24 and 48 hours (Figure 4.5, blue bars). In contrast, M1 polarisation of BV2 and RAW264.7 cells by LPS diminished the decrease of cell viability caused by the mannosylated clodronate liposome treatment observed for the unstimulated or M2 polarised cells even after 48 hours of liposome treatment (Figure 4.4, green bars). Within the experimental group of LPS treated cells, BV2 and RAW264.7 cells showed a trend towards reduced metabolic activity when treated with mannosylated clodronate liposomes compared to control liposomes or no treatmnent, but this decrease was not significant (Figure 4.5). By fluorescence I observed that $iNOS^+$ RAW 264.7 cells were not associated with liposomes, at least by qualitative analysis of a small number of cells (Figure 4.5).


A
Untreated
IL4
LPS
F4/80 DAPI liposomes
50µm
B
polarised BV2 (24h)
polarised BV2 (48h)
Absorbance
untreated
control 1:50
clodronate 1:50
ns
--
IL4
LPS
C
polarised RAW 264.7 (24h)
polarised RAW 264.7 (48h)

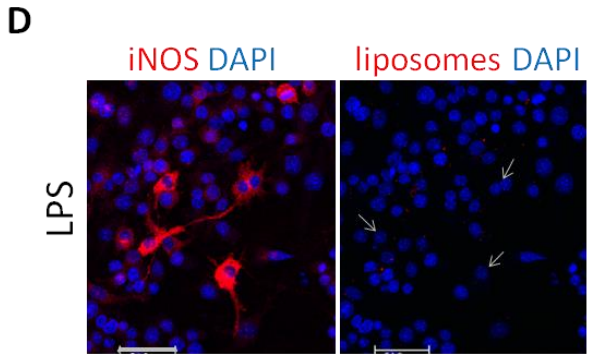


Figure 4.5: *In vitro* M1 polarisation subsides the decrease of cell viability upon treatment with mannosylated clodronate liposomes. Formasan absorbance as a measure of viability of non-polarised (black pattern bars) or polarised (blue pattern and green pattern bars) BV2 (A) and RAW264.7 (B) upon treatment with mannosylated control or clodronate liposomes (1:50 dilution in culture medium) for 24h or 48 hours. Polarisation of cells was achieved by treatment with 20ng/ml IL-4 or 100ng/ml LPS 24 hours prior to the liposome treatment (n=3; $p<0.05$, one-way ANOVA with Dunnett's multiple comparison test). Absorbances of untreated non-polarised cells are normalised to 1. Visualisation of DiD positive control liposomes associated with unpolarised or polarised RAW 264.7 (top panel) or BV2 (bottom panel) cells by fluorescence (C). Spatial correlation of iNOS expressing RAW 264.7 cells with DiD control liposomes (6 hours treatment) on the same field of view (D). Scale bars 50 µm

4.4.2 IL-4 model of CNS inflammation

Moving on from the *in vitro* setting, an IL-4 induced CNS inflammation model was employed as a proof-of-principle experiment for *in vivo* M2 cell polarisation. 100ng of murine recombinant IL-4 were injected intracerebrally into the left striatum and the timecourse of microglial response and MRC1 upregulation assessed immunohistohcemically. Increased numbers of $Iba1^{+}$ cells, an indication of a robust microglial response, compared to the contralateral hemisphere were observed as early as 24 hours after intracerebral IL-4 injection (Figure 4.6A, B; $p=0.0603$ at 6h, $p=0.0223$ at 24h, $p=0.0132$ at 48h, $p=0.0008$ at 72 h with two tailed unpaired t-test for IL-4 and contralateral hemispheres at respective timepoints). Upregulation of Iba1 and increased

numbers of microglial cells were also prominent at 24, 48 and 72 hours after IL-4 injection (p=0.002, one-way ANOVA), with a peak of microglial respnonse at 48 hours (Figure 4.6B). The number of microglia in the contralateral non-injected hemispheres did not vary significantly across the timecourse study (p=0.0832, one-way ANOVA; Figure 4.6, pattern bars).

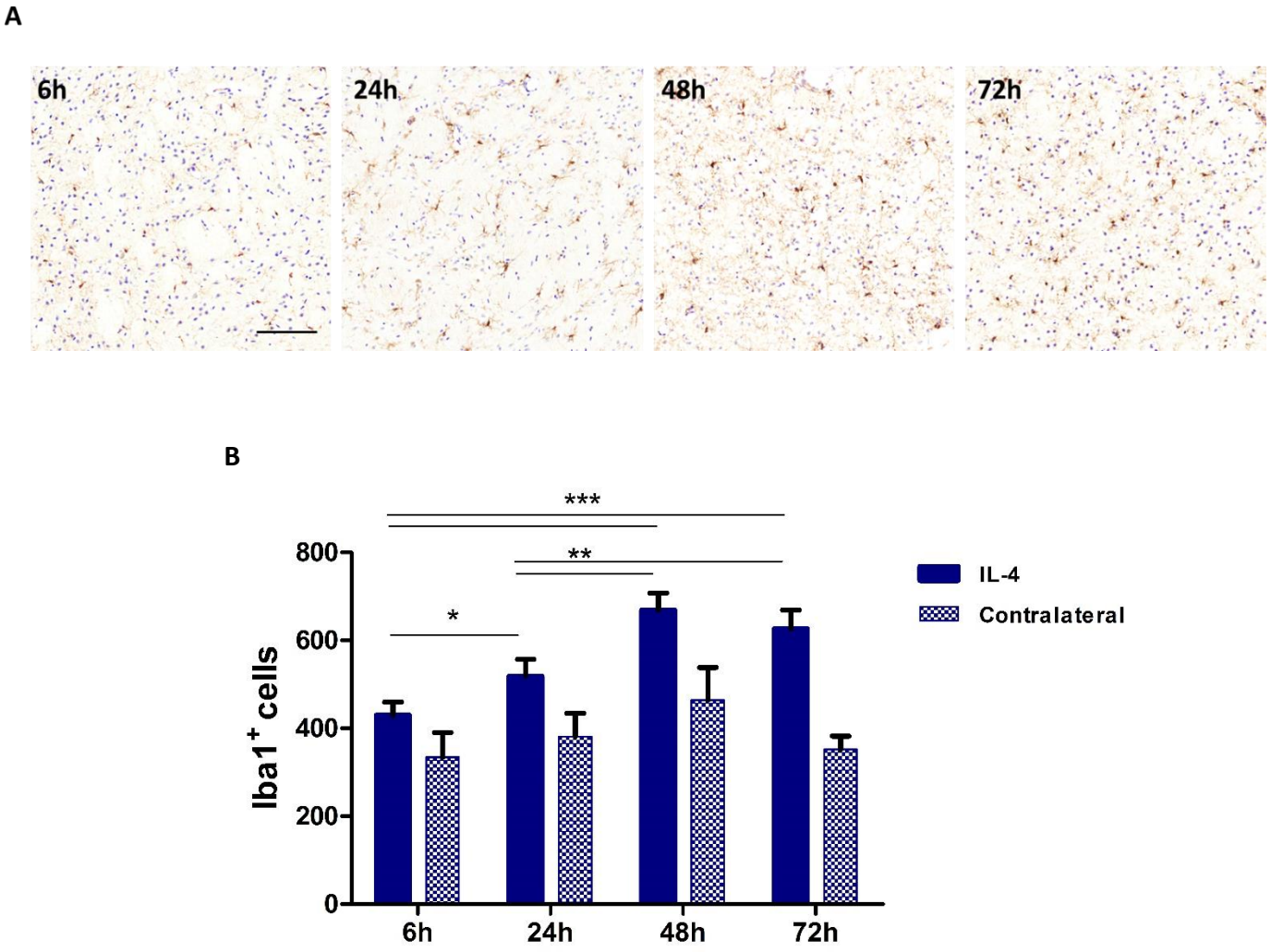
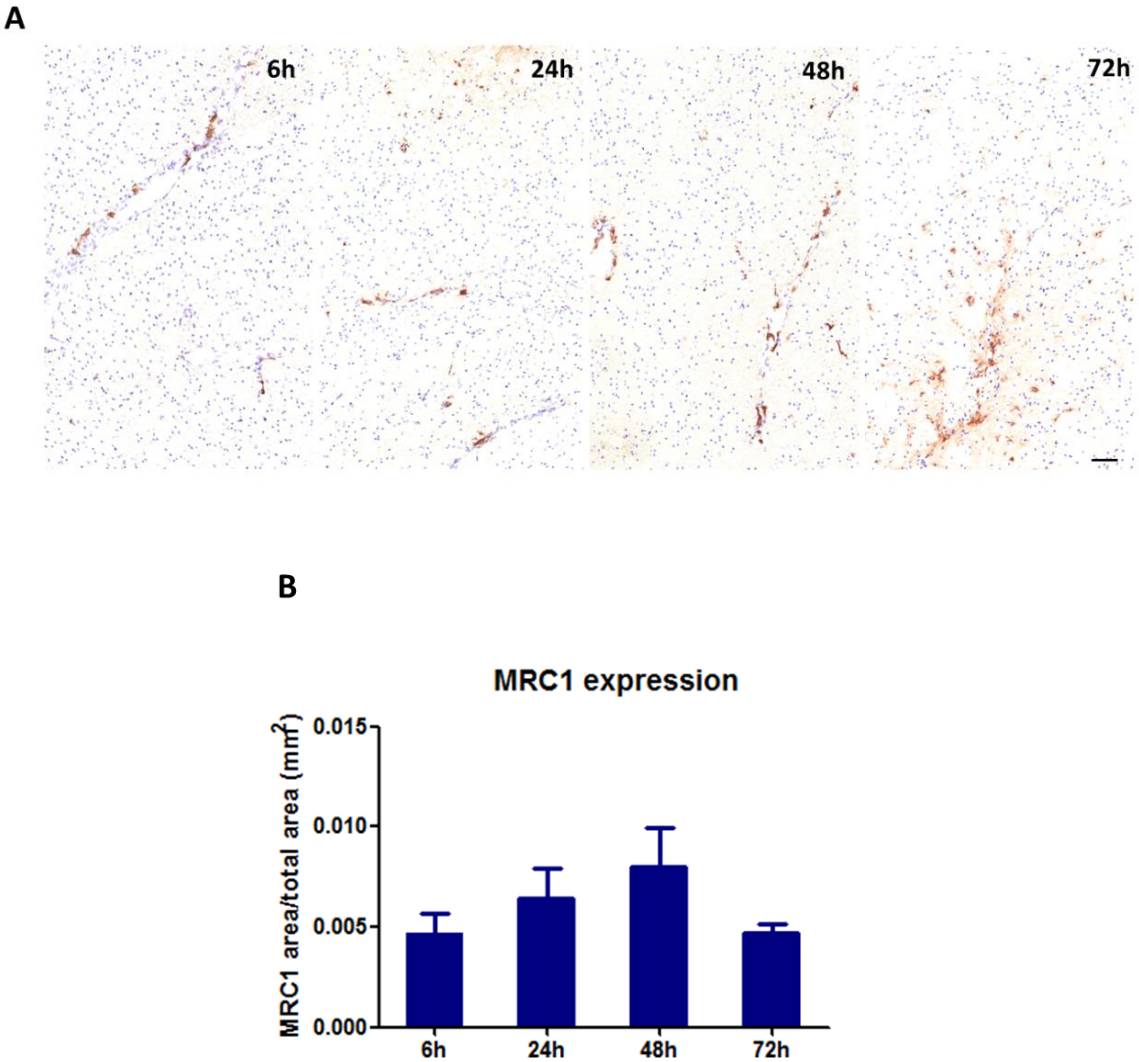


Figure 4.6: Microglial response after intracerebral injection of IL-4. (A) Representative striatal images for Iba1 IHC (brown stain) of mice intracerebrally challenged with IL-4. (B) Quantitation of Iba1^{+} cells in the striatum of mice intracerebrally injected with 100ng of murine recombinant IL-4 (n=3, 3 fields of view per section, 3 sections per animal; p=0.002 one way ANOVA with Newman-Keuls multiple comparison test for IL-4 hemispheres; p=0.0832 one way ANOVA for contralateral hemispheres). Scale bars 100 µm.

With regards to M2 activation specifically throughout the 72 hour timecourse study, MRC1 upregulation was in accordance with the Iba1 activation pattern with a peak of MRC1 expression at 48 hours after IL-4 injection (Figure 4.7A, B). Using double immunofluorescent staining of striatal regions of the IL-4 injected hemispheres, we observed a cellular M2 signature by identifiyng MRC1^{+} vessels (CD31 marker) and microglia (Iba1 marker). Astrocytes (GFAP marker) did not seem to adopt an M2 phenotype, although we did not investigate astrocytic polarisation extensively (Figure 4.7C).



C

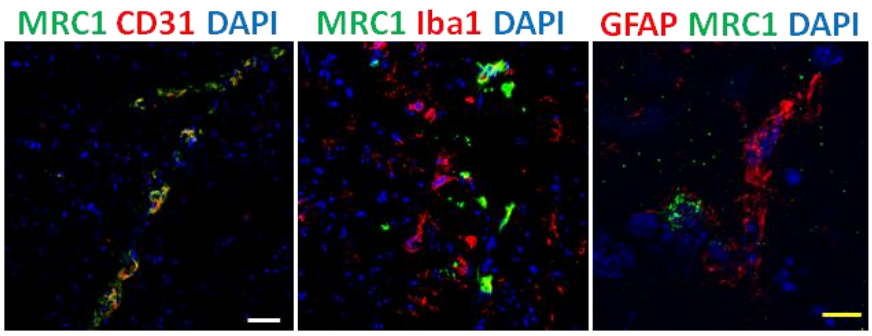
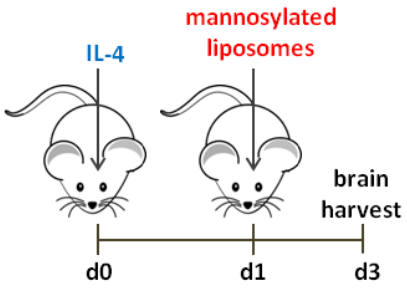


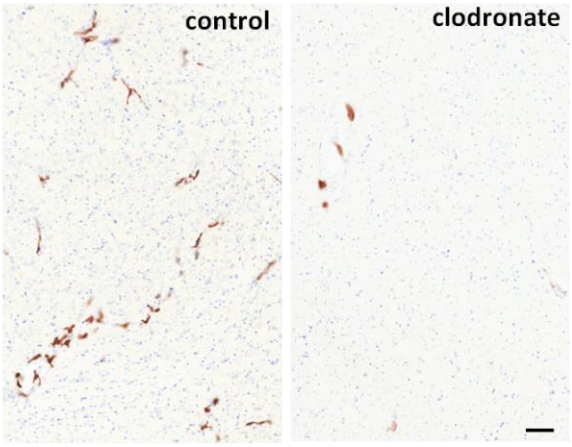
Figure 4.7: MRC1 upregulation after intracerebral injection of IL-4. (A) Representative striatal IHC images for MRC1 expression in mice intracerebrally challenged with 100ng of murine recombinant IL-4. (B) Quantitation of MRC1 expression in hemispheres injected with IL-4 (n=3, 3 sections per brain; one-way ANOVA p=0.2954). (C) Immunofluorescence for double labelling of $MRC1^+$ vessels, microglia and astrocytes 48 hours after intracerebral IL-4 injection. Scale bars 50 µm (A, B white) or 20 µm (B, yellow).

Having defined the time course of MRC1 upregulation in the IL-4 challenged brain, I sought to assess the efficiency of *in vivo* $MRC1^+$ cell depletion using the mannosylated clodronate liposome approach. Control or clodronate liposomes were intracerebrally injected in the brain 24 hours after intracerebral injection of IL-4. MRC1 depletion was assessed after 48 hours by IHC (see Figure 4.8A for schematic). A significant decrease in MRC1 expression was observed in the brains of mice injected with mannosylated clodronate liposome compared to the brains of mice injected with control liposomes (Figure 4.8B, C). Although the $MRC1^+$ cell ablation was not complete, we observed a consistent, average 61% depletion in our experimental model. Migroglial infiltration remained unaffected by the liposome injections as revealed by Iba1 immunostaining and quantitation (Figure 4.8D, E). Moreover, fluorescent control liposomes were localised to $Iba1^+$ and $CD31^+$ cells 6 hours after intracerebral administration in the IL-4 challenged brain (Figure 4.8F)

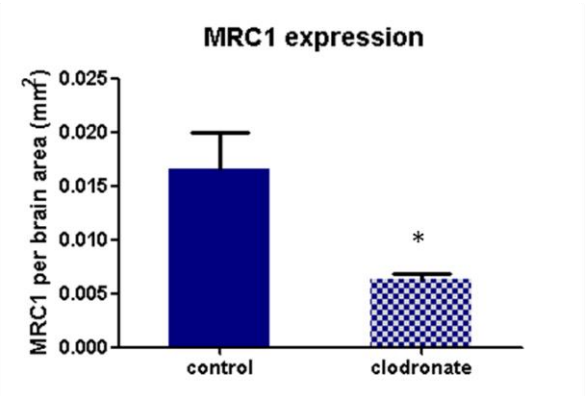
A


mannosylated
liposomes
IL-4
brain
harvest
d0
d1
d3

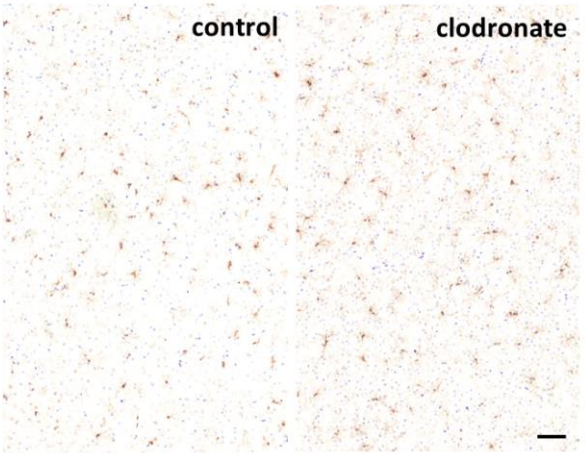
B


control
clodronate

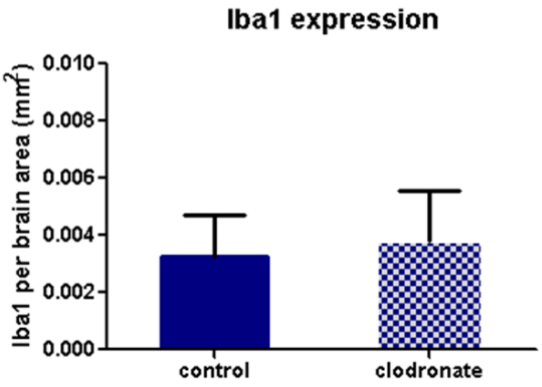
C


MRC1 expression
MRC1 per brain area (mm²)
0.025
0.020
0.015
0.010
0.005
0.000
*
control
clodronate

D


control
clodronate

E


Iba1 expression
Iba1 per brain area (mm²)
0.010
0.008
0.006
0.004
0.002
0.000
control
clodronate

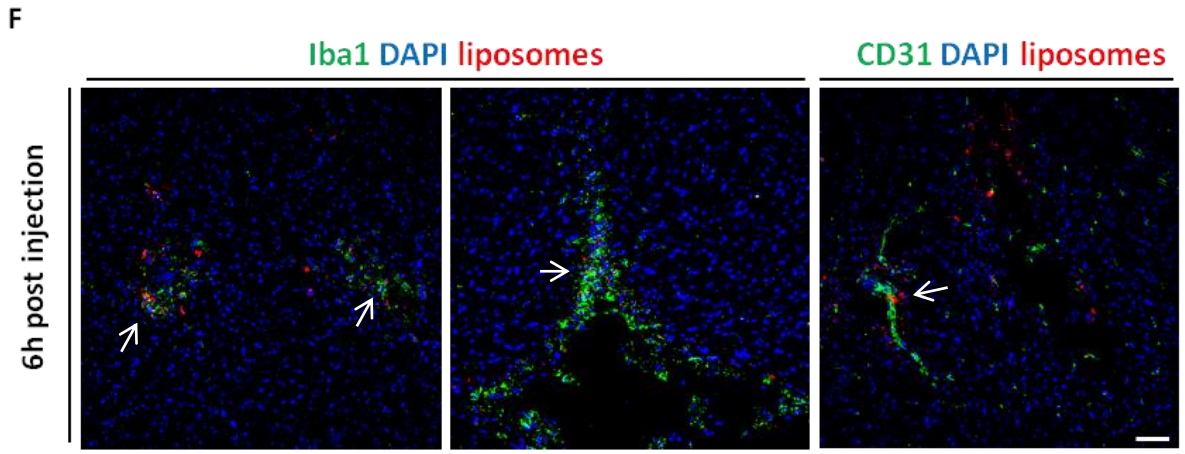


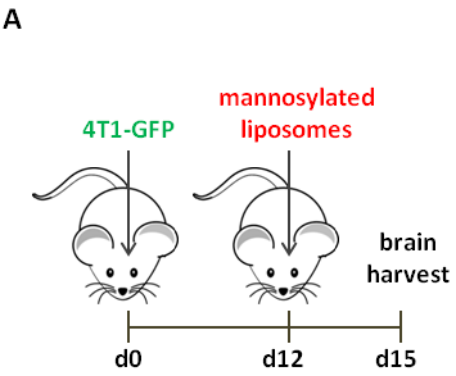
Figure 4.8: *In vivo* depletion of MRC1$^+$ cells by intracerebral injection of mannosylated clodronate liposomes. (A) Schematic presentation of the experimental design. (B) Representative IHC images for MRC1 expression from striatal areas of brains injected with mannosylated control or clodronate liposomes 24 hours after intracerebral injection of 100ng murine recombinant IL-4. (C) Quantitation of MRC1 expression in hemispheres injected with control or clodronate liposomes (n=3, 6 sections per animal, two tailed unpaired t-test p=0.042). (D) Representative IHC images for Iba1 expression from striatal regions of brains injected with mannosylated control or clodronate liposomes 24 hours after intracerebral injection of 100ng murine recombinant IL-4. (E) Quantitation of Iba1 expression in hemispheres injected with control or clodronate liposomes (n=3, 6 sections per animal, two tailed unpaired t-test p=0.7095). (F) Fluorescent co-localisation of control liposomes with Iba1 and CD31 6 hours after intracerebral injection in the IL-4 challenged brain. Scale bars 50 µm.

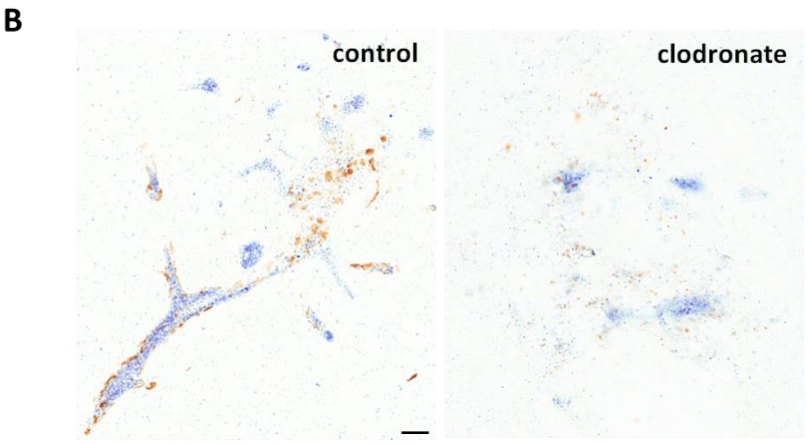
4.4.3 The mannosylated liposomes approach in the metastatic brain

4.4.3.1 Validation of MRC1 depletion in the 4T1-GFP model

Next, to investigate the effect of MRC1$^+$ microglia in the metastatic brain, the clodronate liposome approach was used in our 4T1-GFP metastatic model. Intracerebral administration of the liposomes was performed as previously. Since in the previous results chapter a drop in MRC1$^+$ microglia infiltration in the metastatic brain at day 10 before its peak at day 14 was observed (Figure 3.8), I reasoned that administration of

liposomes 12 days after 4T1-GFP injection would possibly provide an effective approach to MRC1^{+} cell depletion at an early timepoint (see Figure 4.9A for schematic). Three days after intracerebral injection of mannosylated liposomes in the metastatic brain, we observed a decrease in MRC1 expression around the cresyl violet tumour foci (Figure 4.9B) which was statistically significant between control and clodronate liposome injected animals both as a function of tumour area (C) or in absolute area (D) (Figure 4.9C, D). Depletion of MRC1^{+} microglia in the 4T1-GFP metastatic brain was also qualitatively demonstrated by double immunofluorescence of a small number of brain sections (Figure 4.9E).





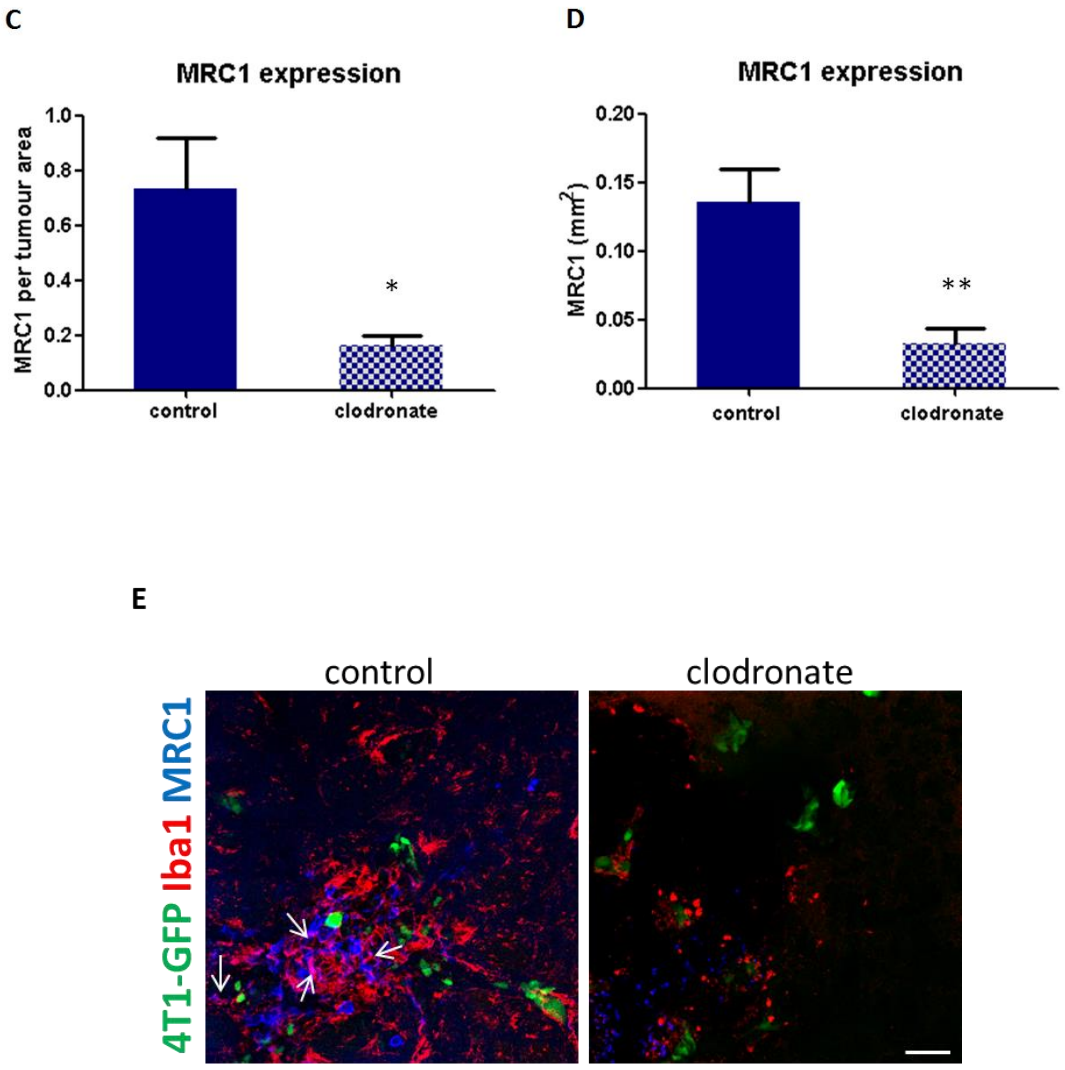
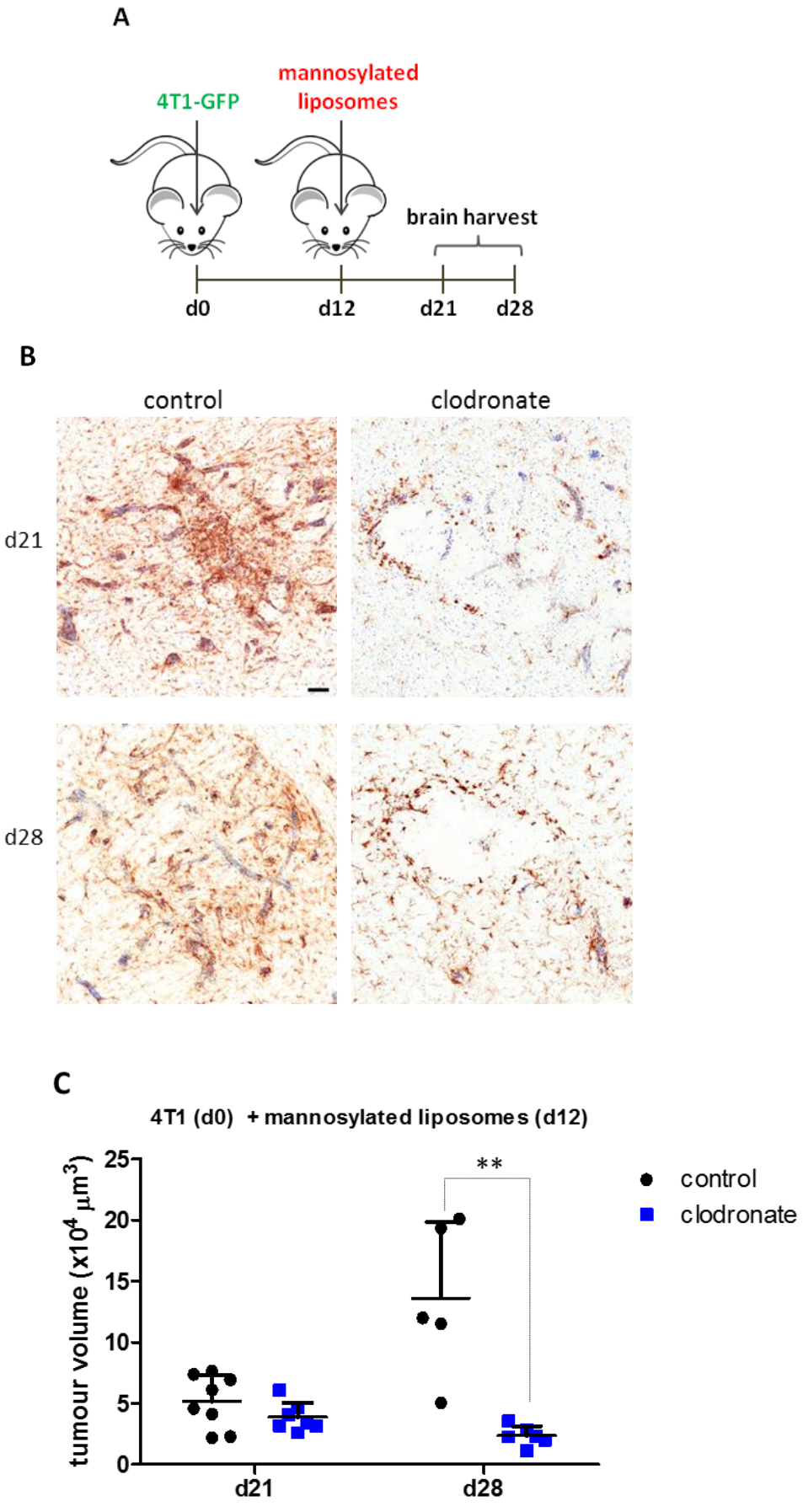


Figure 4.9: *In vivo* depletion of MRC1$^+$ microglia in the 4T1-GFP metastatic brain. (A) Schematic presentation of the experimental design. (B) Representative IHC images for MRC1 expression from striatal regions of metastatic brains three days after injection with mannosylated control or clodronate liposomes. Quantitation of MRC1 expression normalised to tumour area (C) or as absolute immunostained area (D) in brains bearing 4T1 metastases three days after intracerebral injection of mannosylated control or clodronate liposomes) [n=4; analysis inclusive of sections spanning the 4T1-GFP region; p= 0.0256, two tailed unpaired t-test (C); p=0.0083, two tailed unpaired t-test (D)]. (E) Representative fluorescent images for MRC1$^+$ microglia from striatal regions of brains bearing 4T1-GFP metastases three days after injection with mannosylated control or clodronate liposomes. Arrows indicate MRC1$^+$ microglia. Scale bar 50 µm.

4.4.3.2 Metastasis burden

To test the hypothesis that depletion of MRC1^{+} microglia would alter metastasis burden, tumour burden was assessed either 9 or 16 days after liposome injection (see Figure 4.10A for schematic). Quantitation of tumour burden in the 4T1-GFP metastatic brain 9 days after clodronate liposome administration (day 21) showed a trend towards decreased tumour volume between the control and clodronate injected animals (Figure 4.10B, C). However, the difference in tumour burden between the two experimental groups became statistically significant 16 days after liposome injection (day28), since the 4T1-GFP foci in the control animals continued to proliferate whilst tumour volumes in the clodronate animals decreased further (Figure 4.10C). Moreover, an obvious microglial phenotype alteration was evident in animals injected with mannosylated clodronate liposomes. Microglial cells in close vicinity to 4T1-GFP foci in the striatum adopted the amoeboid phenotype, a phenomenon that persisted up to day 16 after liposome injection (Figure 4.10B). It is important to mention that this pattern was not universal since not every brain slice examined showed this microglial phenotype alteration. Microglial cells and infiltration in the control liposome injected animals presented with the typical pattern already seen for the 4T1-GFP model (described in Chapter 3). Additionally, sham intracerebral injections were performed as an additional control for the liposome injection. No significant changes in tumour volume or microglial activation were observed in the PBS injected animals bearing 4T1-GFP metastases compared to the mannosylated control liposome injected animals (Figure 4.10D).


A
4T1-GFP
mannosylated liposomes
brain harvest
d0
d12
d21
d28
B
control
clodronate
d21
d28
C
4T1 (d0) + mannosylated liposomes (d12)
tumour volume (x10^4 µm^3)
25
20
15
10
5
0
**
d21
d28
control
clodronate

D

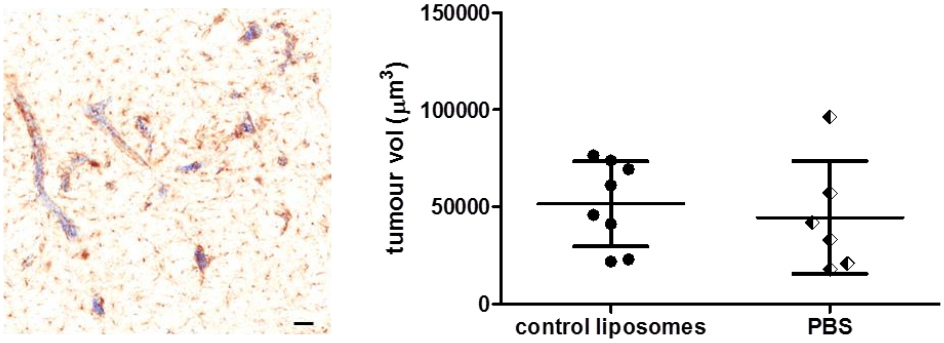
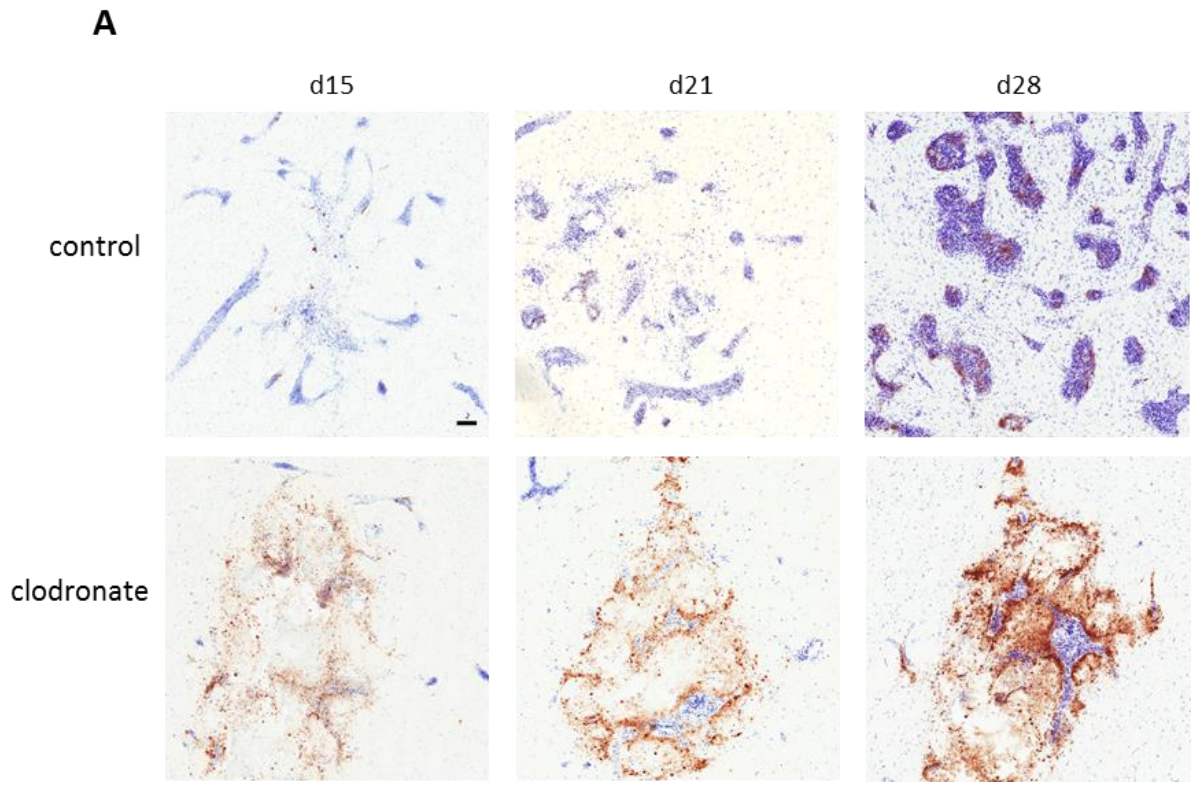


Figure 4.10: Metastatic tumour burden after intracerebral injection of mannosylated clodronate liposomes. (A) Schematic presentation of the experimental design. (B) Representative IHC images for Iba1 expression for the control and clodronate liposome injected animals at days 21 and 28 after tumour cell injection. (C) Quantitation of intracranial tumour burden for mice intracerebrally injected with mannosylated control or clodronate liposomes 12 days after intracerebral 4T1-GFP tumour cell injection (n=5-8; p=0.1898, two tailed unpaired t-test for experimental groups at day 21; p=0.0017, two tailed unpaired t-test for experimental groups at day 28; p=0.0214, two tailed unpaired t-test for clodronate liposome groups). (D) Control PBS injection at day 12 does not affect microglial activation or tumour burden (p=0.6132, two tailed unpaired t-test) at day 21. Scale bars 50 μm.

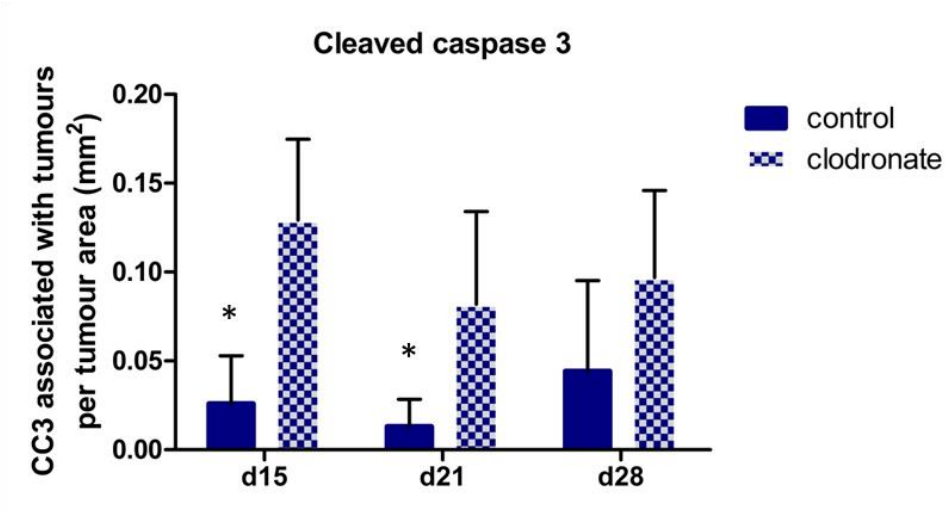
4.4.3.3 Tumour apoptosis

Having observed a significant tumour decrease in the metastatic brains injected with mannosylated clodronate liposomes, I investigated whether those tumours were more apoptotic than tumours in animals injected with control liposomes. Cleaved caspase 3 (CC3), a biomarker indicative of apoptotic death, was expressed in the control liposome injected brains at days 15, 21 and 28 of the tumour timecourse study at basal levels (Figure 4.11A, B). As shown by IHC and immunofluorescence staining (Figure 4.11A, C, D), individual cells within the tumour foci were positive for cytoplasmic and perinuclear CC3 protein. Increased levels of CC3 expression were evident in the clodronate liposome injected animals as shown by both IHC and immunofluorescent staining (Figure 4.11A, C).

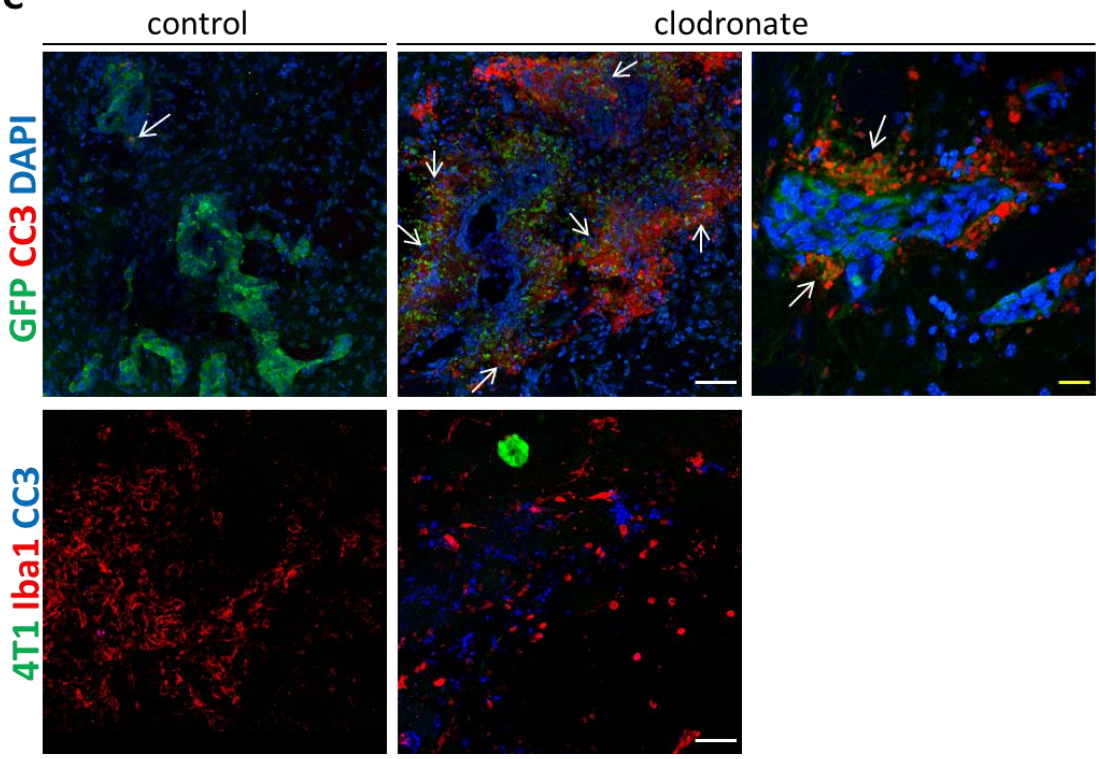
Quantitation of CC3 immunohistochemical expression in close association with the cresyl violet metastatic foci revealed a significant increase of CC3 in the clodronate liposome injected animals compared to the control liposome injected animals at days 15 and 21 (Figure 4.11B, p=0.0278 and p=0.0396, respectively). This effect had subsided by day 28, when the expression of CC3 was still higher in the clodronate liposome injected animals than the controls, but not significantly (Figure 4.11B, p=0.1348). Interestingly, in the clodronate liposomes injected animals, CC3 was not only cytoplasmic/perinuclear, but also extracellular (Figure 4.11A, C, D). Using double immunofluorescence, CC3 expression was localised to GFP positive 4T1 tumour cells and sparsely in microglia in the clodronate liposomes injected animals at days 21 and 28 of the timecourse study (Figure 4.11C, D).



B


Cleaved caspase 3
CC3 associated with tumours per tumour area (mm²)
0.20
0.15
0.10
0.05
0.00
*
*
d15
d21
d28
control
clodronate

C


control
clodronate
GFP CC3 DAPI
4T1 Iba1 CC3

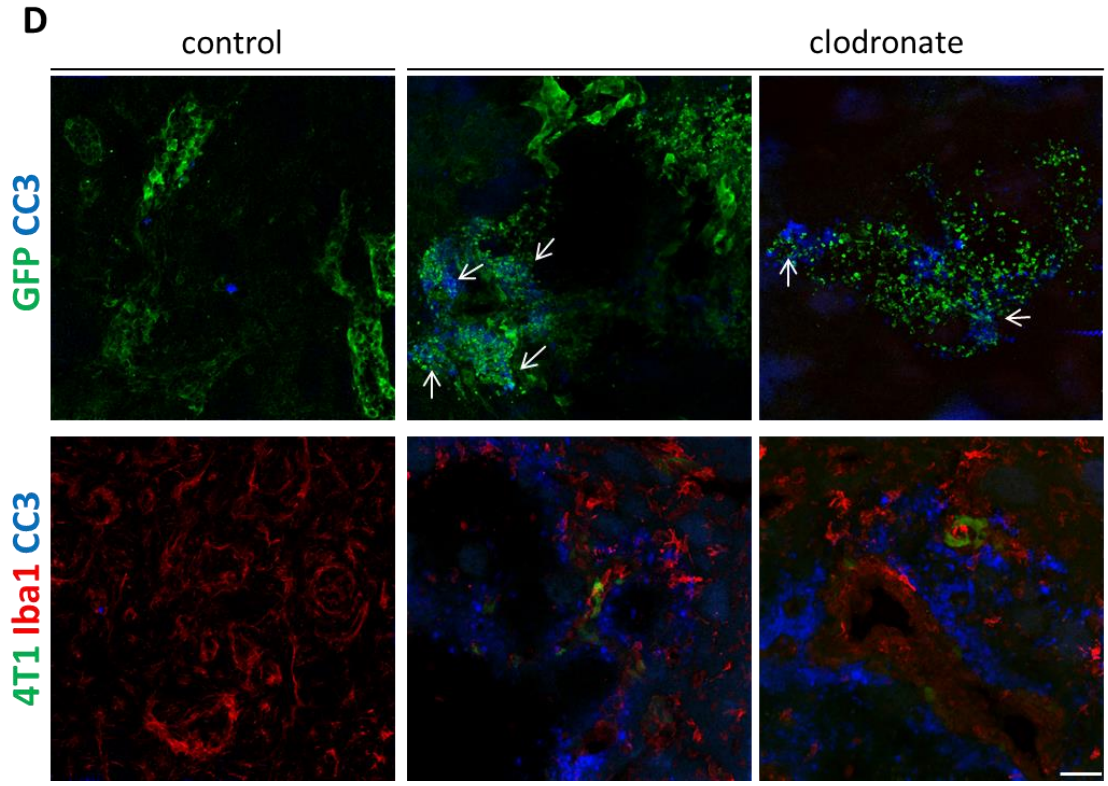


Figure 4.11: Levels of apoptosis in metastatic brains injected with mannosylated control or clodronate liposomes. (A) Representative striatal IHC images for CC3 expression at days 15, 21 and 28 in metastatic brains intracerebrally injected with mannosylated control or clodronate liposomes 12 days after 4T1-GFP cell injection. (B) Quantitation of tumour apoptosis, as indicated by CC3 expression around the metastatic foci, at days 15, 21 and 28 in metastatic brains injected with control or clodronate liposomes (n=3 for d15, p=0.0278 two-tailed unpaired t-test; n=4-5 for day 21, p=0.0396 two-tailed unpaired t-test; n=5 for day 28, p=0.1348 two-tailed unpaired t-test). Immunofluorescent images for co-localisation of CC3 with GFP (for 4T1-GFP cells) or Iba1 in control or clodronate liposomes injected animals at days 21 (C) and 28 (D) of the timecourse study. Arrows indicate co-localisation of markers. Scale bars 50 µm (B, C, D) or 20 µm (C, yellow).

4.4.3.4 Tumour vascularity

M2 like macrophages/microglia are considered to be pro-angiogenic and, thus, linked to tumour vascularisation. To this end, the vascularity of the tumours in the metastatic brains intracerebrally injected with either mannosylated control or clodronate liposomes was assessed. The endothelial marker CD31 was immunohistochemically detected in the metastatic brains of both control and clodronate liposome injected mice (Figure 4.12).

CD31 positive vessels were associated with 4T1-GFP foci in both the control liposome and clodronate liposome injected animals 3, 9 and 16 days after liposome injection.

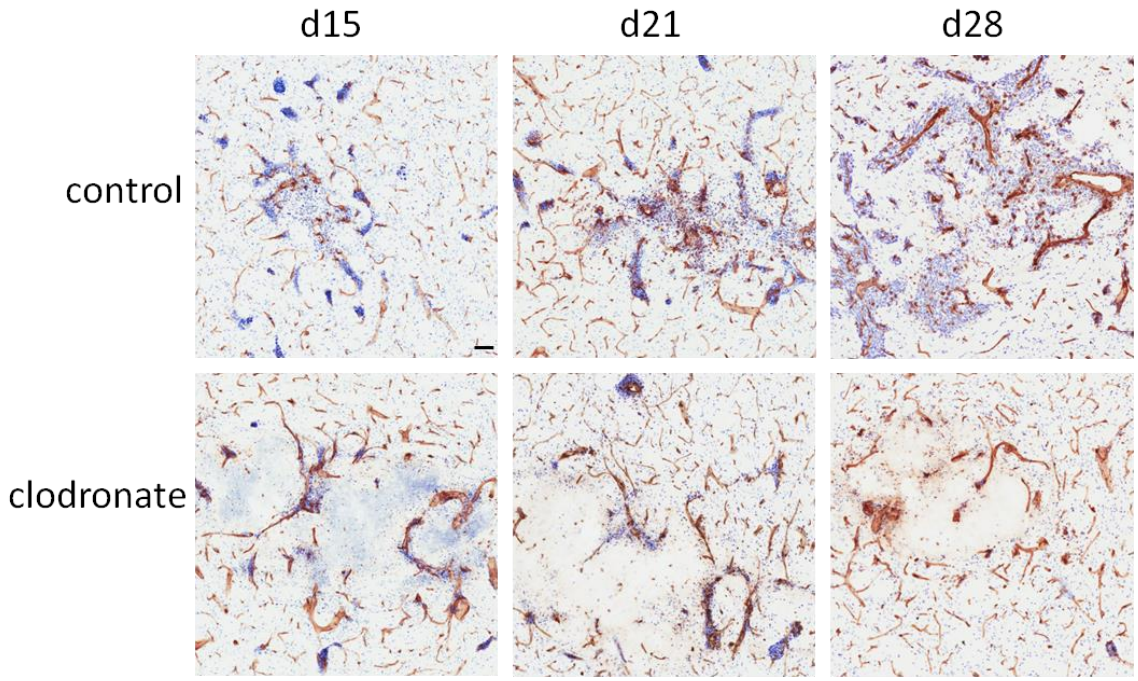
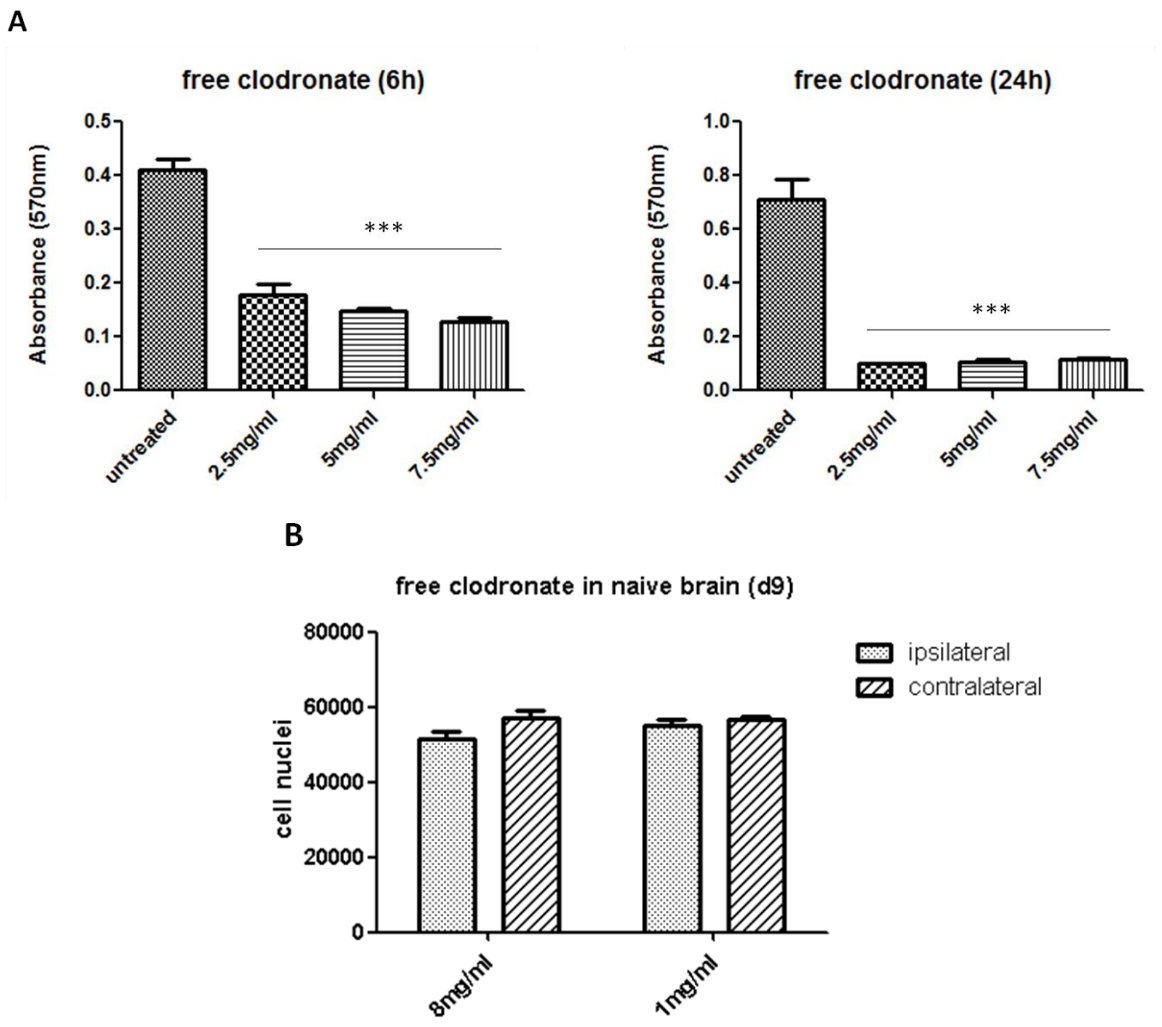


Figure 4.12: Vascularity of 4T1-GFP tumours in metastatic brains injected with mannosylated control or clodronate liposomes. Representative IHC images for CD31 positive vessels at days 15, 21 and 28 in metastatic brains intracerebrally injected with control or clodronate liposomes 12 days after 4T1-GFP cell injection. Scale bars 50 µm.

4.4.4 Control experiments in naïve mouse brains

In order to determine potential side effects from a leakage of clodronate out of the liposomes or from dying microglia, *in vitro* and *in vivo* experiments using free clodronate were performed. Treatment of 4T1-GFP cells with clodronate salt at doses of 2.5mg/ml, 5mg/ml and 7.5mg/ml in the culture medium significantly reduced their viability as early as 6 hours into the treatment as measured by the MTT assay (Figure 4.13A). The effect of free clodronate on 4T1 cells' viability was robust and persisted 24 hours after treatment (Figure 4.13A). To assess its effect *in vivo***,** free clodronate was injected intrastriatally at a

high (8mg/ml) and low dose (1ml/ml) in naïve mouse brains. 9 days later, a timepoint that corresponds to day 21 of the microglial depletion/4T1-GFP model experiment, quantitation of the number of cell nuclei in the ipsilateral and contralateral hemispheres revealed minimal differences due to clodronate administration at both doses studied (Figure 4.13B). Moreover, the number of cell nuclei in the clodronate injected hemispheres was comparable to the number of cell nuclei in PBS injected animals (Figure 4.13C). Iba1 and CC3 expression at day 9 were negligible in brains injected with either dose of free clodronate (Figure 4.13D).



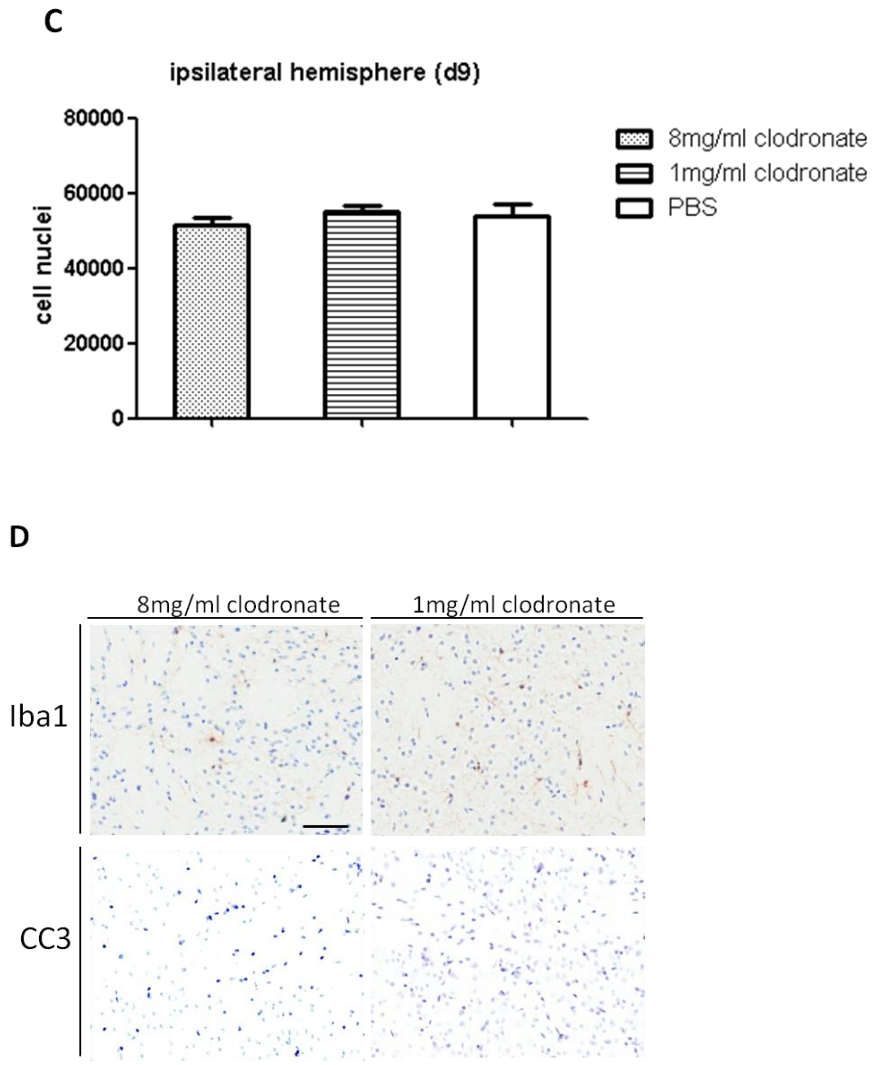
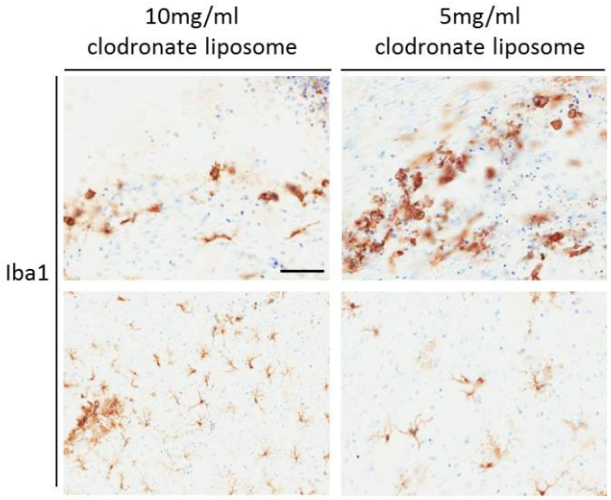


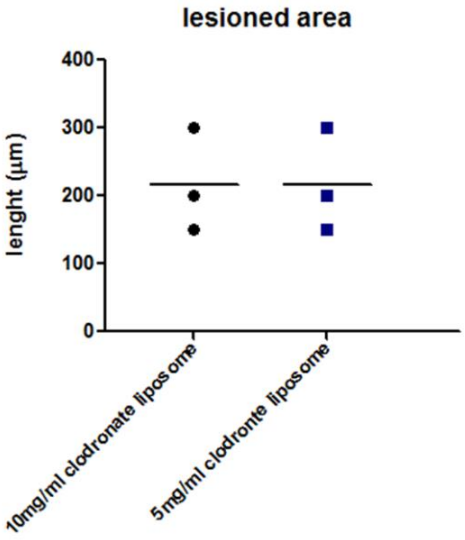
Figure 4.13: Effect of free clodronate on cell context *in vitro* and *in vivo*. (A) Cell viability of 4T1-GFP cells was assessed by MTT assay upon treatment with 2.5mg/ml, 5mg/ml and 7.5mg/ml clodronate salt for 6 and 24 hours. Graphs are representative of two independent experiments performed in triplicate per point ($p<0.0001$, one-way ANOVA with Dunnett's multiple comparison test). (B) Quantitation of cell nuclei in ipsilateral and contralateral hemispheres 9 days after intracerebral injection of 8mg/ml or 1mg/ml free clodronate (n=3; 3 fields of view per section, 6 sections per animal; $p>0.05$, two-way ANOVA). (C) Quantitation of cell nuclei in ipsilateral hemispheres 9 days after injection with free clodronate or PBS (n=2-3; 3 fields of view per section, 6 sections per animal; $p=0.4254$, one-way ANOVA). (D) Representative IHC images for Iba1 and CC3 expression in the striatum of mice intracerebrally injected with 8mg/ml or 1mg/ml free clodronate (d9). Scale bar 50 µm.

As an additional control for our clodronate liposome depletion experiments, intracerebral injections of mannosylated clodronate liposomes in naïve brains were performed. 10mg/ml and 5mg/ml clodronate encapsulated in liposomes was used to assess its effect in non-challenged brains. Intracerebral administration of 10mg/ml and 5mg/ml mannosylated clodronate liposomes caused Iba1 upregulation and microglial activation in the brain (Figure 4.14A). For both concentrations of clodronate liposomes we observed similar extent of microglial infiltration (ramified cells) and activation (amoeboid cells; although potentially perivascular macrophages as discussed in chapter 3) (Figure 4.14A, B). Expression of CC3 was also observed in brains injected with both concentrations of clodronate liposomes close to the injection site (Figure 4.14C), although quantitation of its expression levels in the injected hemispheres revealed non-significant differences between free clodronate and encapsulated clodronate injected brains (Figure 4.14D). Immunofluorescent staining showed that CC3 was expressed by Iba1 microglia cells and not neurons, vessels or astrocytes, although GFAP was upregulated in the injected hemispheres (Figure 4.14E).

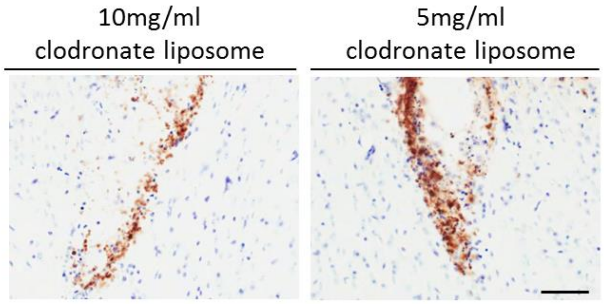
A


10mg/ml
clodronate liposome
5mg/ml
clodronate liposome
Iba1

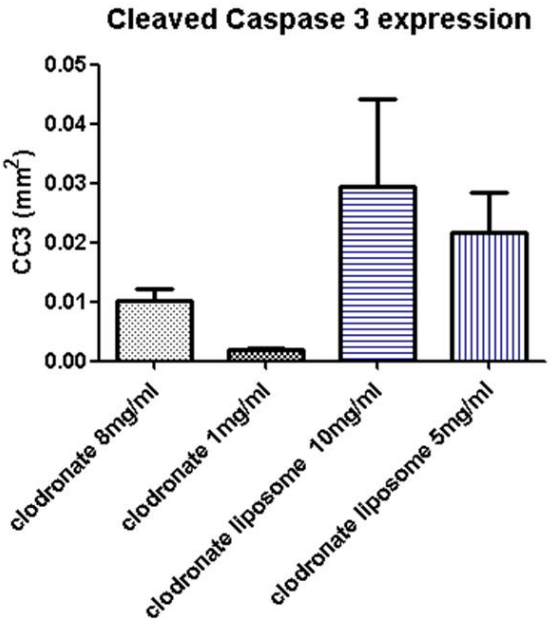
B


lesioned area
lenght (µm)
400
300
200
100
0
10mg/ml clodronate liposome
5mg/ml clodronte liposome

C


10mg/ml
clodronate liposome
5mg/ml
clodronate liposome

D


Cleaved Caspase 3 expression
CC3 (mm2)
0.05
0.04
0.03
0.02
0.01
0.00
clodronate 8mg/ml
clodronate 1mg/ml
clodronate liposome 10mg/ml
clodronate liposome 5mg/ml

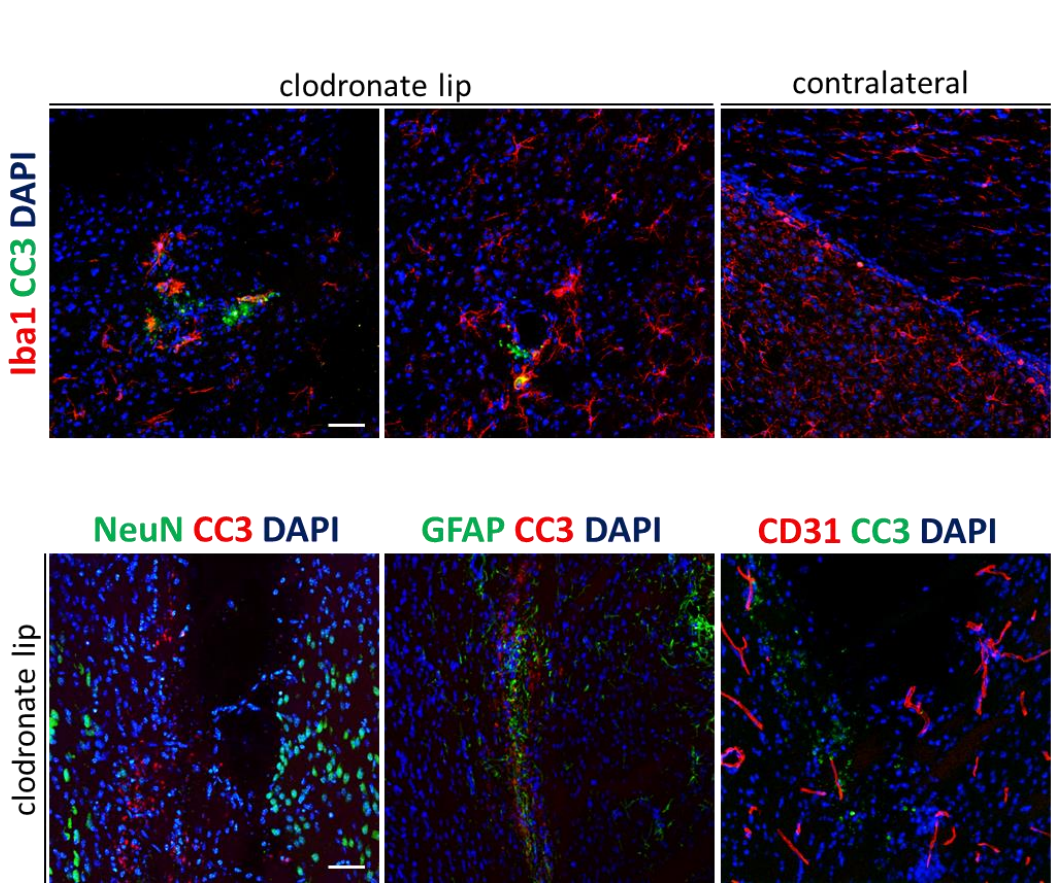


Figure 4.14: Effect of mannosylated clodronate liposomes in the naïve brain. (A) Representative IHC images showing microglial activation 9 days after intracerebral injection with mannosylated liposomes containing 10mg/ml or 5mg/ml clodronate. (B) Quantitation of the rostrocaudal length of the region bearing the amoeboid microglial phenotype (n=3; p=1, two-tailed unpaired t-test). (C) IHC detection of apoptosis, as indicated by staining for CC3, 9 days after intracerebral injection with mannosylated liposomes containing 10mg/ml or 5mg/ml clodronate. (D) Quantitation of expression of CC3 in mouse brains 9 days after injection with free clodronate (black pattern bars; 8mg/ml and 1mg/ml) or liposome encapsulated clodronate (blue pattern bars; 10mg/ml and 5mg/ml) (n=2-3; p=0.079, one-way ANOVA). (E) Immunofluorescent co-localisation of CC3 with microglia (Iba1), neurons (NeuN), astrocytes (GFAP) and vessels (CD31). Scale bars 50 µm

4.5 Discussion

Tumour associated macrophages (TAMs) are promising targets for cancer treatment. Different approaches for targeting TAMs or clinically relevant subsets of TAMs have been reported. Having previously shown that both M1 and M2 cells co-exist in the tumour microenvironment of brain metastases, the possibility of targeting the pro-tumourigenic M2 microglia in brain metastasis was investigated. Given that MRC1 was identified as an M2 phenotypic marker in our experimental brain metastasis model, I exploited the mannosylated liposome approach to target M2 microglia specifically and reasoned that this depletion would reduce intracranial tumour burden.

Initially, to evaluate the specificity of the mannosylated liposomes against differentially polarised cells *in vitro* experiments were performed with microglia and macrophages polarised to an M1 or M2 phenotype. In the literature, it is very well documented that LPS treatment induces M1 macrophage polarisation, whilst IL-4 treatment induces M2 polarisation (Murray et al, 2014). In our hands, LPS treated cells showed upregulation of iNOS and IL-4 treated cells upregulation of MRC1. In this system, the mannosylated clodronate liposomes affected the viability of IL-4 treated cells, whilst this effect appeared to subside with LPS treatment and, thus, M1 polarisation. Decrease in cell metabolic activity and viability was also evident for both unpolarised microglial cells and macrophages (M0 state) incubated with the clodronate liposomes compared to the control, which is in accordance with published data and might be attributed to the basal levels of MRC1 expression and the intrinsic phagocytic nature of those cells (Miron et al, 2013). In support of that hypothesis, control liposome uptake by M0 (control, non-polarised), M1 (LPS treated) and M2 (IL-4 treated) cells *in vitro* was observed by

fluorescent microscopy, although from qualitative observations using a small number of cells it appears that strongly M1 skewed iNOS$^+$ cells did not readily take up liposomes. These experiments propose the efficiency of mannosylated clodronate liposomes in reducing the viability of M2-like macrophages/microglia specifically, *in vitro*, although an increase of the experimental group sizes or quantification of the absorbance at later timepoints (e.g. 72 hours) could provide a more robust significance of the data .

Subsequently, the effect of mannosylated clodronate liposomes was assessed *in vivo.* As a proof-of-principle experimental approach, mouse IL-4 was intracerebrally injected to induce an M2 CNS inflammatory response. Indeed, a microglial response (Iba1 expression) and upregulation of the M2 marker MRC1 were evident as early as 6 hours after IL-4 injection. Both Iba1 and MRC1 protein expression peaked 48 hours after the IL-4 injection, a timecourse that is in accordance with previous studies (Kawahara et al, 2012). Intracerebral injection of mannosylated clodronate liposomes 24 hours after the IL-4 injection and before the MRC1 expression peak conferred a significant decrease in MRC1$^+$ cells *in vivo* (Figure 4.8B). Importantly, MRC1 is expressed by both microglia and endothelial cells in the IL-4 challenged brain, thus MRC1$^+$ cells rather than MRC1$^+$ microglia were depleted in this setting. This experiment provided evidence of the functionality and specificity of the mannosylated liposome method *in vivo* and is to our knowledge the first time such kind of proof-of-principle approach is applied in a CNS inflammation model.

At this point it is important to mention that the route of liposome administration was an important consideration for the liposomes studies. Efficient delivery of liposome encapsulated drugs in rodent brains after intravenous injection has been reported in the

case of antibody directed liposomes. For instance, targeted brain delivery can be mediated by directing the liposomes against the rat transferrin receptor which is specifically upregulated on the brain endothelium (Huwyler et al, 1996). However, clodronate liposomes do not readily cross the BBB and, thus, do not deplete brain resident microglia when delivered systemically (Fulci et al, 2007). Intracerebral delivery of liposomes in pre-clinical rodent models is not very well characterised in the literature. Delivery of DNA-liposomes in rodent brains was described in 1996 for gene therapy in experimental gliomas (Zhu et al, 1996). More recently, Miron et al described intracerebral injection of mannosylated liposomes in the corpus callosum (Miron et al, 2014). Injection of liposomes in the cortex was performed by Faustino and colleagues when studying the role of microglia in a rat model of neonatal stroke (Faustino et al, 2011). Thus, I chose to deliver the liposomes intrastriatally into the IL-4 challenged and metastatic brain as performed for the 4T1-GFP cell injection. Intracerebrally injected fluorescent control liposomes were found to colocalise with Iba1 positive microglia in IL-4 challenged brain 6 hours after injection. Although a small lesion on the brain tissue at the injection site was observed for those early timepoints of our liposomes studies, this might have to do with increased sensitivity of the tissue when perfusing the animals for brain harvesting, since such histology was not observed for either the control or clodronate liposome injected animals for the later timepoints (e.g d21, data not shown).

Another potential issue for the *in vivo* studies was the possibility of collateral damage due to the intratumoral clodronate liposome delivery. Intracerebral delivery of mannosylated clodronate liposomes in naïve brains elicited mild microglial activation, which was qualitatively more intense than that observed for the PBS injection but less pronounced than that observed for both 4T1-GFP cell and IL-4 injections. Importantly, expression of

the apoptotic marker cleaved caspase 3 nine days after injection of clodronate liposomes in naïve brains was significantly lower than that in 4T1-GFP brains and comparable to its expression levels in 4T1-GFP brains injected with the control liposomes. Together these findings indicate that the intratumoral clodronate liposome delivery does not cause collateral damage in the metastatic brain. Another potential source of collateral damage is clodronate leakage from either the liposomes or apoptotic cells. The control experiments using free clodronate in the naïve mouse brain provide an estimation that such a scenario due to clodronate leakage from the liposomes or apoptotic cells might not be highly probable because minimal expression of CC3 and changes in total cell numbers were observed in those brains when compared to contralateral or PBS injected hemispheres. In support to this, efflux transporter systems located on brain capillary endothelial cells serve to actively transport harmful metabolites, xenobiotic substances and Aβ peptides out of the brain (Sun et al, 2002; Shibata et al, 2000) which might explain the absence of any inflammatory activation in brains nine days after intracerebral injection with free clodronate. However, it should be noted that brain cells may have different susceptibility to clodronate than cancer cells. Although previous studies have shown that clodronate does not significantly affect melanoma cell viability and that intratumoral administration of free clodronate in melanoma xenografts did not affect tumour growth *in vivo* (Webster et al, 2014), in this study free clodronate significantly reduced breast cancer cell (4T1) viability. This finding is in accordance with studies showing that bisphosphonates such as clodronate and zoledronate reduce the viability of breast cancer cell lines (Senaratne et al, 2000). Studies with clodronate intracerebrally injected in 4T1 metastatic brains were not performed thus the possibility that free clodronate may contribute to cancer cell death *in vivo* too cannot be excluded.

Based on the same rational as for the IL-4 model, the mannosylated clodronate liposome approach was applied to the well described 4T1-GFP metastatic model. Although as described in Chapter 3 the abundance of $MRC1^+$ microglia did not significantly change over the 21 day timecourse study, liposomes were injected at day 12 taking into account the slight decrease of microglial polarisation at day 10. The depletion of $MRC1^+$ cells was assessed and confirmed 3 days after mannosylated clodronate liposomes injection by immunostaining. Some $Iba1^+$ cells in close association with tumour foci in the striatum of clodronate liposomes injected animals adopted an amoeboid morphology, probably indicative of an activated phenotype. Microglial cells in the metastatic brains of control liposomes or PBS injected animals did not acquire such morphology, suggesting that this alteration is related to M2 depletion. Moreover, similar patterns of this phenotypic activation were observed in brains of naïve animals injected with clodronate liposomes, although to a lesser extent. It can be postulated, therefore, that this phenotypic pattern is due to the depletion of the very few $MRC1^+$ microglial cells in the naïve brain (Chapter 3). Although M1 polarisation was not quantitated, $iNOS^+$ microglia were observed in clodronate liposome injected brains (not shown). Given the dynamic equilibrium of M1 and M2 cells, an increase in $iNOS^+$ microglia in the metastatic brain might be a potential scenario warranting further investigation. Miron and colleagues observed an increase in M1 cells following M2 microglial depletion (Miron et al, 2013), which in our experimental model could account for the decreased intracranial tumour burden observed in the metastatic brain in clodronate liposome injected animals.

Intracranial administration of mannosylated clodronate liposomes resulted in decreased tumour burden in the clodronate liposome injected animals compared to control liposome injected mice. Tumour decrease was associated with increased expression of

CC3 compared to control animals. In the clodronate liposome injected brains, CC3 was primarily expressed by GFP positive tumour cells and occasionally by microglial cells. Since staining for GFP and Iba1 was not performed on the same brain sections, there is a possibility that CC3 might be expressed by other brain resident cells that undergo apoptosis as a result of the death of microglia. Moreover, expression of CC3 extracellularly was observed. Release of caspases to the cell exterior has been reported in the literature by both apoptotic and viable cells (Hentze et al, 2001; Garcia-Faroldi et al, 2013). Although the exact role of such a phenomenon has not been comprehensively studied, there are indications of induction of intercellular inflammatory signalling, at least in the case of extracellular caspases in the CNS (Viviani et al, 2000; Berta et al, 2014). Vascularity of the tumours in the clodronate liposomes treated animals was determined based on a report of decreased vessel density in subcutaneous mouse tumours treated with clodronate liposomes (Zeisberger et al, 2006). However, by visual examination only there didn't appear to be any significant changes in vascularised tumours in the clodronate liposome treated animals compared to the control liposome treated animals at any timepoint. This observation may suggest M2 microglia induce additional non-vascular mechanisms to support tumour growth in the brain. Additionally, it should be considered investigating vessel density at different timepoints between days 15 and 28 since vessel depletion at an early timepoint in the metastatic brain may have an effect on tumour growth. MRC1 expression on vessels has not been investigated in the metastatic brain as part of this thesis, thus the possibility that it occurs similarly to the IL-4 challenged brain cannot be excluded. In such a scenario, MRC1 expression on $CD31^{+}$ blood vessels could account for vessel depletion upon mannosylated clodronate liposomes administration.

In conclusion, it has been shown that mannosylated clodronate liposomes reduce cell viability of microglia and macrophages *in vitro*. Moreover, M2 polarised cells seem to be more sensitive to the clodronate liposome treatment compared to M1 polarised cells, although additional experiments are warranted to further corroborate the susceptibility of differentially polarised cells to the mannosylated liposome treatment. Most importantly, intracerebral injection of mannosylated clodronate liposomes efficiently depleted $MRC1^+$ (M2) cells in IL-4 challenged murine brains. Furthermore, intracerebrally injected mannosylated clodronate liposomes at an early stage (possibly accounting for *in vivo* depletion of M2 microglia) significantly reduced intracranial tumour burden in the metastatic brain. Increased levels of apoptosis, indicated by cleaved caspase 3 expression, were associated with 4T1 tumour foci in the animals injected with clodronate liposomes compared to those injected with control liposomes. Thus, targeting the anti-inflammatory M2 microglial population could be of therapeutic benefit in brain metastasis. However, a few aspects of this project not thoroughly investigated yet necessitate further research. For instance, the diffusion of mannosylated liposomes once intracerebrally injected in the metastatic brain and quantitation of $iNOS^+$ (M1) and $MRC1^+/Arg1^+$ (M2) microglia throughout the metastatic brain should be considered for the validation of this model. Moreover, and taking into account the contradictory results on the *in vitro* and *in vivo* effects of free clodronate, intracerebral administration of free clodronate in the metastatic brain should be added to our control experiments. Another important control that should be included in this study is the use of non-mannosylated clodronate liposomes *in vivo* in order to determine their efficiency in depleting microglia but not $MRC1^+$ cells, such as endothelial cells. In this context, this control would also contribute in determining whether mannosylation of liposomes increases their specificity

towards the M2 phenotype in comparison with the non mannosylated liposomes *in vitro*. Finally, although it was not a priority of this study, further investigation could provide insights into the M1/M2 molecular signatures that sustain metastatic outgrowth in the brain.

Chapter 5

Effect of myeloid specific Krüppel-like factor 4 knock out on the growth of experimental brain metastases

5.1 Introduction

In our previous studies it was demonstrated that *in vivo* depletion of MRC1^{+} microglia at an early timepoint decreased intracranial tumour burden in the intracerebral 4T1-GFP brain metastasis model. In order to further validate those results, the possibility of employing a non-invasive genetic mouse model of deficient M2 microglia polarisation was explored. To this end, a recently described mouse line of myeloid specific Krüppel-like factor 4 (KLF4) knock-out in which myeloid cells are deficient of the KLF4 transcription factor, an important regulator of M2 macrophage polarisation, was chosen to be used (Liao et al, 2011).

For their studies, Liao and colleagues generated a mouse line of myeloid specific KLF4 knock-out by crossing *Klf4*$^{fl/fl}$ mice with LysM$^{cre/cre}$ mice. Both strains have been previously described in the literature. The Cre-loxP system, widely used for mouse genome tailoring, exploits the ability of the bacteriophage P1 derived recombinase Cre to catalyse DNA recombination between two consensus recognition (loxP) sites (Nagy, 2000). The LysM-Cre mouse, in which the Cre recombinase gene is under the control of the endogenous LysM promoter, allows for specific Cre mediated deletion of target genes in myeloid cells (Clausen et al, 1999). The gene targeting strategy involved flanking of *Klf4* exons 2 and 3 with Cre/loxP sites (Katz et al, 2002). Deletion of the flanked genomic area produces a frameshift mutation in exon 4 and, thus, loss of *Klf4* expression. The myeloid specific KLF4 KO was achieved through the LysM-Cre mouse.

KLF4 belongs to the KLF superfamily of zinc finger transcription factors that bind to DNA elements and regulate numerous aspects of cell differentiation. KLF4 has been implicated in diverse cellular processes including myelopoiesis, cellular stemness and monocyte

differentiation (Feinberg et al, 2007; Alder et al, 2008). Recently, Liao's team identified KLF4 as a critical regulator of macrophage polarisation under inflammatory conditions. Using both *in vitro* and *in vivo* approaches, Liao et al showed that KLF4 is essential for robust polarisation towards the M2 phenotype and, importantly, that KLF4 deficient macrophages present with enhanced M1 phenotypic and functional characteristics. More specifically, KLF4 deficient macrophages presented with reduced capacity for inducing M2 transcripts (Arg1, MRC1) compared to wild type cells under IL-4 induced inflammatory stress, whilst they expressed significantly more M1 transcripts (iNOS, TNF-a, COX2) under LPS stimulation. *In vivo*, the myeloid KLF4 deficient mouse line (LYSK) revealed delayed wound healing due to increased expression of iNOS compared to the wild type line (LYSM) (Liao et al, 2011). Other groups have also corroborated the role of KLF4 in macrophage polarisation in the context of inflammatory disease, such as alcohol liver disease and obesity (Saha et al, 2015; Luan et al, 2015).

5.2 Aims

Primary aims of this chapter were:

1. To investigate intracranial tumour growth in LYSM and LYSK mice intracerebrally injected with syngeneic mouse cancer cell lines (breast, lung, melanoma).
2. To validate the microglia specific knock-out of KLF4 and assess M2 polarisation in LYSK mice in response to brain metastasis.

5.3 Methods

LYSM and LYSK mice were intracerebrally injected with EO771-GFP, B16F10-GFP or LLC-GFP as described in section 2.5.5.1. Brains were harvested by perfusion-fixation on day 14 after tumour cell injection. Tumour volumes were calculated by quantitation of the tumour foci area (cresyl violet counterstain) on brain sections 50 µm apart spanning the metastatic lesion. Microglial infiltration was assessed by Iba1 IHC and areas were quantified on brain sections 50 µm apart spanning the metastatic lesion. Again, by referring to microglia throughout this chapter, one is referring to the mixed microglia/macrophage population. Immunofluorescence was performed on 10 µm thick brain or liver sections using anti-KLF4 and anti-MRC1 antibodies (section 2.12.1). Quantitation of fluorescent co-localisation was performed using the Image J plugin.

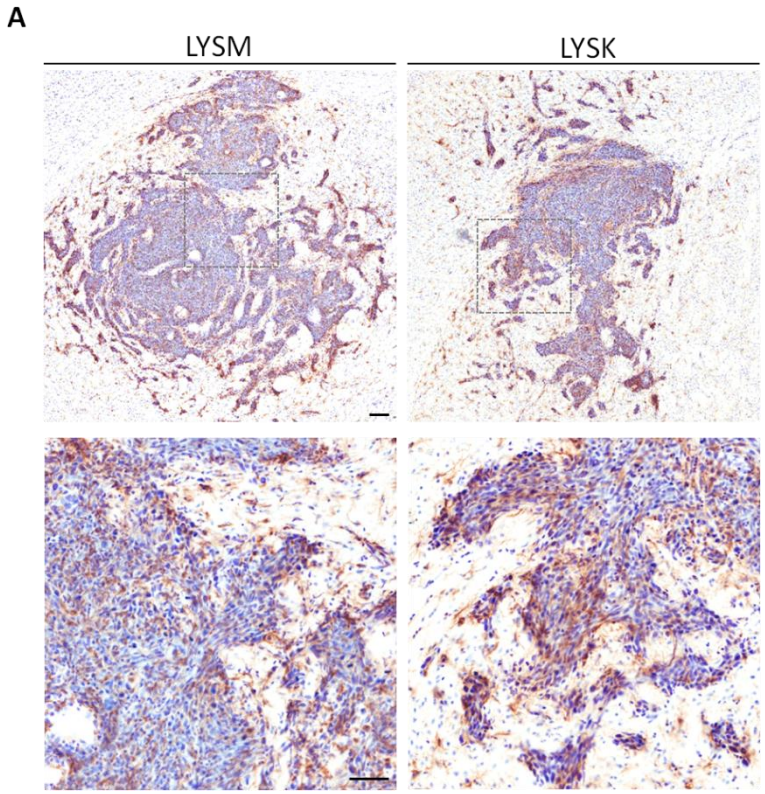
5.4 Results

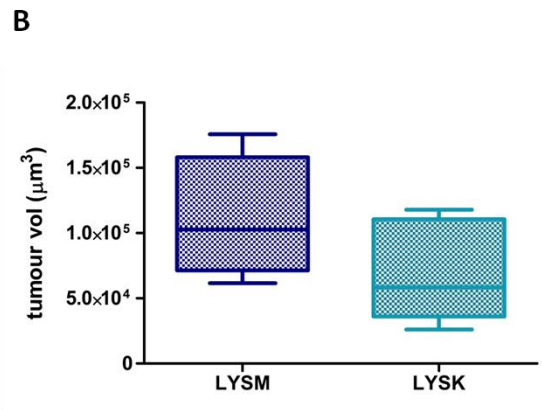
5.4.1 Intracranial metastasis burden in LYSM and LYSK mice

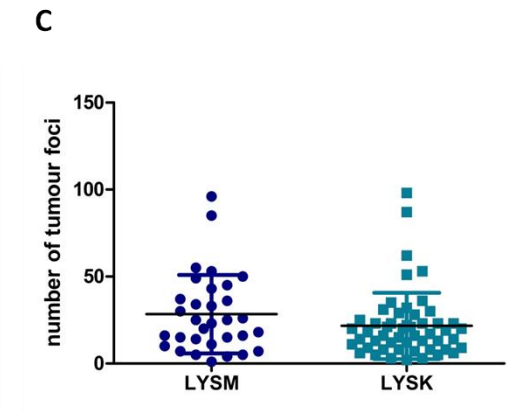
5.4.1.1 Metastasis burden in LYSM/LYSK mice injected with EO771 cells

Intracranial tumour growth of breast, lung and melanoma tumours in LYSM and LYSK mice using the intracerebral metastatic model was investigated. Initially, tumour growth of mammary carcinoma EO771 cells in the brains of LYSM and LYSK mice was assessed. Both mouse lines developed large intracranial EO771 tumours by day 14 which presented with a solid tumour core and smaller tumour foci invading into the adjacent parenchyma (Figure 5.1A). Intracranial tumour burden was not significantly different between LYSK and LYSM mice, although there was a trend towards decreased tumour volume in LYSK

animals compared to wild type LYSM (Figure 5.1B). Moreover, there were no significant differences in the number of metastatic foci present in the metastatic brains of LYSM and LYSK mice (Figure 5.1C). Infiltration of Iba1^{+} microglia cells was prominent in both LYSM and LYSK mice (Figure 5.1A) and the microglial infiltration area positively correlated with tumour area on brain sections from both LYSM and LYSK mice (Figure 5.1D).







D

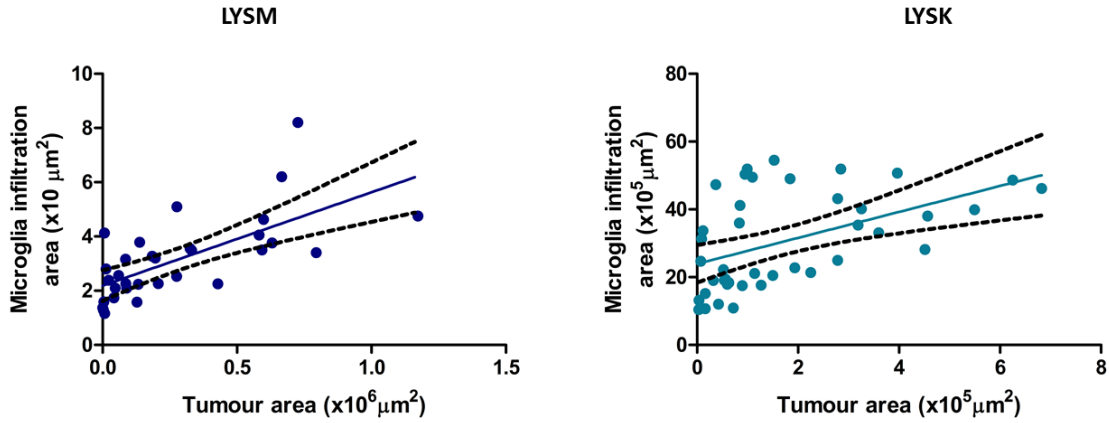
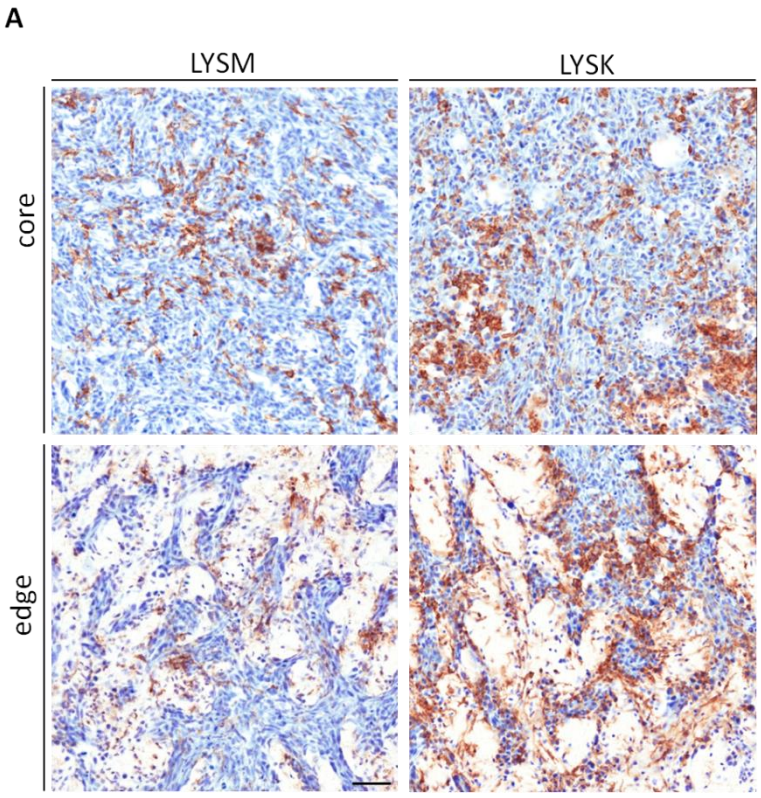


Figure 5.1: Tumour growth and microglia infiltration of EO771 tumours in LYSM and LYSK mice. (A) Representative IHC images for Iba1 in brains of mice 14 days after intracerebral injection with $5x10^2$ EO771 mammary carcinoma cells. Magnified images of the insets are shown in the bottom panel [scale bars 100μm (top), 50μm (bottom)]. Quantitation of tumour volumes (B) (p=0.1482, unpaired two-tailed t test) and number of metastatic foci (C) (p=0.1456, unpaired two-tailed t test) in brains of LYSM and LYSK mice intracerebrally injected with EO771 cells at day 14 (n=4-6). Correlation of microglia infiltration area with tumour area on brain sections of LYSM (D, left) (r^2=0.4564) and LYSK (D, right) (r^2=0.2377) mice.

5.4.1.2 Metastasis burden in LYSM/LYSK mice injected with LLC cells

The growth of lung cancer LLC cells intracerebrally injected in LYSM and LYSK mice was also investigated. $2x10^3$ intracerebrally injected LLC cells produced large metastases in the brains of both mouse lines by day 14. LLC tumours presented with a solid tumour core and smaller foci at the edge of tumours, invading into the adjacent parenchyma (Figure 5.2A). IHC revealed prominent infiltration of the cores and edges of the LLC tumours by $Iba1^+$ microglia cells in both LYSM and LYSK mice (Figure 5.2A). As for the EO771 model, intracranial tumour burden was not significantly different between LYSK and LYSM mice, although there was a trend towards decreased tumour volume in LYSK

compared to LYSM mice (Figure 5.2B). Moreover, there were no significant differences in the number of metastatic foci present in the metastatic brains of LYSM and LYSK mice, although a trend towards increased numbers of metastatic foci was evident for the LYSK animals (Figure 5.2C). Microglial infiltration defined as Iba1 positive immunostaining within the infiltration area positively correlated with tumour area on brain sections from both LYSM and LYSK mice (Figure 5.2D).



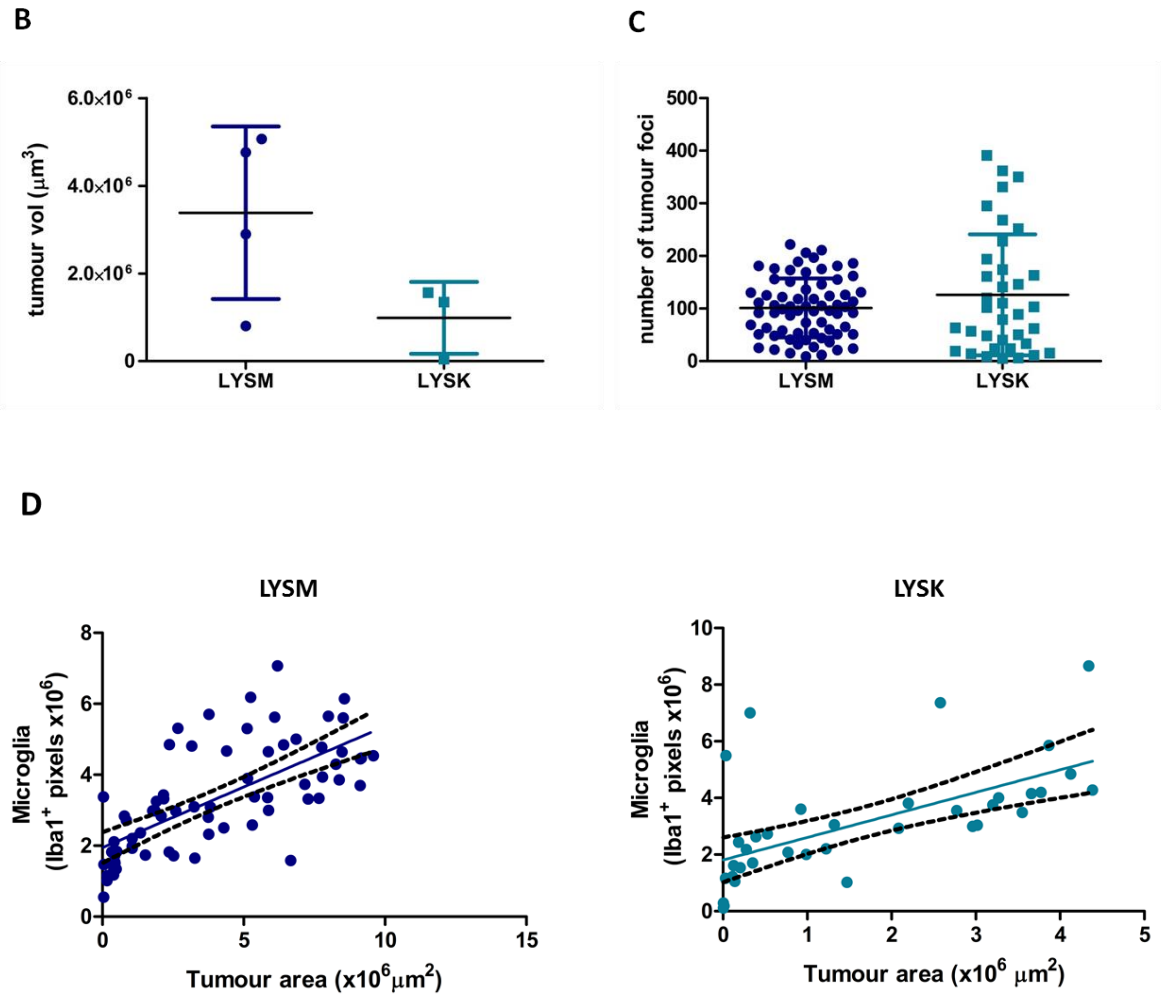
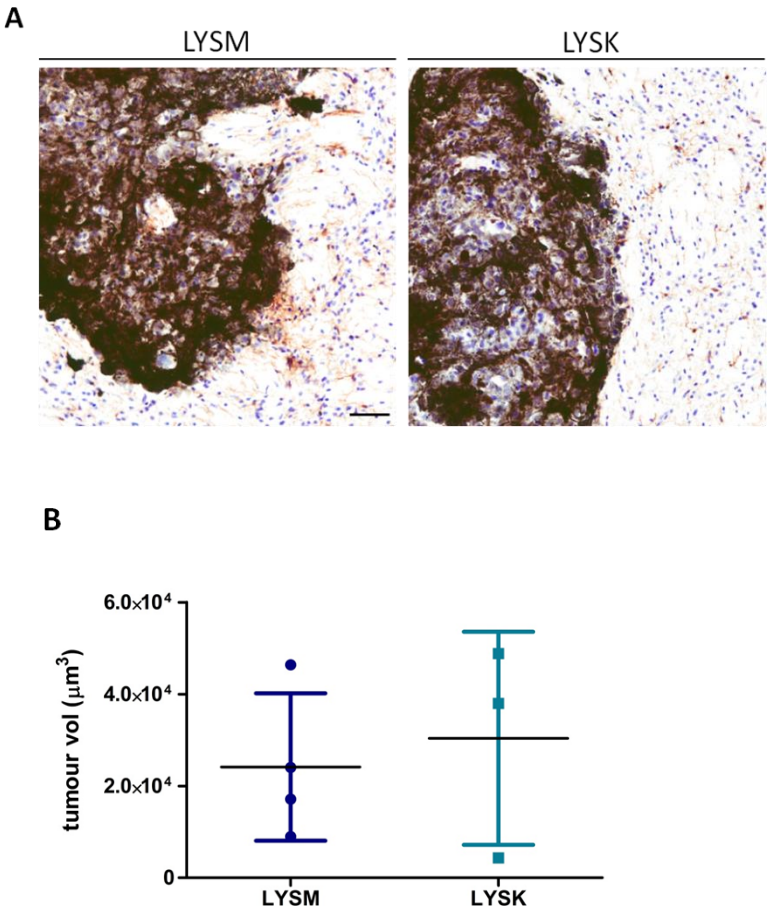


Figure 5.2: Tumour growth and microglia infiltration of LLC tumours in LYSM and LYSK mice. (A) Representative IHC images for Iba1 in brains of mice 14 days after intracerebral injection with $2x10^3$ LLC lung carcinoma cells. Images from the core and edges of the tumours are shown for both mouse lines (scale bars 50 µm). Quantitation of tumour volumes (B) (p=0.1088, unpaired two-tailed t test) and number of metastatic foci (C) (p=0.1363, unpaired two-tailed t test) in brains of LYSM and LYSK mice intracerebrally injected with LLC cells at day 14 (n=3-4). Correlation of Iba1 positive pixels within the microglia infiltration area with tumour area on brain sections of LYSM (C, left) (r^2=0.4719) and LYSK (C, right) (r^2=0.3819) mice.

5.4.1.3 Metastasis burden in LYSM/LYSK mice injected with B16F10 cells

The growth of a mouse melanoma cell line intracerebrally injected in LYSM and LYSK mice was investigated. $2x10^3$ B16F10 cells intracerebrally injected produced small metastases in the brains of both mouse lines at day 14 that grew as solid, minimally invasive tumours (Figure 5.3A). IHC revealed relatively weak infiltration of the melanoma tumour, defined by the dark brown melanin pigment, by $Iba1^+$ microglia cells in both LYSM and LYSK mice (Figure 5.3A). However, as for the previous two models, intracranial tumour burden was not different between LYSM and LYSK mice for the B16F10 tumours (Figure 5.3B). The microglial infiltration area correlated positively with tumour area on brain sections from both LYSM and LYSK mice, albeit less strongly compared to LLC and EO771 tumours ($r^2 \leq 0.16$, Figure 5.3C).



C

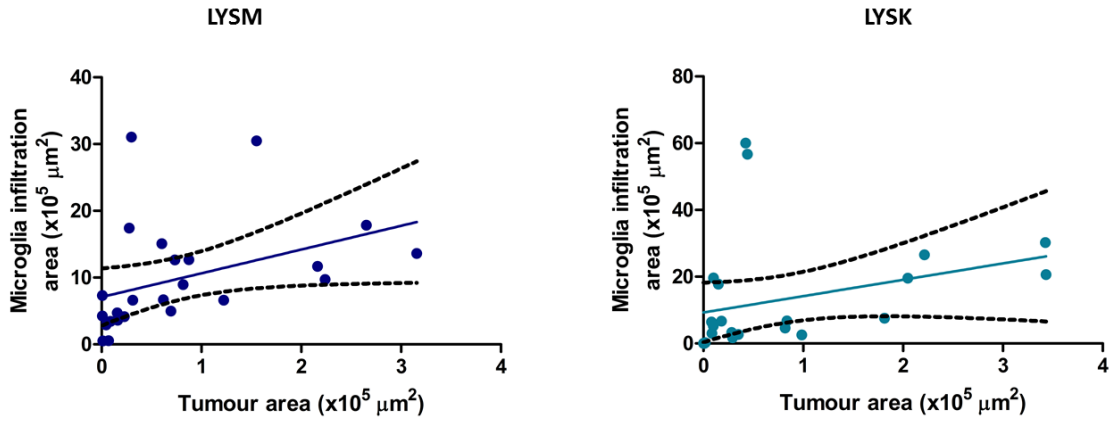


Figure 5.3: Tumour growth and microglia infiltration of B16F10 tumours in LYSM and LYSK mice. (A) Representative IHC images for Iba1 (brown) in brains of mice 14 days after intracerebral injection with $2x10^3$ B16F10 melanoma cells (dark brown owed to melanin). (Scale bars 50 µm). (B) Quantitation of tumour volumes (p= 0.6878, unpaired two-tailed t test) in brains of LYSM and LYSK mice intracerebrally injected with B16F10 cells at day 14 (n=3-4). Correlation of the microglia infiltration area with tumour area on brain sections of LYSM (C, left) (r^2= 0.1605) and LYSK (C, right) (r^2= 0.07086) mice.

5.4.2 Validation of the KLF4 knock-out in the LYS model

Given that no significant differences in intracranial tumour volumes were observed between LYSM and LYSK mice, the deletion of KLF4 in LYSK mice was investigated by immunostaining of liver and brain sections. However, by double immunofluorescent staining for Iba1 and KLF4 on brain sections of LYSM and LYSK mice bearing experimental EO771 mammary metastases, we identified $KLF4^+$ microglia in both mouse lines (Figure 5.4A). Quantitation of the co-localisation of KLF4 with Iba1 reveals non-significant differences in the expression levels of microglia derived KLF4 between the LYSM and LYSK mice (p>0.1, Figure 5.4B). Moreover, the expression of KLF4 by macrophages was assessed in livers of LYSK and LYSM mice, given that livers are also populated by resident macrophages. However, in non-challenged livers there was negligible KLF4 expression

and, thus, no KLF4^{+} macrophages were identified in the liver of either mouse line (Figure 5.4C).

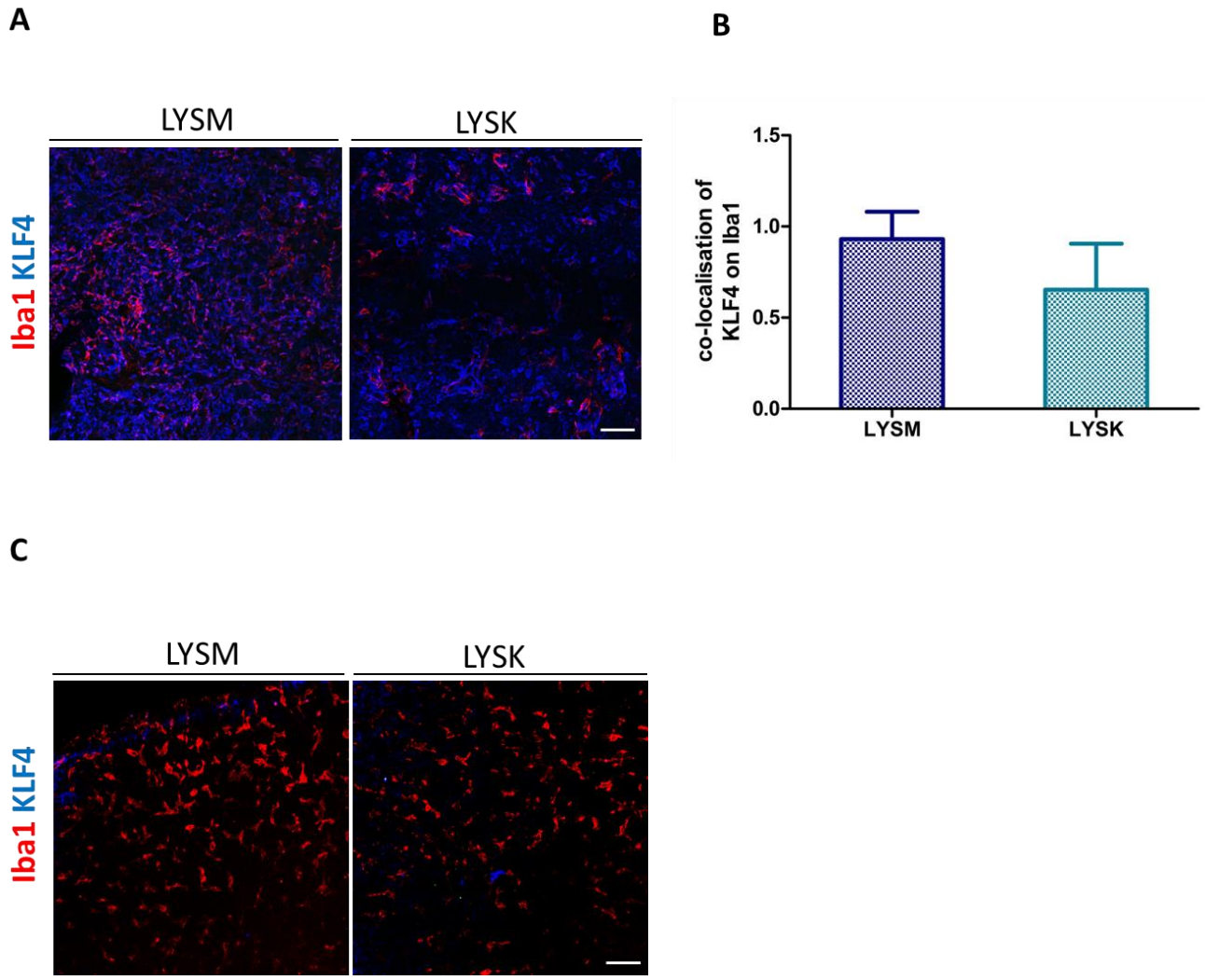


Figure 5.4: Validation of the myeloid KLF4 knock out in LYSK mice. (A) Double immunofluorescence for Iba1 (microglia) and KLF4 in the brains of LYSM and LYSK intracerebrally injected with 5x10^{2} EO771 cells (day 14). (B) Quantitation of the co-localisation of KLF4 on Iba1 in control (LYSM) and KLF4 knock-out (LYSK) mice (unpaired two tailed t test, p=0.1069; n=4, 2-3 sections per animal). (C) Double immunofluorescence for Iba1 (resident macrophages) and KLF4 in livers of LYSM and LYSK mice bearing intracranial EO771 metastases. Scale bars 50 µm.

Finally, microglial M2 polarisation in metastatic brains of LYSM and LYSK mice was assessed. To this end, immunofluorescent staining for the microglia specific M2 marker MRC1 on brain sections from mice intracerebrally injected with EO771 and LLC tumour

cells was performed. In contrast to expectations, brain metastatic LLC and EO771 tumours were infiltrated by $MRC1^{+}$ cells at day 14 after induction of intracranial metastases (Figure 5.5A, B).

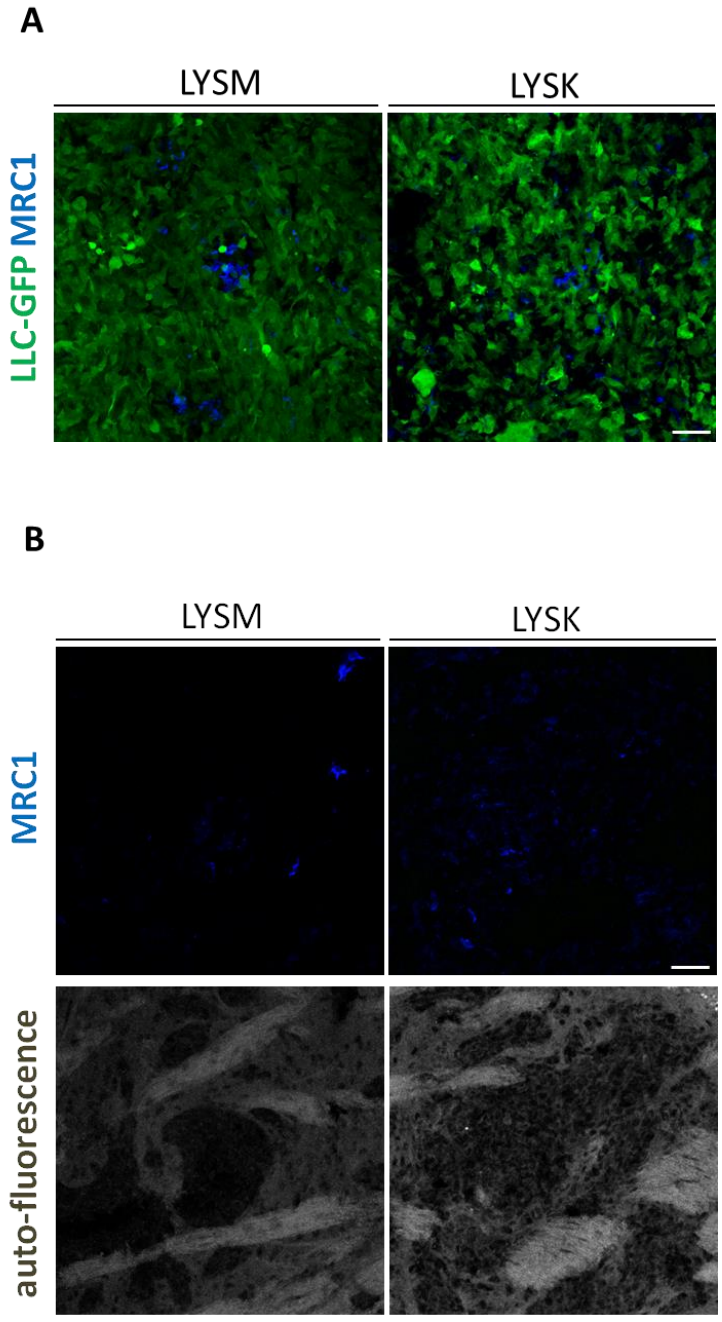


Figure 5.5: M2 microglia in the metastatic brains of LYSM and LYSK mice. Immunofluorescence for MRC1 (M2 marker) in the metastatic brains of LYSM and LYSK mice intracerebrally injected with LLC-GFP (A) and EO771 (B) tumour cells. Auto-fluorescence images of the corresponding fluorescent images (B) reveal the location of the tumours. Scale bars 50 µm.

5.5 Discussion

Different molecules have been implicated in the specific polarisation of macrophages. In this chapter we investigated the effect of myeloid knock-out of the transcription factor KLF4, which has been implicated in M2 macrophage polarisation (Liao et al, 2011), on the growth of brain metastases.

Efficient gene targeting on microglia using the Cre-loxP/LysM approach has been described in the literature (Kavanagh et al, 2015). However, others report low gene recombination efficiency in microglia of LysM/Cre animals that present with efficient gene targeting in peripheral myeloid cells (Goldmann et al, 2013). In this model, KLF4 expressing microglia were identified in the metastatic brains of both LYSM (wild type KLF4) and LYSK (KLF4 deficient) mice by double immunofluorescence. Although there was a small decrease in $KLF4^{+}$ microglia in LYSK brains compared to LYSM, their presence in the inflamed brain is indicative of inefficient microglial targeting. Preliminary results on intracranial tumour burden and morphology of EO771, LLC and B16F10 metastatic tumours showed no significant differences between LYSM and LYSK mice, which could be attributed to inefficient KLF4 microglial targeting and polarisation to the M2 phenotype. However, an increase in experimental group sizes should be considered in order to validate potential statistical significance between the two mouse lines. For instance, G power analysis of the pilot data presented here could determine the group sizes required for future experiments. In addition, quantitation of tumour burden for the two mouse lines at timepoints different than day 14 could also yield potential statistically significant differences.

Liao and colleagues have confirmed the KLF4 knock-out in peritoneal macrophages and BMDMs, but have not assessed KLF4 gene targeting in resident macrophage populations (Liao et al, 2011). Thus, further quantitative analysis of the KLF4 knock-out in tissue resident and peripheral macrophages of the LYSK mouse line is needed in order to validate the data on tumour burden for this model. KLF4 expression in non-challenged livers of the LYSM and LYSK mice bearing experimental brain metastases was not observed. However, this may reflect the lack of macrophage activation and hence KLF4 induction. Thus, the KLF4 knock-out in non-CNS resident macrophages should be assessed under inflammatory conditions, preferably M2-like inflammatory stress. Finally, when considering the large EO771 and LLC intracranial tumours, there are higher chances of compromised BBB and, thus, easier influx of circulating monocytes than for the smaller B16F10 tumours. Assuming that peripheral myeloid cells of the LYSK mice carry the KLF4 knock-out, although not yet validated, the contribution of M1-like circulating macrophages to the trend towards decreased tumour burden observed in LYSK mice should be considered.

In Chapter 1, a very strong positive correlation between intracranial 4T1 tumour burden and microglia infiltration was showed. Here, the correlation of tumour growth and microglial activation was also investigated. Those two parameters are positive correlated for all primary tumour types and mouse lines studied. No differences were observed between LYSM and LYSK mice, a finding which is indicative of constant microglial activation, irrespective of the phenotype and potential M1-M2 shifts. However, relatively weak microglial activation in response to the B16F10 tumours compared with the EO771 and LLC tumours was observed. Similarly, a recent study on experimental B16 melanoma brain metastases showed microglial infiltration of intracranial tumours, although to a

lesser extent than other immune cell infiltration (Amit et al, 2013). Moreover, the aforementioned observations are in accordance with published data on human brain metastatic melanoma tumours, which exhibit decreased peritumoral microglial infiltration in comparison to lung cancer brain metastases (Berghoff et al, 2013).

In conclusion, further validation of the LYSM/LYSK model as a tool to study the contribution of M2 microglia to metastatic growth is needed. This model does not provide absolute elimination of the M2 phenotype in the brain, contrary to what would have been expected (Liao et al, 2011). Although the expression of KLF4 by microglia in the metastatic brains of both LYSM and LYSK suggests inefficient knock-out, microglial polarisation should be further validated under other inflammatory stresses. For instance, microglial polarisation should be tested in the context of an IL-4 induced M2-like neuroinflammatory model (described in Chapter 4) and an M1-like neuroinflammatory model, induced by pro-inflammatory stimuli such as IL-1β or TNF. Investigation of the microglial phenotype under the aforementioned conditions will provide answers about potential stimuli-specific polarisation of microglia in the LYSM/LYSK mice and allow us to draw conclusions as to whether the findings are tumour specific or not. Importantly, the polarisation of circulating macrophages activated by M1 and M2 stimuli should be also investigated, in order to corroborate the contribution of peripheral polarised macrophages in brain metastasis. Finally, alternative models of M2 microglia targeting should be employed, such as the recently described approach of *in vivo* TAM re-education towards the M1 phenotype by antibody targeting (Georgoudaki et al, 2016), in order to investigate the effect of M1 and M2 microglia in the development of brain metastasis.

Chapter 6

Discussion and future directions

6.1 General discussion

The inflammatory response to brain metastasis is poorly studied. The work in this thesis suggests that microglia, the brain resident macrophages, are important effectors of the inflammatory response to experimental brain metastases at the early stages of tumour progression and that targeting specific subpopulations could be of therapeutic benefit.

The homing of microglia/macrophages in human and murine brain metastases has been reported in the literature. However, a more detailed investigation of the microglial response to brain metastases at its early stages was lacking. In this work microglial infiltration of experimental 4T1 breast cancer brain metastases was investigated across a 28 day timecourse study and sustained microglial infiltration of the metastatic foci was seen. This is, to our knowledge, the first study demonstrating a dynamic association between microglia and tumour cells at the early stages of metastatic outgrowth in the brain. Moreover, a strong positive correlation between microglial infiltration and intracranial tumour burden was evident. In support of the hypothesis that microglia are important effectors of the inflammatory response to brain metastasis, microglial infiltration of experimental EO771, LLC and B16F10 metastases in a C57BL/6 model (LYSM) also showed a positive correlation with tumour area. Similarly, Lorger's group reported microglial infiltration of experimental parenchymal brain metastases (Rippaus et al, 2016). A study by Zhai and colleagues has demonstrated sustained microglial infiltration of experimental gliomas (Zhai et al, 2010). Interestingly, however, Ajami et al reported only a transient microglial infiltration of EAE brains with a significant decline in the number of $Iba1^{+}$ resident cells as disease progressed to complete paralysis (Ajami et al, 2011). Thus, the microglial response to malignant cells appears to be a robust feature

of the tumour microenvironment and further investigation of the functional crosstalk between microglia and tumours cells in the metastatic brain could provide useful insights about the progression of metastasis.

Phenotypic analysis of microglia in the metastatic brain revealed the presence of both pro-inflammatory M1 ($iNOS^+$, $COX2^+$) and anti-inflammatory M2 ($Arg1^+$, $MRC1^+$) cells during the early stages of metastatic outgrowth. A recent study by Rippaus et al also reported mixed M1 and M2 macrophage populations in the murine metastatic brain (Rippaus et al, 2016). In the context of cancer, M1 like cells can exert cytotoxicity whilst M2 like cells can promote progression via their pro-survival and pro-angiogenic functions. Thus, the balanced coupling of the M1 and M2 microglial response during the early stages of metastatic progression might be permissive of the establishment of macrometastases. This hypothesis was tested by employing an *in vivo* M2 microglia depletion approach using mannosylated clodronate liposomes. Successful depletion of $MRC1^+$ M2 cells in an IL-4 induced neuroinflammatory model allowed confident application of this approach to the 4T1 metastatic model and study of the progression of intracranial metastasis. Depletion of $MRC1^+$ microglia lead to a significant decrease in intracranial tumour burden in the metastatic brain. Moreover, altered morphology of microglia and increased expression of CC3 in close association with the tumour foci were evident following M2 microglia depletion. These findings suggested that M2 microglia sustain metastatic outgrowth in the brain and could be exploited for therapy.

A complementary approach to further validate the role of M2 like microglia in the metastatic brain was employed using the LYSM/LYSK mouse line of myeloid specific KLF4 knock out which has been shown to promote M1 polarisation (Liao et al, 2011). This

mouse line has provided a useful tool to study peripheral, non-CNS resident macrophages and the contribution of polarised macrophage to disease. However, in our hands, the LYSK mice failed to show efficient KLF4 targeting in microglia and, consequently, deficient M2 polarisation. The presence of $MRC1^{+}$ cells in the brains of both mouse lines might explain the non-significant decrease in tumour volumes between LYSM and LYSK mice. Further validation of the LYS-KLF4 model in the context of brain metastasis and neuroinflammatory stress could provide information about microglial polarisation and inflammatory activation in the brain in relation to KLF4 signalling (Kaushik et al, 2010). Moreover, upon validation of the KLF4 knock-out in non-CNS myeloid cells, the role of peripheral M2 macrophages in the progression of brain metastasis could be investigated.

6.2 Future directions

The experiments performed for the fulfilment of this thesis set the framework of studying the microglial response to brain metastasis. At this point, only intracerebral models of brain metastasis have been studied and a future step forward would be to further corroborate the findings reported here using syngeneic and xenograft intracardiac models of brain metastasis. For instance, use of the mammary murine 4T1 or human MDA-MB-231 cell lines intracardially injected into BALB/c or SCID mice, respectively. Mimicking of a physiologically relevant metastatic process and human disease will provide a more comprehensive understanding of the microglial response to brain metastasis.

Although microglial activation and phenotypic polarisation in response to brain metastasis has been clearly demonstrated in this study, investigation of the molecular

characteristics of tumour cells and associated polarised microglia would provide additional mechanistic insights into the biology of brain metastasis. It is well established that microenvironmental cues influence tumour cell behaviour but this field is understudied in the context of secondary cancer to the brain. Targeting host and tumour interactions, through the cellular adhesion molecules for instance, could be of therapeutic benefit in brain metastasis (Soto et al, 2016). Knock-out of LFA-1 on breast cancer cells reduces intracranial tumour burden and is associated with changes in host-tumour interactions including altered microglial molecular signatures. Moreover, a functional crosstalk between cancer cells and M2 metastasis infiltrating microglia/macrophages mediated by the inflammatory molecule lymphotoxin-β was recently reported (Rippaus et al, 2016) whilst previous work in our laboratory identified significant upregulation of the inflammatory molecules IL1β, IL6 and MMP2 in the metastatic brain (EO' Brien, DPhil thesis). Analysis of the molecular profiles of polarised microglia and tumour cells in our control and depletion models could yield new candidates for therapy.

The experiments on *in vivo* manipulation of microglia could initiate a series of experimental approaches for microglial harnessing with the aim of therapeutic benefit. Here, a subpopulation of microglia, the M2 like $MRC1^{+}$ cells, was targeted. Given the contradiction of the results obtained from Chapters 4 and 5, alternative approaches of targeting M2 microglia could be employed. For instance, depletion of $MRC1^{+}$ cells using the CD206-DTR mouse model, already discussed in Chapter 4.1, or reprogramming microglia towards the M1 phenotype by antibody targeting should be considered as future options for further validation of our hypothesis (Kambara et al, 2015; Georgoudaki et al, 2016). Moreover targeting of the whole microglial population in a preclinical model

of brain metastasis has not been documented. This could be a complimentary approach to corroborate the role of the anti-inflammatory, M2 microglial population in the progression of brain metastasis relatively to the whole population. Microglia ablation using the CD11b/gancyclovir approach has been previously reported in experimental gliomas, although with opposing outcomes in different studies, probably due to different experimental design (Galarneau et al, 2007; Markovic et al, 2009; Zhai et al, 2011). Moreover, the CSF1R inhibitor PLX3397 has been recently shown to selectively deplete microglia in the murine brain (Elmore et al, 2014). Those approaches implemented appropriately in our preclinical models of brain metastasis to specifically target microglial cells only and not CD11b/CSF1R^{+} peripheral monocytes could provide interesting insights into the role of these brain resident cells in the biology of metastasis. Interestingly, blockade of CSF1R signalling with the brain-penetrant inhibitor BLZ945 in a glioblastoma model confers survival advantage mainly by altering polarisation of microglia/macrophages rather than cell depletion (Pyonteck et al, 2013). This approach would fit nicely into our research objectives since it combines both targeting and re-educating microglia towards the M1 phenotype for therapeutic benefit.

Overall, we propose metastasis associated microglia as a promising target for therapeutic intervention. Although our knowledge of the metastasis specific molecular signatures of microglia and the functional crosstalk between microglia and tumour cells remains vague, further investigation of the afore-mentioned aspects could yield clinically applicable therapeutic modalities. Importantly, harnessing the microglial response to brain metastasis could be used in combination with chemotherapy or radiotherapy as effective multimodal anti-cancer therapy (De Palma and Lewis, 2013).

References

Abraham D, Zins K, Sioud M, Lucas T, Schäfer R, Stanley ER, Aharinejad S. Stromal cell-derived CSF-1 blockade prolongs xenograft survival of CSF-1-negative neuroblastoma. Int J Cancer. 2010 Mar 15;126(6):1339-52.

Acharyya S, Oskarsson T, Vanharanta S, Malladi S, Kim J, Morris PG, Manova-Todorova K, Leversha M, Hogg N, Seshan VE, Norton L, Brogi E, Massagué J. A CXCL1 paracrine network links cancer chemoresistance and metastasis. Cell. 2012 Jul 6;150(1):165-78.

Aguirre K, Miller S. MHC class II-positive perivascular microglial cells mediate resistance to Cryptococcus neoformans brain infection. Glia. 2002 Aug;39(2):184-8.

Aharinejad S, Abraham D, Paulus P, Abri H, Hofmann M, Grossschmidt K, Schäfer R, Stanley ER, Hofbauer R. Colony-stimulating factor-1 antisense treatment suppresses growth of human tumor xenografts in mice. Cancer Res. 2002 Sep 15;62(18):5317-24.

Ajami B, Bennett JL, Krieger C, Tetzlaff W, Rossi FM. Local self-renewal can sustain CNS microglia maintenance and function throughout adult life. Nat Neurosci. 2007 Dec;10(12):1538-43.

Ajami B, Bennett JL, Krieger C, McNagny KM, Rossi FM. Infiltrating monocytes trigger EAE progression, but do not contribute to the resident microglia pool. Nat Neurosci, 2011. 14(9): p. 1142-9.

Alder JK, Georgantas RW 3rd, Hildreth RL, Kaplan IM, Morisot S, Yu X, McDevitt M, Civin CI. Kruppel-like factor 4 is essential for inflammatory monocyte differentiation in vivo. J Immunol. 2008 Apr 15;180(8):5645-52.

Allavena P, Mantovani A. Immunology in the clinic review series; focus on cancer: tumour-associated macrophages: undisputed stars of the inflammatory tumour microenvironment. Clin Exp Immunol. 2012 Feb;167(2):195-205.

Almatroodi SA, McDonald CF, Darby IA, Pouniotis DS. Characterization of M1/M2 Tumour-Associated Macrophages (TAMs) and Th1/Th2 Cytokine Profiles in Patients with NSCLC. Cancer Microenviron. 2016 Apr;9(1):1-11.

Amit M, Laider-Trejo L, Shalom V, Shabtay-Orbach A, Krelin Y, Gil Z. Characterization of the melanoma brain metastatic niche in mice and humans. Cancer Med. 2013 Apr;2(2):155-63.

Axente M, He J, Bass CP, Hirsch JI, Sundaresan G, Zweit J, Pugachev A. Comprehensive approach to coregistration of autoradiography and microscopy images acquired from a set of sequential tissue sections. J Nucl Med. 2011 Oct;52(10):1621-9.

Beerling E, Ritsma L, Vrisekoop N, Derksen PW, van Rheenen J. Intravital microscopy: new insights into metastasis of tumors. J Cell Sci. 2011 Feb 1;124(Pt 3):299-310.

Berghoff AS, Lassmann H, Preusser M, Höftberger R. Characterization of the inflammatory response to solid cancer metastases in the human brain. Clin Exp Metastasis, 2013. 30(1): p. 69-81.

Berta T, Park CK, Xu ZZ, Xie RG, Liu T, Lü N, Liu YC, Ji RR. Extracellular caspase-6 drives murine inflammatory pain via microglial TNF-α secretion. J Clin Invest. 2014 Mar;124(3):1173-86. doi: 10.1172/JCI72230. Epub 2014 Feb 17.

Bertram JS, Janik P. Establishment of a cloned line of Lewis Lung Carcinoma cells adapted to cell culture. Cancer Lett. 1980 Nov;11(1):63-73.

Biswas SK, Mantovani A. Macrophage plasticity and interaction with lymphocyte subsets: cancer as a paradigm. Nat Immunol. 2010 Oct;11(10):889-96.

Bos PD, Zhang XH, Nadal C, Shu W, Gomis RR, Nguyen DX, Minn AJ, van de Vijver MJ, Gerald WL, Foekens JA, Massagué J. Genes that mediate breast cancer metastasis to the brain. Nature. 2009 Jun 18;459(7249):1005-9.

Brantley EC, Guo L, Zhang C, Lin Q, Yokoi K, Langley RR, Kruzel E, Maya M, Kim SW, Kim SJ, Fan D, Fidler IJ. Nitric oxide-mediated tumoricidal activity of murine microglial cells. Transl Oncol. 2010 Dec 1;3(6):380-8.

Butovsky O, Jedrychowski MP, Moore CS, Cialic R, Lanser AJ, Gabriely G, Koeglsperger T, Dake B, Wu PM, Doykan CE, Fanek Z, Liu L, Chen Z, Rothstein JD, Ransohoff RM, Gygi SP, Antel JP, Weiner HL. Identification of a unique TGF-β-dependent molecular and functional signature in microglia. Nat Neurosci. 2014 Jan;17(1):131-43.

Cailhier JF, Partolina M, Vuthoori S, Wu S, Ko K, Watson S, Savill J, Hughes J, Lang RA. Conditional macrophage ablation demonstrates that resident macrophages initiate acute peritoneal inflammation. J Immunol. 2005 Feb 15;174(4):2336-42.

Carbonell WS, Ansorge O, Sibson N, Muschel R. The vascular basement membrane as "soil" in brain metastasis. PLoS One, 2009. 4(6): p. e5857.

Cardona AE, Pioro EP, Sasse ME, Kostenko V, Cardona SM, Dijkstra IM, Huang D, Kidd G, Dombrowski S, Dutta R, Lee JC, Cook DN, Jung S, Lira SA, Littman DR, Ransohoff RM. Control of microglial neurotoxicity by the fractalkine receptor. Nat Neurosci. 2006 Jul;9(7):917-24. Epub 2006 Jun 18.

Cavallaro S. CXCR4/CXCL12 in non-small-cell lung cancer metastasis to the brain. Int J Mol Sci. 2013 Jan 15;14(1):1713-27.

Ceresoli GL, Cappuzzo F, Gregorc V, Bartolini S, Crinò L, Villa E. Gefitinib in patients with brain metastases from non-small-cell lung cancer: a prospective trial. Ann Oncol. 2004 Jul;15(7):1042-7.

Chen EI, Hewel J, Krueger JS, Tiraby C, Weber MR, Kralli A, Becker K, Yates JR 3rd, Felding-Habermann B Adaptation of energy metabolism in breast cancer brain metastases. Cancer Res. 2007 Feb 15;67(4):1472-86.

Chen Q, Boire A, Jin X, Valiente M, Er EE, Lopez-Soto A, Jacob LS, Patwa R, Shah H, Xu K, Cross JR, Massagué J. Carcinoma-astrocyte gap junctions promote brain metastasis by cGAMP transfer. Nature. 2016 May 18;533(7604):493-8.

Chen Q, Zhang XH, Massagué J. Macrophage binding to receptor VCAM-1 transmits survival signals in breast cancer cells that invade the lungs. Cancer cell. 2011;20:538–549.

Cherry JD, Olschowka JA, O'Banion MK1. Neuroinflammation and M2 microglia: the good, the bad, and the inflamed. J Neuroinflammation. 2014 Jun 3;11:98. doi: 10.1186/1742-2094-11-98.

Chhor V, Le Charpentier T, Lebon S, Oré MV, Celador IL, Josserand J, Degos V, Jacotot E, Hagberg H, Sävman K, Mallard C, Gressens P, Fleiss. Characterization of phenotype markers and neuronotoxic potential of polarised primary microglia in vitro. Brain Behav Immun. 2013 Aug;32:70-85.

Clausen BE, Burkhardt C, Reith W, Renkawitz R, Förster I. Conditional gene targeting in macrophages and granulocytes using LysMcre mice. Transgenic Res. 1999 Aug;8(4):265-77.

Coffelt SB, Chen YY, Muthana M, Welford AF, Tal AO, Scholz A, Plate KH, Reiss Y, Murdoch C, De Palma M, Lewis CE. Angiopoietin 2 stimulates TIE2-expressing monocytes to suppress T cell activation and to promote regulatory T cell expansion. J Immunol. 2011 Apr 1;186(7):4183-90.

Colotta F, Allavena P, Sica A, Garlanda C, Mantovani A.Cancer-related inflammation, the seventh hallmark of cancer: links to genetic instability. Carcinogenesis, 2009. 30(7): p. 1073-81.

Condeelis J, Pollard JW. Macrophages: obligate partners for tumor cell migration, invasion, and metastasis. Cell. 2006 Jan 27;124(2):263-6.

Criscuoli ML, Nguyen M, Eliceiri BP. Tumor metastasis but not tumor growth is dependent on Src-mediated vascular permeability. Blood. 2005 Feb 15;105(4):1508-14.

Davalos D, Grutzendler J, Yang G, Kim JV, Zuo Y, Jung S, Littman DR, Dustin ML, Gan WB. ATP mediates rapid microglial response to local brain injury in vivo. Nat Neurosci. 2005 Jun;8(6):752-8.

De Palma M, Lewis CE. Macrophage regulation of tumor responses to anticancer therapies. Cancer Cell. 2013 Mar 18;23(3):277-86.

Dexter DL, Kowalski HM, Blazar BA, Fligiel Z, Vogel R, Heppner GH. Heterogeneity of tumor cells from a single mouse mammary tumor. Cancer Res. 1978; 38:3174–3181.

Donnelly DJ, Gensel JC, Ankeny DP, van Rooijen N, Popovich PG. An efficient and reproducible method for quantifying macrophages in different experimental models of central nervous system pathology. J Neurosci Methods. 2009 Jun 30;181(1):36-44.

Eichler AF, Kuter I, Ryan P, Schapira L, Younger J, Henson JW. Survival in patients with brain metastases from breast cancer: the importance of HER-2 status. Cancer. 2008 Jun;112(11):2359-67.

Eichler AF, Loeffler JS. Multidisciplinary management of brain metastases. Oncologist, 2007. 12(7): p. 884-98.

Elkabes S, DiCicco-Bloom EM, Black IB. Brain microglia/macrophages express neurotrophins that selectively regulate microglial proliferation and function. J Neurosci. 1996 Apr 15;16(8):2508-21.

Elmore MR, Najafi AR, Koike MA, Dagher NN, Spangenberg EE, Rice RA1, Kitazawa M, Matusow B, Nguyen H, West BL, Green KN. Colony-stimulating factor 1 receptor signaling is necessary

for microglia viability, unmasking a microglia progenitor cell in the adult brain. Neuron. 2014 Apr 16;82(2):380-97. doi: 10.1016/j.neuron.2014.02.040.

Eloy JO, Claro de Souza M, Petrilli R, Barcellos JP, Lee RJ, Marchetti JM. Liposomes as carriers of hydrophilic small molecule drugs: strategies to enhance encapsulation and delivery. Colloids Surf B Biointerfaces. 2014 Nov 1;123:345-63.

Erler JT, Bennewith KL, Cox TR, Lang G, Bird D, Koong A, Le QT, Giaccia AJ. Hypoxia-induced lysyl oxidase is a critical mediator of bone marrow cell recruitment to form the premetastatic niche. Cancer Cell. 2009 Jan 6;15(1):35-44.

Faustino JV, Wang X, Johnson CE, Klibanov A, Derugin N, Wendland MF, Vexler ZS. Microglial cells contribute to endogenous brain defenses after acute neonatal focal stroke. J Neurosci. 2011 Sep 7;31(36):12992-3001.

Feinberg MW, Wara AK, Cao Z, Lebedeva MA, Rosenbauer F, Iwasaki H, Hirai H, Katz JP, Haspel RL, Gray S, Akashi K, Segre J, Kaestner KH, Tenen DG, Jain MK. The Kruppel-like factor KLF4 is a critical regulator of monocyte differentiation. EMBO J. 2007 Sep 19;26(18):4138-48.

Fidler IJ. Metastasis: quantitative analysis of distribution and fate of tumor emboli labeled with 125 I-5-iodo-2'-deoxyuridine. J Natl Cancer Inst. 1970 Oct;45(4):773-82.

Fidler IJ. The pathogenesis of cancer metastasis: the 'seed and soil' hypothesis revisited. Nat Rev Cancer, 2003. 3(6): p. 453-8.

Fidler IJ, Yano S, Zhang RD, Fujimaki T, Bucana CD. The seed and soil hypothesis: vascularisation and brain metastases. Lancet Oncol. 2002 Jan;3(1):53-7.

Fitzgerald DP, Palmieri D, Hua E, Hargrave E, Herring JM, Qian Y, Vega-Valle E, Weil RJ, Stark AM, Vortmeyer AO, Steeg PS. Reactive glia are recruited by highly proliferative brain metastases of breast cancer and promote tumor cell colonization Clin Exp Metastasis. 2008;25(7):799-810.

Font-Nieves M, Sans-Fons MG, Gorina R, Bonfill-Teixidor E, Salas-Pérdomo A, Márquez-Kisinousky L, Santalucia T, Planas AM. Induction of COX-2 enzyme and down-regulation of COX-1 expression by lipopolysaccharide (LPS) control prostaglandin E2 production in astrocytes. J Biol Chem. 2012 Feb 24;287(9):6454-68.

Fritz JM, Tennis MA, Orlicky DJ, Lin H, Ju C, Redente EF, Choo KS, Staab TA, Bouchard RJ, Merrick DT, Malkinson AM, Dwyer-Nield LD. Depletion of tumor-associated macrophages slows the growth of chemically induced mouse lung adenocarcinomas. Front Immunol. 2014 Nov 25;5:587.

Fulci G, Dmitrieva N, Gianni D, Fontana EJ, Pan X, Lu Y, Kaufman CS, Kaur B, Lawler SE, Lee RJ, Marsh CB, Brat DJ, van Rooijen N, Stemmer-Rachamimov AO, Hochberg FH, Weissleder R, Martuza RL, Chiocca EA. Depletion of peripheral macrophages and brain microglia increases brain tumor titers of oncolytic viruses. Cancer Res. 2007 Oct 1;67(19):9398-406.

Gabrusiewicz K, Ellert-Miklaszewska A, Lipko M, Sielska M, Frankowska M, Kaminska B. Characteristics of the alternative phenotype of microglia/macrophages and its modulation in experimental gliomas. PLoS One, 2011. 6(8): p. e23902.

Gabrusiewicz K, Rodriguez B, Wei J, Hashimoto Y, Healy LM, Maiti SN, Thomas G, Zhou S, Wang Q, Elakkad A, Liebelt BD, Yaghi NK, Ezhilarasan R, Huang N, Weinberg JS, Prabhu SS, Rao G, Sawaya R, Langford LA, Bruner JM, Fuller GN, Bar-Or A, Li W, Colen RR, Curran MA, Bhat KP, Antel JP, Cooper LJ, Sulman EP, Heimberger AB. Glioblastoma-infiltrated innate immune cells resemble M0 macrophage phenotype. JCI Insight. 2016;1(2).

Gajewski TF, Schreiber H, Fu YX. Innate and adaptive immune cells in the tumor microenvironment. Nat Immunol. 2013 Oct;14(10):1014-22. doi: 10.1038/ni.2703.

Galarneau H, Villeneuve J, Gowing G, Julien JP, Vallières L. Increased glioma growth in mice depleted of macrophages. Cancer Res. 2007 Sep 15;67(18):8874-81.

Garcia-Faroldi G, Melo FR, Rönnberg E, Grujic M, Pejler G. Active caspase-3 is stored within secretory compartments of viable mast cells. J Immunol. 2013 Aug 1;191(3):1445-52.

Gavrilovic IT, Posner JB. Brain metastases: epidemiology and pathophysiology. J Neurooncol. 2005 Oct;75(1):5-14.

Gay LJ, Felding-Habermann B. Contribution of platelets to tumour metastasis. Nat Rev Cancer. 2011 Feb;11(2):123-34.

Georgoudaki AM, Prokopec KE, Boura VF, Hellqvist E, Sohn S, Östling J, Dahan R, Harris RA, Rantalainen M, Klevebring D, Sund M, Brage SE, Fuxe J, Rolny C, Li F, Ravetch JV, Karlsson MC. Reprogramming Tumor-Associated Macrophages by Antibody Targeting Inhibits Cancer Progression and Metastasis. Cell Rep. 2016 May 31;15(9):2000-11.

Ginhoux F, Greter M, Leboeuf M, Nandi S, See P, Gokhan S, Mehler MF, Conway SJ, Ng LG, Stanley ER, Samokhvalov IM, Merad M. Fate mapping analysis reveals that adult microglia derive from primitive macrophages. Science. 2010 Nov 5;330(6005):841-5.

Ginhoux F, Lim S, Hoeffel G, Low D, Huber T. Origin and differentiation of microglia. Front Cell Neurosci. 2013 Apr 17;7:45.

Girard S, Brough D, Lopez-Castejon G, Giles J, Rothwell NJ, Allan SM Microglia and macrophages differentially modulate cell death after brain injury caused by oxygen-glucose deprivation in organotypic brain slices. Glia. 2013 May;61(5):813-24.

Goldmann T, Wieghofer P, Müller PF, Wolf Y, Varol D, Yona S, Brendecke SM, Kierdorf K, Staszewski O, Datta M, Luedde T, Heikenwalder M, Jung S, Prinz M. A new type of microglia gene targeting shows TAK1 to be pivotal in CNS autoimmune inflammation. Nat Neurosci. 2013 Nov;16(11):1618-26.

Gowing G, Vallieres L, Julien JP. Mouse model for ablation of proliferating microgliain acute CNS injuries. Glia, 53 (2006), pp. 331–337.
Granot Z, Henke E, Comen EA, King TA, Norton L, Benezra R. Tumor entrained neutrophils inhibit seeding in the premetastatic lung. Cancer Cell. 2011 Sep 13;20(3):300-14. doi: 10.1016/j.ccr.2011.08.012.

Guerreiro R, Wojtas A, Bras J, Carrasquillo M, Rogaeva E, Majounie E, Cruchaga C, Sassi C, Kauwe JS, Younkin S, Hazrati L, Collinge J, Pocock J, Lashley T, Williams J, Lambert JC, Amouyel P, Goate A, Rademakers R, Morgan K, Powell J, St George-Hyslop P, Singleton A, Hardy J. TREM2 variants in Alzheimer's disease. N Engl J Med. 2013 Jan 10; 368(2):117-27.

Guo W, Giancotti FG. Integrin signalling during tumour progression. Nat Rev Mol Cell Biol. 2004 Oct;5(10):816-26.

Gupta GP, Massagué J. Cancer metastasis: building a framework. Cell. 2006 Nov 17;127(4):679-95.

Gupta GP, Massagué J. Platelets and metastasis revisited: a novel fatty link. J Clin Invest. 2004 Dec;114(12):1691-3.

Gupta GP, Nguyen DX, Chiang AC, Bos PD, Kim JY, Nadal C, Gomis RR, Manova-Todorova K, Massagué J. Mediators of vascular remodelling co-opted for sequential steps in lung metastasis. Nature. 2007 Apr 12;446(7137):765-70.

Hamilton A, Sibson NR. Role of the systemic immune system in brain metastasis. Mol Cell Neurosci, 2013. 53: p. 42-51.

Hanahan D, Weinberg RA. The hallmarks of cancer. Cell. 2000 Jan 7;100(1):57-70.

Hanahan D, Weinberg RA. Hallmarks of cancer: the next generation. Cell. 2011 Mar 4;144(5):646-74.

Harris AL. Hypoxia--a key regulatory factor in tumour growth. Nat Rev Cancer. 2002 Jan;2(1):38-47.

Harrison JK, Jiang Y, Chen S, Xia Y, Maciejewski D, McNamara RK, Streit WJ, Salafranca MN, Adhikari S, Thompson DA, Botti P, Bacon KB, Feng L. Role for neuronally derived fractalkine in mediating interactions between neurons and CX3CR1-expressing microglia. Proc. Natl. Acad. Sci. USA 1998 Sep 1;95(18):10896-901.

Hayashi N, Niikura N, Masuda N, Takashima S, Nakamura R, Watanabe K, Kanbayashi C, Ishida M, Hozumi Y, Tsuneizumi M, Kondo N, Naito Y, Honda Y, Matsui A, Fujisawa T, Oshitanai R, Yasojima H, Yamauchi H, Saji S, Iwata H. Prognostic factors of HER2-positive breast cancer patients who develop brain metastasis: a multicenter retrospective analysis. Breast Cancer Res Treat. 2015 Jan;149(1):277-84.

He BP, Wang JJ, Zhang X, Wu Y, Wang M, Bay BH, Chang AY. Differential reactions of microglia to brain metastasis of lung cancer. Mol Med. 2006 Jul-Aug;12(7-8):161-70.

Hentze H, Schwoebel F, Lund S, Keel M, Ertel W, Wendel A, Jäättelä M, Leist M. In vivo and in vitro evidence for extracellular caspase activity released from apoptotic cells. Biochem Biophys Res Commun. 2001 May 25;283(5):1111-7.

Hinton CV, Avraham S, Avraham HK. Role of the CXCR4/CXCL12 signaling axis in breast cancer metastasis to the brain. Clin Exp Metastasis. 2010 Feb;27(2):97-105.

Holling TM, Schooten E, van Den Elsen PJ. Function and regulation of MHC class II molecules in T-lymphocytes: of mice and men. Hum Immunol. 2004 Apr;65(4):282-90.

Huwyler J, Wu D, Pardridge WM. Brain drug delivery of small molecules using immunoliposomes. Proc Natl Acad Sci U S A. 1996 Nov 26;93(24):14164-9.

Ito D, Imai Y, Ohsawa K, Nakajima K, Fukuuchi Y, Kohsaka S. Microglia-specific localisation of a novel calcium binding protein, Iba1. Brain Res Mol Brain Res. 1998 Jun 1;57(1):1-9.

Ito D, Tanaka K, Suzuki S, Dembo T, Fukuuchi Y. Enhanced expression of Iba1, ionized calcium-binding adapter molecule 1, after transient focal cerebral ischemia in rat brain. Stroke. 2001 May;32(5):1208-15.

Jain S, Harris J, Ware J. Platelets: linking hemostasis and cancer. Arterioscler Thromb Vasc Biol. 2010 Dec;30(12):2362-7.

Jonsson T, Stefansson H, Steinberg S, Jonsdottir I, Jonsson PV, Snaedal J, Bjornsson S, Huttenlocher J, Levey AI, Lah JJ, Rujescu D, Hampel H, Giegling I, Andreassen OA, Engedal K, Ulstein I, Djurovic S, Ibrahim-Verbaas C, Hofman A, Ikram MA, van Duijn CM, Thorsteinsdottir U, Kong A, Stefansson K. Variant of TREM2 associated with the risk of Alzheimer's disease. N Engl J Med. 2013 Jan 10;368(2):107-16.

Kambara K, Ohashi W, Tomita K, Takashina M, Fujisaka S, Hayashi R, Mori H, Tobe K, Hattori Y. In vivo depletion of CD206+ M2 macrophages exaggerates lung injury in endotoxemic mice. Am J Pathol. 2015 Jan;185(1):162-71.

Kang Y, Siegel PM, Shu W, Drobnjak M, Kakonen SM, Cordón-Cardo C, Guise TA, Massagué J. A multigenic program mediating breast cancer metastasis to bone. Cancer Cell. 2003 Jun;3(6):537-49.

Kaplan RN, Riba RD, Zacharoulis S, Bramley AH, Vincent L, Costa C, MacDonald DD, Jin DK, Shido K, Kerns SA, Zhu Z, Hicklin D, Wu Y, Port JL, Altorki N, Port ER, Ruggero D, Shmelkov SV, Jensen KK, Rafii S, Lyden D. VEGFR1-positive haematopoietic bone marrow progenitors initiate the pre-metastatic niche. Nature. 2005 Dec 8;438(7069):820-7.

Katz JP, Perreault N, Goldstein BG, Lee CS, Labosky PA, Yang VW, Kaestner KH. The zinc-finger transcription factor Klf4 is required for terminal differentiation of goblet cells in the colon. Development. 2002 Jun;129(11):2619-28.

Kaushik DK, Gupta M, Das S, Basu A. Krüppel-like factor 4, a novel transcription factor regulates microglial activation and subsequent neuroinflammation. J Neuroinflammation. 2010 Oct 15;7:68.

Kavanagh E, Burguillos MA, Carrillo-Jimenez A, Oliva-Martin MJ, Santiago M, Rodhe J, Joseph B, Venero JL. Deletion of caspase-8 in mouse myeloid cells blocks microglia pro-inflammatory activation and confers protection in MPTP neurodegeneration model. Aging (Albany NY). 2015 Sep;7(9):673-89.

Kawahara K, Suenobu M, Yoshida A, Koga K, Hyodo A, Ohtsuka H, Kuniyasu A, Tamamaki N, Sugimoto Y, Nakayama H. Intracerebral microinjection of interleukin-4/interleukin-13 reduces β-amyloid accumulation in the ipsilateral side and improves cognitive deficits in young amyloid precursor protein 23 mice. Neuroscience. 2012 Apr 5;207:243-60.

Khan AJ, Dicker AP On the merits and limitations of whole-brain radiation therapy. J Clin Oncol. 2013 Jan 1;31(1):11-3.

Khanna C, Hunter K. Modeling metastasis in vivo. Carcinogenesis. 2005 Mar;26(3):513-23.

Kigerl KA, Gensel JC, Ankeny DP, Alexander JK, Donnelly DJ, Popovich PG. Identification of two distinct macrophage subsets with divergent effects causing either neurotoxicity or regeneration in the injured mouse spinal cord. J Neurosci. 2009 Oct 28;29(43):13435-44.

Kim LS, Huang S, Lu W, Lev DC, Price JE. Vascular endothelial growth factor expression promotes the growth of breast cancer brain metastases in nude mice. Clin Exp Metastasis. 2004;21(2):107-18.

Komohara Y, Ohnishi K, Kuratsu J, Takeya M. Possible involvement of the M2 anti-inflammatory macrophage phenotype in growth of human gliomas. J Pathol. 2008 Sep;216(1):15-24.

Kreutzberg GW. Microglia, the first line of defence in brain pathologies. Arzneimittelforschung. 1995 Mar;45(3A):357-60.

Lalancette-Hébert M, Gowing G, Simard A, Weng YC, Kriz J.Selective ablation of proliferating microglial cells exacerbates ischemic injury in the brain. J Neurosci. 2007 Mar 7;27(10):2596-605.

Laoui D, Movahedi K, Van Overmeire E, Van den Bossche J, Schouppe E, Mommer C, Nikolaou A, Morias Y, De Baetselier P, Van Ginderachter JA. Tumor-associated macrophages in breast cancer: distinct subsets, distinct functions. Int J Dev Biol. 2011;55(7-9):861-7.

Lawson LJ, Perry VH, Gordon S. Turnover of resident microglia in the normal adult mouse brain. Neuroscience. 1992;48(2):405-15.

Lehenkari PP, Kellinsalmi M, Näpänkangas JP, Ylitalo KV, Mönkkönen J, Rogers MJ, Azhayev A, Väänänen HK, Hassinen IE. Further insight into mechanism of action of clodronate: inhibition of mitochondrial ADP/ATP translocase by a nonhydrolyzable, adenine-containing metabolite. Mol Pharmacol. 2002 May;61(5):1255-62.

Li W, Graeber MB. The molecular profile of microglia under the influence of glioma. Neuro Oncol. 2012 Aug;14(8):958-78.

Liao X, Sharma N, Kapadia F, Zhou G, Lu Y, Hong H, Paruchuri K, Mahabeleshwar GH, Dalmas E, Venteclef N, Flask CA, Kim J, Doreian BW, Lu KQ, Kaestner KH, Hamik A, Clément K, Jain MK. Krüppel-like factor 4 regulates macrophage polarization. J Clin Invest. 2011 Jul;121(7):2736-49.

Lim SY, Gordon-Weeks A, Allen D, Kersemans V, Beech J, Smart S, Muschel RJ. Cd11b(+) myeloid cells support hepatic metastasis through down-regulation of angiopoietin-like 7 in cancer cells. Hepatology. 2015 Aug;62(2):521-33.

Lin EY, Nguyen AV, Russell RG, Pollard JW. Colony-stimulating factor 1 promotes progression of mammary tumors to malignancy. J Exp Med. 2001 Mar 19;193(6):727-40.

Liu J, Zhang N, Li Q, Zhang W, Ke F, Leng Q, Wang H, Chen J, Wang H. Tumor-Associated Macrophages Recruit CCR6+ Regulatory T Cells and Promote the Development of Colorectal Cancer via Enhancing CCL20 Production in Mice. PLoS One. 2011; 6(4): e19495.

Liu KK, Dorovini-Zis K. Regulation of CXCL12 and CXCR4 expression by human brain endothelial cells and their role in CD4+ and CD8+ T cell adhesion and transendothelial migration. J Neuroimmunol. 2009 Oct 30;215(1-2):49-64.

Liu Y, Kosaka A, Ikeura M, Kohanbash G, Fellows-Mayle W, Snyder LA, Okada H. Premetastatic soil and prevention of breast cancer brain metastasis. Neuro Oncol. 2013 Jul;15(7):891-903.

Lobbezoo DJ, van Kampen RJ, Voogd AC, Dercksen MW, van den Berkmortel F, Smilde TJ, van de Wouw AJ, Peters FP, van Riel JM, Peters NA, de Boer M, Peer PG, Tjan-Heijnen VC. Prognosis of metastatic breast cancer: are there differences between patients with de novo and recurrent metastatic breast cancer? Br J Cancer. 2015 Apr 28;112(9):1445-51.

Lonser RR, Song DK, Klapper J, Hagan M, Auh S, Kerr PB, Citrin DE, Heiss JD, Camphausen K, Rosenberg SA. Surgical management of melanoma brain metastases in patients treated with immunotherapy. J Neurosurg. 2011 Jul;115(1):30-6.

Lorger M, Felding-Habermann B. Capturing Changes in the Brain Microenvironment during Initial Steps of Breast Cancer Brain Metastasis. Am J Pathol. 2010 Jun; 176(6): 2958–2971.

Luan B, Yoon YS, Le Lay J, Kaestner KH, Hedrick S, Montminy M. CREB pathway links PGE2 signaling with macrophage polarization. Proc Natl Acad Sci U S A. 2015 Dec 22;112(51):15642-7.

Luzzi KJ, MacDonald IC, Schmidt EE, Kerkvliet N, Morris VL, Chambers AF, Groom AC. Multistep nature of metastatic inefficiency: dormancy of solitary cells after successful extravasation and limited survival of early micrometastases. Am J Pathol. 1998 Sep;153(3):865-73.

Marabelle A, Kohrt H, Sagiv-Barfi I, Ajami B, Axtell RC, Zhou G, Rajapaksa R, Green MR, Torchia J, Brody J, Luong R, Rosenblum MD, Steinman L, Levitsky HI, Tse V, Levy R. Depleting tumor-specific Tregs at a single site eradicates disseminated tumors. J Clin Invest. 2013 Jun;123(6):2447-63.

Marín-Teva JL, Dusart I, Colin C, Gervais A, van Rooijen N, Mallat M. Microglia promote the death of developing Purkinje cells. Neuron. 2004 Feb 19;41(4):535-47.

Markovic DS, Vinnakota K, Chirasani S, Synowitz M, Raguet H, Stock K, Sliwa M, Lehmann S, Kälin R, van Rooijen N, Holmbeck K, Heppner FL, Kiwit J, Matyash V, Lehnardt S, Kaminska B, Glass R, Kettenmann H. Gliomas induce and exploit microglial MT1-MMP expression for tumor expansion. Proc Natl Acad Sci U S A. 2009 Jul 28;106(30):12530-5.

Martinez FO, Gordon S. The M1 and M2 paradigm of macrophage activation: time for reassessment. F1000Prime Rep. 2014 Mar 3;6:13.

Martinez FO, Gordon S, Locati M, Mantovani A. Transcriptional profiling of the human monocyte-to-macrophage differentiation and polarization: new molecules and patterns of gene expression. J Immunol. 2006 Nov 15;177(10):7303-11.

Matsuo Y, Amano S, Furuya M, Namiki K, Sakurai K, Nishiyama M, Sudo T, Tatsumi K, Kuriyama T, Kimura S, Kasuya Y. Involvement of p38alpha mitogen-activated protein kinase in lung metastasis of tumor cells. J Biol Chem. 2006 Dec 1;281(48):36767-75.

McGowan PM, Simedrea C, Ribot EJ, Foster PJ, Palmieri D, Steeg PS, Allan AL, Chambers AF. Notch1 inhibition alters the CD44hi/CD24lo population and reduces the formation of brain metastases from breast cancer. Mol Cancer Res. 2011 Jul;9(7):834-44.

Minn AJ, Gupta GP, Siegel PM, Bos PD, Shu W, Giri DD, Viale A, Olshen AB, Gerald WL, Massagué J. Genes that mediate breast cancer metastasis to lung. Nature. 2005 Jul 28;436(7050):518-24.

Mildner A, Schmidt H, Nitsche M, Merkler D, Hanisch UK, Mack M, Heikenwalder M, Brück W, Priller J, Prinz M. Microglia in the adult brain arise from Ly-6ChiCCR2+ monocytes only under defined host conditions. Nat Neurosci. 2007 Dec;10(12):1544-53.

Miron VE, Boyd A, Zhao JW, Yuen TJ, Ruckh JM, Shadrach JL, van Wijngaarden P, Wagers AJ, Williams A, Franklin RJ, ffrench-Constant C. M2 microglia and macrophages drive oligodendrocyte differentiation during CNS remyelination. Nat Neurosci. 2013 Sep;16(9):1211-8.

Mittelbronn M, Dietz K, Schluesener HJ, Meyermann R. Local distribution of microglia in the normal adult human central nervous system differs by up to one order of magnitude. Acta Neuropathol. 2001 Mar;101(3):249-55.

Morrison HW, Filosa JA. A quantitative spatiotemporal analysis of microglia morphology during ischemic stroke and reperfusion. J Neuroinflammation. 2013 Jan 11;10:4. doi: 10.1186/1742-2094-10-4.

Murray PJ, Allen JE, Biswas SK, Fisher EA, Gilroy DW, Goerdt S, Gordon S, Hamilton JA, Ivashkiv LB, Lawrence T, Locati M, Mantovani A, Martinez FO, Mege JL, Mosser DM, Natoli G, Saeij JP, Schultze JL, Shirey KA, Sica A, Suttles J, Udalova I, van Ginderachter JA, Vogel SN, Wynn TA. Macrophage activation and polarization: nomenclature and experimental guidelines. Immunity. 2014 Jul 17;41(1):14-20.

Murray PJ, Wynn TA. Protective and pathogenic functions of macrophage subsets. Nat Rev Immunol. 2011 Oct 14;11(11):723-37.

Nagy A. Cre recombinase: the universal reagent for genome tailoring. Genesis. 2000 Feb;26(2):99-109.

Nguyen DX, Bos PD, Massagué J. Metastasis: from dissemination to organ-specific colonization. Nat Rev Cancer. 2009 Apr;9(4):274-84.

Nimmerjahn A, Kirchhoff F, Helmchen F. Resting Microglial Cells Are Highly Dynamic Surveillants of Brain Parenchyma in Vivo Science. 2005 May 27;308(5726):1314-8.

Noy R. and Pollard JW. Tumor-associated macrophages: from mechanisms to therapy. Immunity. 2014 Jul 17; 41(1): 49–61.

O'Brien ER, Kersemans V, Tredwell M, Checa B, Serres S, Soto MS, Gouverneur V, Leppert D, Anthony DC, Sibson NR. Glial activation in the early stages of brain metastasis: TSPO as a diagnostic biomarker. J Nucl Med. 2014 Feb;55(2):275-80.

Ohsawa K, Imai Y, Kanazawa H, Sasaki Y, Kohsaka S. Involvement of Iba1 in membrane ruffling and phagocytosis of macrophages/microglia. J Cell Sci. 2000 Sep;113 (Pt 17):3073-84.

Okuda H, Xing F, Pandey PR, Sharma S, Watabe M, Pai SK, Mo YY, Iiizumi-Gairani M, Hirota S, Liu Y, Wu K, Pochampally R, Watabe K. miR-7 suppresses brain metastasis of breast cancer stem-like cells by modulating KLF4. Cancer Res. 2013 Feb 15;73(4):1434-44.

Olson JK, Miller SD. Microglia initiate central nervous system innate and adaptive immune responses through multiple TLRs. J Immunol. 2004 Sep 15;173(6):3916-24.

Omuro AM, Kris MG, Miller VA, Franceschi E, Shah N, Milton DT, Abrey LE. High incidence of disease recurrence in the brain and leptomeninges in patients with nonsmall cell lung carcinoma after response to gefitinib. Cancer. 2005 Jun 1;103(11):2344-8.

Padua D, Zhang XH, Wang Q, Nadal C, Gerald WL, Gomis RR, Massagué J. TGFbeta primes breast tumors for lung metastasis seeding through angiopoietin-like 4. Cell. 2008 Apr 4;133(1):66-77.

Paolicelli RC, Bolasco G, Pagani F, Maggi L, Scianni M, Panzanelli P, Giustetto M, Ferreira TA, Guiducci E, Dumas L, Ragozzino D, Gross CT. Synaptic pruning by microglia is necessary for normal brain development. Science. 2011 Sep 9;333(6048):1456-8.

Panni RZ, Linehan DC, DeNardo DG. Targeting tumor-infiltrating macrophages to combat cancer. Immunotherapy. 2013 Oct;5(10):1075-87.

Parakalan R, Jiang B, Nimmi B, Janani M, Jayapal M, Lu J, Tay SS, Ling EA, Dheen ST. Transcriptome analysis of amoeboid and ramified microglia isolated from the corpus callosum of rat brain. BMC Neurosci. 2012 Jun 14;13:64. doi: 10.1186/1471-2202-13-64.

Pardridge WM. The blood-brain barrier: bottleneck in brain drug development. NeuroRx, 2005. 2(1): p. 3-14.

Parkhurst CN, Yang G, Ninan I, Savas JN, Yates JR 3rd, Lafaille JJ, Hempstead BL, Littman DR, Gan WB. Microglia promote learning-dependent synapse formation through brain-derived neurotrophic factor. Cell. 2013 Dec 19;155(7):1596-609.

Patchell RA. The management of brain metastases. Cancer Treat Rev. 2003 Dec;29(6):533-40.

Pease NJ, Edwards A and Moss LJ. Effectiveness of whole brain radiotherapy in the treatment of brain metastases: a systematic review. Palliat Med, 2005. 19(4): p. 288-99.

Pepe G, Calderazzi G, De Maglie M, Villa AM, Vegeto E. Heterogeneous induction of microglia M2a phenotype by central administration of interleukin-4. J Neuroinflammation. 2014 Dec 31;11:211.

Perry VH, Holmes C. Microglial priming in neurodegenerative disease. Nat Rev Neurol. 2014 Apr;10(4):217-24. doi: 10.1038/nrneurol.2014.38. Epub 2014 Mar 18.

Perry VH, Hume DA, Gordon S. Immunohistochemical localization of macrophages and microglia in the adult and developing mouse brain. Neuroscience. 1985 Jun;15(2):313-26.

Perry VH, Teeling J. Microglia and macrophages of the central nervous system: the contribution of microglia priming and systemic inflammation to chronic neurodegeneration. Semin Immunopathol. 2013 Sep;35(5):601-12.

Pieńkowski T, Zielinski CC. Trastuzumab treatment in patients with breast cancer and metastatic CNS disease. Ann Oncol. 2010 May;21(5):917-24.

Pollard JW. Tumour-educated macrophages promote tumour progression and metastasis. Nat Rev Cancer. 2004 Jan;4(1):71-8.

Ponomarev ED, Maresz K, Tan Y, Dittel BN. CNS-derived interleukin-4 is essential for the regulation of autoimmune inflammation and induces a state of alternative activation in microglial cells. J Neurosci. 2007 Oct 3;27(40):10714-21.

Provenzano PP, Keely PJ. The role of focal adhesion kinase in tumor initiation and progression. Cell Adh Migr. 2009 Oct-Dec; 3(4): 347–350.

Psaila B, Lyden D. The metastatic niche: adapting the foreign soil. Nat Rev Cancer. 2009 Apr;9(4):285-93.

Pukrop T, Dehghani F, Chuang HN, Lohaus R, Bayanga K, Heermann S, Regen T, Van Rossum D, Klemm F, Schulz M, Siam L, Hoffmann A, Trümper L, Stadelmann C, Bechmann I, Hanisch UK, Binder C. Microglia promote colonization of brain tissue by breast cancer cells in a Wnt-dependent way. Glia. 2010 Sep;58(12):1477-89.

Pukrop T, Klemm F, Hagemann T, Gradl D, Schulz M, Siemes S, Trümper L, Binder C. Wnt 5a signaling is critical for macrophage-induced invasion of breast cancer cell lines. Proc Natl Acad Sci U S A. 2006 Apr 4;103(14):5454-9.

Pyonteck SM, Akkari L, Schuhmacher AJ, Bowman RL, Sevenich L, Quail DF, Olson OC, Quick ML, Huse JT, Teijeiro V, Setty M, Leslie CS, Oei Y, Pedraza A, Zhang J, Brennan CW, Sutton JC, Holland EC, Daniel D, Joyce JA. CSF-1R inhibition alters macrophage polarization and blocks glioma progression. Nat Med. 2013 Oct;19(10):1264-72.

Pyonteck SM, Gadea BB, Wang HW, Gocheva V, Hunter KE, Tang LH, Joyce JA.Deficiency of the macrophage growth factor CSF-1 disrupts pancreatic neuroendocrine tumor development. Oncogene. 2012 Mar 15;31(11):1459-67.

Qian B, Deng Y, Im JH, Muschel RJ, Zou Y, Li J, Lang RA, Pollard JW. A distinct macrophage population mediates metastatic breast cancer cell extravasation, establishment and growth. PLoS One. 2009 Aug 10;4(8):e6562.

Qian BZ, Li J, Zhang H, Kitamura T, Zhang J, Campion LR, Kaiser EA, Snyder LA, Pollard JW. CCL2 recruits inflammatory monocytes to facilitate breast-tumour metastasis. Nature. 2011 Jun 8;475(7355):222-5.

Quail DF, Joyce JA. Microenvironmental regulation of tumor progression and metastasis. Nat Med. 2013 Nov;19(11):1423-37.

Quezada SA and Peggs KS. Exploiting CTLA-4, PD-1 and PD-L1 to reactivate the host immune response against cancer. Br J Cancer, 2013. 108(8): p. 1560-5.

Rao S, Sengupta R, Choe EJ, Woerner BM, Jackson E, Sun T, Leonard J, Piwnica-Worms D, Rubin JB. CXCL12 mediates trophic interactions between endothelial and tumor cells in glioblastoma. PLoS One. 2012;7(3):e33005.

Rath M, Müller I, Kropf P, Closs EI, Munder M. Metabolism via Arginase or Nitric Oxide Synthase: Two Competing Arginine Pathways in Macrophages. Front Immunol. 2014 Oct 27;5:532.

Raz A, McLellan WL, Hart IR, Bucana CD, Hoyer LC, Sela BA, Dragsten P, Fidler IJ. Cell surface properties of B16 melanoma variants with differing metastatic potential. Cancer Res. 1980 May; 40(5):1645-51.

Reymond N, d'Água BB, Ridley AJ. Crossing the endothelial barrier during metastasis. Nat Rev Cancer. 2013 Dec;13(12):858-70.

Rietkötter E, Bleckmann A, Bayerlová M, Menck K, Chuang HN, Wenske B, Schwartz H, Erez N, Binder C, Hanisch UK, Pukrop T. Anti-CSF-1 treatment is effective to prevent carcinoma invasion induced by monocyte-derived cells but scarcely by microglia. Oncotarget. 2015 Jun 20;6(17):15482-93.

Rippaus N, Taggart D, Williams J, Andreou T, Wurdak H, Wronski K, Lorger M. Metastatic site-specific polarization of macrophages in intracranial breast cancer metastases. Oncotarget. 2016 May 18. doi: 10.18632/oncotarget.9445.

Riss TL, Moravec RA, Niles AL, Duellman S, Benink HA, Worzella TJ, Minor L. Cell Viability Assays. Assay Guidance Manual (eBook Chapter), 2015.

Roses RE, Paulson EC, Sharma A, Schueller JE, Nisenbaum H, Weinstein S, Fox KR, Zhang PJ, Czerniecki BJ. HER-2/neu overexpression as a predictor for the transition from in situ to invasive breast cancer. Cancer Epidemiol Biomarkers Prev. 2009 May;18(5):1386-9.

Saha B, Bala S, Hosseini N, Kodys K, Szabo G. Krüppel-like factor 4 is a transcriptional regulator of M1/M2 macrophage polarization in alcoholic liver disease. J Leukoc Biol. 2015 Mar 4; 97(5):963-973.

Saijo K, Crotti A, Glass CK. Regulation of microglia activation and deactivation by nuclear receptors Glia. 2013 Jan;61(1):104-11.

Saijo K, Glass CK. Microglial cell origin and phenotypes in health and disease. Nat Rev Immunol. 2011 Oct 25;11(11):775-87.

Sanford DE, Belt BA, Panni RZ, Mayer A, Deshpande AD, Carpenter D, Mitchem JB, Plambeck-Suess SM, Worley LA, Goetz BD, Wang-Gillam A, Eberlein TJ, Denardo DG, Goedegebuure SP, Linehan DC. Inflammatory monocyte mobilization decreases patient survival in pancreatic cancer: a role for targeting the CCL2/CCR2 axis. Clin Cancer Res. 2013 Jul 1;19(13):3404-15.

Sarkar S, Döring A, Zemp FJ, Silva C, Lun X, Wang X, Kelly J, Hader W, Hamilton M, Mercier P, Dunn JF, Kinniburgh D, van Rooijen N, Robbins S, Forsyth P, Cairncross G, Weiss S, Yong VW. Therapeutic activation of macrophages and microglia to suppress brain tumor-initiating cells. Nat Neurosci. 2014 Jan;17(1):46-55.

Seike T, Fujita K, Yamakawa Y, Kido MA, Takiguchi S, Teramoto N, Iguchi H, Noda M. Interaction between lung cancer cells and astrocytes via specific inflammatory cytokines in the microenvironment of brain metastasis. Clin Exp Metastasis. 2011 Jan;28(1):13-25.

Senaratne SG, Pirianov G, Mansi JL, Arnett TR, Colston KW. Bisphosphonates induce apoptosis in human breast cancer cell lines. Br J Cancer. 2000 Apr;82(8):1459-68.

Serres S, Soto MS, Hamilton A, McAteer MA, Carbonell WS, Robson MD, Ansorge O, Khrapitchev A, Bristow C, Balathasan L, Weissensteiner T, Anthony DC, Choudhury RP, Muschel RJ, Sibson NR. Molecular MRI enables early and sensitive detection of brain metastases. Proc Natl Acad Sci U S A. 2012 Apr 24;109(17):6674-9.

Shibata M, Yamada S, Kumar SR, Calero M, Bading J, Frangione B, et al. Clearance of Alzheimer's amyloid-ss(1-40) peptide from brain by LDL receptor-related protein-1 at the blood-brain barrier. J Clin Invest 106: 1489–1499, 2000.

Sica A, Mantovani A. Macrophage plasticity and polarization: in vivo veritas. J Clin Invest. 2012 Mar;122(3):787-95.

Sica A, Schioppa T, Mantovani A, Allavena P. Tumour-associated macrophages are a distinct M2 polarised population promoting tumour progression: potential targets of anti-cancer therapy. Eur J Cancer. 2006 Apr;42(6):717-27.

Song MS, Salmena L, Pandolfi PP. The functions and regulation of the PTEN tumour suppressor. Nat Rev Mol Cell Biol. 2012 Apr 4;13(5):283-96.

Soto MS, O'Brien ER, Andreou K, Scrace SF, Zakaria R, Jenkinson MD, O'Neill E, Sibson NR. Disruption of tumour-host communication by downregulation of LFA-1 reduces COX-2 and e-NOS expression and inhibits brain metastasis growth. Oncotarget. 2016 Jul 20.

Soto MS, Serres S, Anthony DC, Sibson NR. Functional role of endothelial adhesion molecules in the early stages of brain metastasis. Neuro Oncol. 2014 Apr;16(4):540-51.

Steeg PS. Targeting metastasis. Nat Rev Cancer. 2016 Apr;16(4):201-18.

Strauss KI, Barbe MF, Marshall RM, Raghupathi R, Mehta S, Narayan RK. Prolonged cyclooxygenase-2 induction in neurons and glia following traumatic brain injury in the rat. J Neurotrauma. 2000 Aug;17(8):695-711.

Strell C, Entschladen F. Extravasation of leukocytes in comparison to tumor cells. Cell Commun Signal. 2008 Dec 4;6:10.

Sugiura K, Stock CC. Studies in a tumor spectrum. I. Comparison of the action of methylbis (2-chloroethyl)amine and 3-bis(2-chloroethyl)aminomethyl-4-methoxymethyl -5-hydroxy-6-methylpyridine on the growth of a variety of mouse and rat tumors. Cancer. 1952 Mar;5(2):382-402.

Sun H, Dai H, Shaik N, Elmquist WF Drug efflux transporters in the CNS. Adv Drug Deliv Rev. 2003 Jan 21;55(1):83-105.

Szulzewsky F, Pelz A, Feng X, Synowitz M, Markovic D, Langmann T, Holtman IR, Wang X, Eggen BJ, Boddeke HW, Hambardzumyan D, Wolf SA, Kettenmann H. Glioma-associated microglia/macrophages display an expression profile different from M1 and M2 polarization and highly express Gpnmb and Spp1. PLoS One. 2015 Feb 6;10(2):e0116644.

Takahashi K, Rochford CD, Neumann H. Clearance of apoptotic neurons without inflammation by microglial triggering receptor expressed on myeloid cells-2. J Exp Med. 2005 Feb 21;201(4):647-57.

Thiery JP, Acloque H, Huang RY, Nieto MA. Epithelial-mesenchymal transitions in development and disease. Cell. 2009 Nov 25;139(5):871-90.

Tjensvoll K, Oltedal S, Heikkilä R, Kvaløy JT, Gilje B, Reuben JM, Smaaland R, Nordgård O. Persistent tumor cells in bone marrow of non-metastatic breast cancer patients after primary surgery are associated with inferior outcome. BMC Cancer. 2012 May 28;12:190.

Tominaga N, Kosaka N, Ono M, Katsuda T, Yoshioka Y, Tamura K, Lötvall J, Nakagama H, Ochiya T. Brain metastatic cancer cells release microRNA-181c-containing extracellular vesicles capable of destructing blood-brain barrier. Nat Commun. 2015 Apr 1;6:6716.

Trujillo JA, Fleming EL, and Perlman S. Transgenic CCL2 expression in the central nervous system results in a dysregulated immune response and enhanced lethality after coronavirus infection. J Virol, 2013. 87(5): p. 2376-89.

Turtzo LC, Lescher J, Janes L, Dean DD, Budde MD, Frank JA. Macrophagic and microglial responses after focal traumatic brain injury in the female rat. J Neuroinflammation. 2014 Apr 24;11:82. doi: 10.1186/1742-2094-11-82.

Valastyan S, Weinberg RA. Tumor metastasis: molecular insights and evolving paradigms. Cell. 2011 Oct 14;147(2):275-92.

Valiente M, Obenauf AC, Jin X, Chen Q, Zhang XH, Lee DJ, Chaft JE, Kris MG, Huse JT, Brogi E, Massagué J. Serpins promote cancer cell survival and vascular co-option in brain metastasis. Cell. 2014 Feb 27;156(5):1002-16.

van der Loos CM. Multiple Immunoenzyme Staining: Methods and Visualizations for the Observation With Spectral Imaging. J Histochem Cytochem. 2008 Apr; 56(4): 313–328.

van Rooijen N, Hendrikx E. Liposomes for specific depletion of macrophages from organs and tissues. Methods Mol Biol. 2010;605:189-203.

van Rooijen N, Sanders A, van den Berg TK. Apoptosis of macrophages induced by liposome-mediated intracellular delivery of clodronate and propamidine. J Immunol Methods. 1996 Jun 14;193(1):93-9.

van Rooijen N, van Kesteren-Hendrikx E. Clodronate liposomes: perspectives in research and therapeutics. J Liposome Res. 2002 Feb-May;12(1-2):81-94.

van Rooijen N, van Nieuwmegen R. Elimination of phagocytic cells in the spleen after intravenous injection of liposome encapsulated dichloromethylene-diphosphonate: An enzyme-histochemical study. Cell Tissue Res. 1984; 238, 355-358.

Verney C, Monier A, Fallet-Bianco C, Gressens P. Early microglial colonization of the human forebrain and possible involvement in periventricular white-matter injury of preterm infants. J Anat. 2010 Oct;217(4):436-48.

Viviani B, Corsini E, Galli CL, Padovani A, Ciusani E, Marinovich M. Dying neural cells activate glia through the release of a protease product. Glia. 2000 Oct;32(1):84-90.

Villanueva MT. Cell signalling: Stuck in the middle of chemoresistance and metastasis. Nat Rev Clin Oncol. 2012 Sep;9(9):490. doi: 10.1038/nrclinonc.2012.129. Epub 2012 Jul 31.

Webster MR, Kamat C, Connis N, Zhao M, Weeraratna AT, Rudek MA, Hann CL, Freel Meyers CL. Bisphosphonamidate clodronate prodrug exhibits selective cytotoxic activity against melanoma cell lines. Mol Cancer Ther. 2014 Feb;13(2):297-306. doi: 10.1158/1535-7163.MCT-13-0315. Epub 2013 Dec 5.

Weiss LM. Comparative histologic study of 43 metastasizing and nonmetastasizing adrenocortical tumors. Am J Surg Pathol. 1984 Mar;8(3):163-9.

Williams CB, Yeh ES, Soloff AC. Tumor-associated macrophages: unwitting accomplices in breast cancer malignancy. NPJ Breast Cancer. 2016;2. pii: 15025. Epub 2016 Jan 20.

Wu X, Schulte BC, Zhou Y, Haribhai D, Mackinnon AC, Plaza JA, Williams CB, Hwang ST. Depletion of M2-like tumor-associated macrophages delays cutaneous T-cell lymphoma development in vivo. J Invest Dermatol. 2014 Nov;134(11):2814-22.

Wyckoff JB, Wang Y, Lin EY, Li JF, Goswami S, Stanley ER, Segall JE, Pollard JW, Condeelis J. Direct visualization of macrophage-assisted tumor cell intravasation in mammary tumors. Cancer Res. 2007 Mar 15;67(6):2649-56.

Wynn TA, Chawla A, Pollard JW. Macrophage biology in development, homeostasis and disease. Nature. 2013 Apr 25;496(7446):445-55.

Xing F, Kobayashi A, Okuda H, Watabe M, Pai SK, Pandey PR, Hirota S, Wilber A, Mo YY, Moore BE, Liu W, Fukuda K, Iiizumi M, Sharma S, Liu Y, Wu K, Peralta E, Watabe K. Reactive astrocytes promote the metastatic growth of breast cancer stem-like cells by activating Notch signalling in brain. EMBO Mol Med. 2013 Mar;5(3):384-96.

Yamasaki R, Lu H, Butovsky O, Ohno N, Rietsch AM, Cialic R, Wu PM, Doykan CE, Lin J, Cotleur AC, Kidd G, Zorlu MM, Sun N, Hu W, Liu L, Lee JC, Taylor SE, Uehlein L, Dixon D, Gu J, Floruta CM, Zhu M, Charo IF, Weiner HL, Ransohoff RM. Differential roles of microglia and monocytes in the inflamed central nervous system. J Exp Med. 2014 Jul 28;211(8):1533-49.

Yoshimasu T, Sakurai T, Oura S, Hirai I, Tanino H, Kokawa Y, Naito Y, Okamura Y, Ota I, Tani N, Matsuura N. Increased expression of integrin alpha3beta1 in highly brain metastatic subclone of a human non-small cell lung cancer cell line. Cancer Sci. 2004 Feb;95(2):142-8.

Zeisberger SM, Odermatt B, Marty C, Zehnder-Fjällman AH, Ballmer-Hofer K, Schwendener RA. Clodronate-liposome-mediated depletion of tumour-associated macrophages: a new and highly effective antiangiogenic therapy approach. Br J Cancer. 2006 Aug 7;95(3):272-81. Epub 2006 Jul 11.

Zhai H, Heppner FL, Tsirka SE. Microglia/macrophages promote glioma progression. Glia. 2011 Mar;59(3):472-85.

Zhang J, Yang PL, Gray NS. Targeting cancer with small molecule kinase inhibitors. Nat Rev Cancer. 2009 Jan;9(1):28-39.

Zhang L, Zhang S, Yao J, Lowery FJ, Zhang Q, Huang WC, Li P, Li M, Wang X, Zhang C, Wang H, Ellis K, Cheerathodi M, McCarty JH, Palmieri D, Saunus J, Lakhani S, Huang S, Sahin AA, Aldape KD, Steeg PS, Yu D. Microenvironment-induced PTEN loss by exosomal microRNA primes brain metastasis outgrowth. Nature. 2015 Nov 5;527(7576):100-4.

Zhong H, De Marzo AM, Laughner E, Lim M, Hilton DA, Zagzag D, Buechler P, Isaacs WB, Semenza GL, Simons JW. Overexpression of hypoxia-inducible factor 1alpha in common human cancers and their metastases. Cancer Res. 1999 Nov 15;59(22):5830-5.

Zhu J, Zhang L, Hanisch UK, Felgner PL, Reszka R. A continuous intracerebral gene delivery system for in vivo liposome-mediated gene therapy. Gene Ther. 1996 Jun;3(6):472-6.